ABSTRACT

FRANK H. CORNEW. An Analysis of Methods for Accurate Modeling of Advective-Dominated Transport (Under the direction of CASS T. MILLER.)

Finite element modeling of sharp front advective-dispersive-reactive transport is not accurate for highly advective or reactive problems. Two techniques were studied with the goal of accurately modeling these problems: an *h*-adaptive method that adjusted element lengths, and Petrov-Galerkin upwinding which used weighting functions of higher polynomial order than that of the basis functions.

Finite element models were constructed using linear and quadratic basis functions in one spatial dimension. The *h*-adaptive method was shown to give good results with linear and quadratic basis functions. Petrov-Galerkin upwinding also yielded excellent results. This method was implemented for both classes of basis functions, but was studied only for the linear case.

The benefits of Petrov-Galerkin upwinding depend on user defined parameters that regulate the amount of upwinding applied to the solution. Taylor series and Fourier analyses of the finite element truncation error as well as numerical experimentation were performed to define optimal upwinding parameters. Published results by other investigators were reproduced, and an automated method of deriving optimal upwinding parameters was developed.

Analysis and operation of the Petrov-Galerkin models indicated that optimal levels of upwinding are a function of the gradient across each element. This observation led to a new upwinding scheme that adjusts the upwinding condition at each element as a function of the local gradient. Significantly better results were obtained with the new method relative to existing Petrov-Galerkin formulations.

The utility of this technique will be greatly enhanced when optimal upwinding conditions are described as a function of dimensionless model parameters such as Péclet, Courant, and Damköhler numbers, and the method is generalized to multiple spatial dimensions.

Acknowledgment

This work would not have been possible with out the help of my parents, Richard and Chrystel Cornew, my advisor, Dr. Casey Miller, and Beverly Brooks. The patience and support exhibited by all of these individuals is greatly appreciated. Furthermore, I thank Dr. Andrew Balber for general professional advice and inspiration, and Elizabeth Nelson for technical assistance. C.L. Lassiter and Donna Simmons have provided valuable administrative support for which I am grateful.

TABLE OF CONTENTS

LIST OF FIGURES

LIST OF TABLES

ABBREVIATIONS

ADR .....Advective Dispersive Reactive
BG.....Bubnov-Galerkin
FD .....Finite Difference
FE.....Finite Element
GU.....Gradient Upwinding
Im .....Imaginary part of a complex number
LHS.....Left-Hand-Side
LLE.....Linear Local Equilibrium
LM.....Levenberg-Marquardt
LPG.....Linear basis function Petrov-Galerkin code
PDE.....Partial Differential Equation
PG .....Petrov-Galerkin
QPG .....Quadratic basis function Petrov-Galerkin code
Re.....Real part of a complex number
RHS.....Right-Hand-Side
SU/PG.....Streamline-Upwind/Petrov Galerkin
1-D .....One Dimensional in space
2-D .....Two Dimensional in space
3-D .....Three Dimensional in space

NOTATION

a_λ.....Numerical amplification factor

$a_{a\text{-}\lambda}$.....Analytical amplification factor

C.....Concentration (m/l^3)

C_x^t.....Concentration at time t and location x (m/l^3)

C_a.....Analytical or exact concentration (m/l^3)

C^m.....Maximum concentration (m/l^3)

$C^{m\text{-}}$.....Maximum negative concentration (m/l^3)

C^{mo}.....Maximum concentration at t=0 (m/l^3)

C_n.....Numerical concentration (m/l^3)

Cr.....Mesh Courant Number

Da.....Mesh Damköhler Number

D_h.....Hydrodynamic dispersion coefficient (l^2/t)

E_i.....Integral measure of the overall error

E_d.....Discrete measure of the overall error

E_p.....Peak depression error

E_o.....Maximum oscillation error

E_s.....Phase shift error

E_m.....Mass preservation error

F_i.....ith-order Taylor series coefficient

i.....Square root of -1

k_1.....First-order decay coefficient (t^{-1})

M_i.....Modifying function of polynomial order i

N.....Polynomial order of basis functions

N_i.....ith basis function

n_n.....Number of nodes

Pe.....Mesh Péclet Number

R_f.....Retardation factor for linear local equilibrium sorption

T.....Truncation error (m/l^3)

W_i.....ith weighting function

v_x.....Mean solute pore velocity (l/t)

x_L.....Length of spatial domain (l)

x_a^m.....Spatial location of maximal analytic concentration (l)

x_n^m.....Spatial location of maximal numeric concentration (l)

α.....N+1 degree uniform upwinding parameter
α_i.....ith-order N+1 degree Gradient Upwinding parameter
α^e.....Element specific N+1 degree upwinding parameter
α_m.....N+1 degree uniform upwinding parameter for middle nodes
α^u.....Upgradient element N+1 degree upwinding parameter
β.....N+2 degree uniform upwinding parameter
β_i.....ith-order N+2 degree Gradient Upwinding parameter
β_c.....N+2 degree uniform upwinding parameter for corner nodes
β^d.....Downgradient element N+2 degree upwinding parameter
β^e.....Element specific N+2 degree upwinding parameter
β_m.....N+2 degree uniform upwinding parameter for middle nodes
β^u.....Upgradient element N+2 degree upwinding parameter
Δt.....Time step size (t)
Δx.....Distance between spatial nodes (l)
μ.....Peak location of a Gaussian source (l)
ξ.....Dimensionless natural coordinate spatial dimension
σ_x.....Standard deviation of a Gaussian source (l)
$\overline{\sigma_x}$.....Dimensionless standard deviation of a Gaussian source

1 INTRODUCTION

Groundwater is relied on throughout the world as a clean and abundant water source. In 1985, groundwater provided drinking water for as much as 50% of the population, as well as for 35% of the municipalities in the United States (Conservation Foundation, 1985). It is thought that humans have developed wells to access groundwater over the past seven millennia (Eliason, 1990).

The high quality of groundwater is due to filtration and biological activity that occur in the subsurface environment. This quality is threatened by contamination from industrial, agricultural, residential, and environmental sources. Industrial sources are responsible for a great deal of groundwater contamination. Inappropriate or outdated waste disposal strategies, process design, and material handling policies, as well as accidental release of toxics all pollute groundwater. The perception that groundwater quality is mainly threatened by industrial activity is understandable, but industry is not the only source of groundwater contamination.

Widespread agricultural use of pesticides, herbicides, and fertilizers also has a significant impact on groundwater quality. Approximately 545 million kg. of agricultural pesticides are used annually in the United States (Ritter, 1990). These substances are applied directly to the ground, and have been used repeatedly on large land areas for long periods of time. The resulting accumulations of pesticides and fertilizers observed in groundwater may therefore be large and toxic (Burkart et al., 1990).

Residential sources such as municipal landfill leachate and wastewater also contribute to groundwater contamination. It is important to note that approximately one third of the population of the United States uses septic systems for wastewater disposal (Environmental Protection Agency, 1986). Septic systems are therefore responsible for the greatest volume of anthropogenic effluent discharged into the groundwater zone in this country (Robertson et al., 1990).

Leaking underground storage tanks are common causes of agricultural, industrial and residential groundwater pollution. Leaking petrochemical tanks are commonplace, and may be located in a variety of settings such as residences, gasoline stations or tank farms. Leaks result from corrosion of old tanks or from improper installation of new ones. Many abandoned tanks exist in unknown locations, increasing the potential for groundwater contamination (Dickinson, 1990). Known sources are serious enough: at least 750,000 gallons of high level radioactive waste mixed with aqueous and organic waste have leaked from tanks at the Hanford nuclear reservation in Washington state (Levi, 1992).

Fresh water in the subsurface may also be contaminated by salt water intrusion and mineral leaching. While these sources may be considered to be of environmental origin, they are frequently induced or aggravated by human demand on groundwater (Bear, 1979). While this type of problem is not as dire as leaking tanks of radioactive organic solvents, salt water intrusion can reduce the utility of groundwater resources to the same extent as other types of contamination. The cost of desalinating seawater was recently reported to be approximately four U.S. dollars per 1000 gallons (Abelson, 1991), which is certainly a tractable cost for low level production, but is prohibitive for large volumes.

Groundwater quality is clearly at risk from the above factors. Protection and remediation of this resource require accurate characterization of the hydrological environment in the subsurface, as well as above the ground surface. Modeling was initially used to describe groundwater flow to locate production wells and predict their performance. In the past fifteen years, transport modeling of contaminants in groundwater has been routinely used to simulate the impact and fate of these contaminants as they interact with the subsurface environment.

Numerical modeling methods have been effectively applied to contaminant transport in groundwater. Such methods can address complex situations involving various modes of sorption and decay, as well as multiple contaminant phases. The cornerstone of such transport models is the advective-dispersive-reactive (ADR) equation. While numerical methods can solve this equation, the scope of the problems they can accurately model is constrained by algorithmic limitations, as well as by computational overhead.

This work addresses the limitations of finite element (FE) modeling of ADR transport. This method, for the most part, accurately models the ADR equation, but can exhibit numerical dispersion and oscillations under model configurations that involve advective-dominated transport and sharp fronts (Bear, 1979). Unfortunately, avoiding this undesirable

behavior results in significant computational expense when the standard FE formulation is used. Techniques were examined that involve modifications of the mathematical structure of FE models, as well as methods that alter the implementation of the model to produce more accurate solutions.

2 BACKGROUND AND LITERATURE REVIEW

2.1 Modeling

In 1856, Henri Darcy published the results of his research on water flow through sand filters used to supply potable water to the French city of Dijon (Darcy, 1856). His efforts resulted in Darcy's law, which, by extension, mathematically describes groundwater flow in the subsurface. This development is therefore the foundation of mathematical modeling of groundwater dynamics.

Transport modeling in groundwater permits the assessment of the impact and fate of contaminants as they interact with the subsurface environment. Until recently, most of the developments in hydrogeological modeling addressed groundwater flow problems related to water well production and siting. Groundwater flow modeling is also an important component of transport modeling, since transport cannot be modeled unless the direction and velocity of the groundwater are known. Modeling contaminant transport in groundwater still has a long history - in an indirect sense. The ADR equation is a member of a class of partial differential equations (PDE's) that is of interest in many scientific disciplines (Guymon et al., 1970). It is classified as parabolic for transient problems and elliptic for stationary problems. The transient case arises when the partial derivative of the concentration with respect to time is not zero. Conversely, the stationary case results for zero values of the concentration's partial temporal derivative.

Advection-dominated transport is considered to be a difficult problem to model with numerical methods, due to the nonsymmetry of convection operators present in such problems (Hughes and Brooks, 1979). This asymmetry leads to oscillations in solutions derived from methods that correctly model symmetrical problems. Expressions that are similar to the ADR equation are used to describe heat transport in solid materials, vorticity transport in viscous fluid dynamics as well as energy transfer in reservoirs (Christie et al., 1976; Heinrich et al., 1977). There has been significant research interest in these fields over the years, and the expertise gained relates directly to transport modeling in groundwater.

Ironically, many developments in flow and transport modeling have resulted from research related to petroleum exploration (Hughes, 1987; Langtangen, 1990). In this case, modeling efforts were directed at locating and extracting a resource which, after use, might return to the subsurface as petrochemical contaminants.

Computational models may be classified into two basic types: analytical and numerical. Analytical models use closed-form expressions to provide exact or approximate solutions to the problem. They have the advantage of providing results only for the locations and times desired, but are limited by a number of factors. Their utility is restricted to very specific combinations of problem conditions, such as source type, domain shape, boundary conditions, hydrological conditions, and reaction types (Bear, 1979).

2.2 Numerical Models

Numerical models rely on various methods to approximate PDE's. In this case, the PDE of interest describes transport of contaminants in groundwater - the ADR equation. Most numerical methods solve PDE's by expressing them as a system of algebraic expressions that approximate the solution at specific points in time and space. The system is then solved to produce solutions of the PDE at each of the solution points. Many intermediate solution points may be required in order to obtain solutions at a set of desired solution points. The numerical methods used to solve groundwater related problems are typically classified as Eulerian or Lagrangian. These two classes may also be hybridized to generate Eulerian-Lagrangian models, in which components of the transport problem are isolated and solved by the different schemes.

2.2.1 Lagrangian Methods

Lagrangian, or particle tracking methods model contaminant transport by transporting units of contaminant mass (particles) through the modeled environment. Each mass unit is advected in the direction of groundwater flow, and then dispersed by increasing its volume, and then degraded as dictated by the appropriate reaction kinetics. This methodology has been implemented in a formal mathematical framework as well as with stochastic processes.

The random walk method advects contaminant mass in a straightforward fashion. For every time step a mass unit will travel a distance equal to the product of the timestep length and the groundwater flow velocity in the direction of groundwater flow (Prickett et al., 1981). The dispersive component of the problem is then modeled as a random process, and

the mass represented by the mass unit is degraded as required by the reactive processes in the model.

Other numerical Lagrangian methods such as continuous forward particle tracking and single step reverse particle tracking have been hybridized with Eulerian methods to model different aspects of ADR transport (Yeh, 1988). Lagrangian modeling of advection may be combined with Eulerian modeling of dispersion with good results.

Lagrangian methods have the advantage of allowing the mesh Courant number (Cr) of the model to be greater than unity. This means that the mean advective transport that occurs between timepoints can occur over distances that are longer than the separation between spatial solution points. The Cr is the ratio of these two quantities, and one of the fundamental constraints on Eulerian models is that this ratio must not be greater than one. Lagrangian models do not have to observe this restriction, and therefore require fewer solution steps than Eulerian methods to model transport over a given period of time. While the Cr does not restrict timestep size in Lagrangian models of the ADR equation, real world problems impose other timestep size limitations on this model class. These restrictions result from heterogeneous hydrogeological parameters as well as common reactive processes. Lagrangian methods may therefore be difficult to implement for groundwater transport problems involving complex subsurface media (Yeh, 1988).

These techniques are intuitively simple and easily implemented, but they tend to be computationally intensive, as many discrete mass units must be moved in order to provide sufficient resolution to describe a continuous concentration profile throughout the domain. This drawback is somewhat compensated for by the suitability of these methods for parallel processing, as they involve many independent solutions of the same problem.

2.2.2 Eulerian Methods

Eulerian methods treat the domain as a fixed framework of control volumes delimited by solution points or nodes. Mass balance is maintained in the control volumes while the total mass they contain varies.

The two main Eulerian schemes are the finite difference (FD) and FE methods. FD methods are based on discrete approximations of the derivatives of the dependent variable. A system of difference equations is then created from these approximations, which is then solved for the dependent variables at each node. The accuracy of a FD solution is a function

of the method used to approximate the derivatives, the order of the approximations, as well as the model parameters

Finite differences are one of the more popular numerical solution methods for PDE's, as they are simple to implement. A significant drawback to FD methods is that they cannot precisely represent curved boundaries in two or three dimensional space. This is because FD grids must be constructed of parallel straight lines or flat surfaces. Representing curved boundaries with FD grids is analogous to describing a smooth edged disk with flat, square tiles, or building a sphere out of cubic blocks. The grid may also be refined in order to describe boundaries accurately. Unfortunately, the grid parallelism requirement generates superfluous nodes within the domain, which results in unnecessary computational overhead.

Finite differences have been used to solve PDE's for a long time and were first applied to modeling of contaminant transport in 1962 (Huyakorn and Pinder, 1983; Istok, 1989). In fact, finite difference approximations of derivatives for solving PDE's were used and studied by Bessel, Euler, Gauss, Laplace, and Newton; the origins of FD methods therefore date back to the eighteenth century (Ames, 1977; Pinder and Gray, 1977). The applications of FD methods are so ubiquitous that problems involving salami processing have been addressed with FD models (Imre and Környev, 1990).

Finite elements are a more recent development, making their first appearance as a method for solving PDE's in 1960 (Zienkiewicz, 1977). ADR transport was first modeled with finite elements in 1968 (Price et al., 1968), and has been a very active area of research since then (Westerink and Shea, 1989).

The accuracy of both FE and FD solutions is a function of hydrological parameters, node spacing, and timestep size. The FE method has several advantages over finite differences. It generally provides solutions with greater accuracy for a given number of degrees of freedom, compared to solutions from FD models (Gray and Pinder, 1976; van Genuchten, 1976). FE models are also more flexible: anisotropic and heterogeneous aquifer properties are incorporated with greater ease than in FD models. While FE models may require greater computational effort than FD models for the same number of nodes, the flexibility of FE grids may result in solutions of better quality with less computational effort, due to reduction of the number of nodes (Istok, 1989). The FE method also allows for direct solution for the dependent variable at points in the domain that do not lie on nodes through the use of the basis functions contained in the model structure. While FD solutions

provide results only at the nodes, independent interpolation techniques may still be applied to obtain data at non-nodal locations.

The spaces demarcated by gridlines in FE models are referred to as elements. In this case, nodes may be placed exactly where they are needed, and gridlines are not required to be parallel or even straight. Element boundaries can be deformed to precisely match any physical feature of the domain through the use of natural or isoparametric coordinates (Huyakorn and Pinder, 1983). This allows precise representation of boundaries and other domain features such as sources, sinks, and variations in physical parameters.

Equations are developed in FE models that are based on interpolated approximations of the dependent variables over each element. These equations are then numerically integrated to yield a system of equations that can be solved for dependent variable values at each node (Bear, 1979). The Rayleigh-Ritz technique was initially used to derive the approximating equations required by FE models. It is based on the calculus of variations, and does not necessarily produce results for as broad a range of problems as the Galerkin method described below (Istok, 1989). The Rayleigh-Ritz method produces basis functions that are defined over the entire domain, and must also respect the domain's boundary conditions. Its applicability is therefore limited to regions that have relatively simple geometries (Huyakorn and Pinder, 1983).

B.G. Galerkin developed an alternate method for deriving FE formulations in 1915. Bubnov independently arrived at a similar approach in 1913, so this procedure is referred to as the Bubnov-Galerkin (BG) method (Pinder and Gray, 1977). This technique is a subset of the method of weighted residuals, and has become the preferred method for FE model formulation. Since the basis functions that this method produces are defined only over each element, more complicated domain geometries are tractable by this method. The two methods employ basis functions that are subject to the same constraints, but the superiority of the BG method arises from its ability to represent the domain in a piecewise fashion (Huyakorn and Pinder, 1983).

Finite element solutions are based on interpolations of the problem at hand. Obviously, interpolation accuracy is a function of the polynomial order of the interpolating or basis functions. Higher-order polynomials can potentially produce better fits of complicated solution profiles than lower-order polynomials (Zienkiewicz, 1977; Press et al., 1989), but increasing the order of the basis functions results in increased computational overhead of the finite element scheme. This increase results from both greater mathematical complexity

and an increase in degrees of freedom, as additional nodes are required by higher-order basis functions for a given number of elements (Pinder and Gray, 1977). Experimentation on various types of basis functions resulted in the observation that quadratic Lagrangian basis functions performed better than linear ones (van Genuchten, 1976). Surprisingly, the same investigator reported that cubic basis functions did not perform as well as the quadratic functions when longer time steps were used. This investigator also noted that while first- and second-order continuous Hermitean basis functions were usually more accurate than their Lagrange polynomial counterparts, they can be unstable when modeling advection-dominated flow.

2.2.3 Matrix Solution Techniques

Numerical models rely on various methods to approximate PDE's. Most numerical methods solve PDE's by expressing them as a system of equations in matrix form that approximate the PDE at specific points in time and space. The system is then solved to produce solutions of the PDE at each of the desired locations. Solution methods fall into two general classes: direct and iterative. Direct solvers such as Gauss elimination use one step to arrive at the exact solution, while iterative solvers use a succession of approximate solutions to arrive at an answer that is close to exact. While direct methods are accurate and simple, iterative solvers are generally required in FE transport models in multiple dimensions. This is due to the sparse matrices with large bandwidths that are generated in two- and three-dimensional models (Allen and Curran, 1989; Sharma and Carey, 1989; Liou and Tezduyar, 1990) storage and manipulating such matrices requires a great deal of computer overhead. Nonlinear sorption and reactive processes may also require iterative solution methods (Huyakorn and Pinder, 1983).

While many methods have been applied over the years, iterative solution techniques are a field of current interest. Traditionally, Newton-Raphson and Picard iteration are used for nonlinear problems, and Jacobi iteration, the Gauss-Seidel method, the successive overrelaxation method, and the iterative-alternating-direction-implicit method are applied to linear systems. Iterative solvers based on preconditioned conjugate gradient methods are under development, and have been applied to linear 3-D FE problems (Pini and Gambolati, 1988). Recent work on iterative implicit-explicit methods uses a combination of the grouped element-by-element and generalized minimum residual method and a scheme that assigns implicit or explicit time integration depending on the solution state of linear problems (Liou and Tezduyar, 1990).

2.2.4 Upwinding

The concept of upwinding first appeared in the early 1950's when Allen and Southwell applied upstream differencing to finite difference models (Bouloutas and Celia, 1988). Upstream differencing emphasizes the contribution from upstream or upgradient nodes to the advective portion of the solution at downgradient nodes. Upwinding, or upstream weighting was first applied to finite elements in 1976 (Griffiths and Mitchell, 1979). This technique emphasizes the contribution from the upstream portion of the element through the use of asymmetric weighting functions. The effect of upwinding on FD and FE transport models is to introduce numerical dispersion, thereby smoothing out oscillations. Unfortunately, this can be a disadvantage, as overly diffusive solutions can occur, especially in the case of transient problems (Hughes, 1987).

2.2.4.1 Petrov-Galerkin Upwinding

Petrov-Galerkin (PG) methods upwind FE models by introducing weighting functions that are not identical to the basis functions (Mikhlin, 1964; Hughes, 1987). For ADR modeling, the PG method reduces oscillations in finite element solutions by reducing the asymmetry of the advection matrix (Heinrich and Zienkiewicz, 1979; Barrett and Morton, 1984). As an added benefit, symmetric positive definite matrices are more easily solved by iterative matrix solution techniques such as conjugate gradient methods (Tezduyar et al., 1988).

While PG upwinding eliminates oscillations by increasing the symmetry of components of non-self-adjoint problems such as the ADR equation, it has also been successfully applied to symmetric problems such as the Timoshenko beam problem, the thin Mindlin plate (Loula et al., 1987; Givoli, 1988), as well as the compressible Euler and Navier-Stokes equations (Hughes, 1987; Brueckner and Heinrich, 1991). The latter are not to be confused with the incompressible Navier-Stokes equations, which do contain asymmetric components (de Sampaio, 1991).

Upwinding of FD and FE methods has been criticized in the literature as an ad-hoc technique (Gresho and Lee, 1979; Leonard, 1979b). These investigators propose that many of the good results obtained with upwinding result from trial and error adjustment of upwinding conditions without adequate or appropriate theoretical support. These commentaries suggest that upwinding is at best a solution methodology that should be avoided, and at worst that past investigations of these methods are based on poor science.

2.2.4.2 Weighting Functions

The initial investigation that described PG methods used upwinding with linear and quadratic basis functions (Christie et al., 1976). This investigation used two classes of weighting functions. Weighting functions of the same polynomial order as the basis functions result in N degree upwinding, and weighting functions that are one polynomial degree higher than the basis functions result in N+1 degree upwinding. Further efforts focused on N+1 upwinding of linear, quadratic, and cubic basis functions (Christie and Mitchell, 1978). Other weighting schemes have been proposed, such as formulations that vary the quadrature points used for numerical integration of the elements (Hughes, 1978; Abdel-Hadi et al., 1985; Bermudez et al., 1989), as well as methods that directly add artificial diffusion (Kelly et al., 1980). These are related to PG methods, but are not considered to be as easily implemented, especially for higher dimensional applications on irregular grids (Adornato and Brown, 1987).

2.2.4.3 Optimal Upwinding Parameters

The amount of upwinding applied to the model is usually controlled by user defined upwinding parameters. Many different approaches have been used to define "optimal" upwinding levels, either through parameters, weighting functions or quadrature points. The optimal level of upwinding was described by difference equation analysis and Padé approximation for the steady-state problem in one dimension in the first report on upwinded finite elements (Christie et al., 1976). The focus of that work was the vorticity transport equation, which is similar to the ADR equation. Unfortunately, FE solutions of the transient ADR equation frequently exhibit excessive diffusion and incorrect advective speed when "optimal" upwinding derived for the stationary case is used (Tezduyar and Ganjoo, 1986; Yu and Heinrich, 1986; Pini and Gambolati, 1988; de Sampaio, 1990).

The PG/modified operator approach of de Sampaio uses an optimal N+1 upwinding parameter for linear FE analysis of transient and stationary ADR problems (de Sampaio, 1990). This process arises from modifying the differential operator to make it self adjoint; optimal upwinding arises from approximating the weighting function. The approximation provides an optimal upwinding parameter for the stationary case, but an adjustment of the time weighting factor based on Fourier analysis is needed for transient problems.

The issue of optimal upwinding parameters for N+1 and N+2 degree upwinded finite elements was recently addressed by Westerink and Shea in one dimension for the transient

ADR equation (1989). The upwinding formulation used by these investigators is based on previous work (Christie et al., 1976; Dick, 1983). Dick enhanced the N+1 degree formulation of Christie and Griffiths to include N+2 upwinding for linear basis functions. Westerink and Shea applied this method to linear and quadratic basis functions and used Taylor series analysis up to the fifth-order, Fourier analysis, and numerical experimentation to describe optimal upwinding parameters.

2.2.4.4 Two Dimensional Implementation

A major difficulty in upwinding methodology has been the extension from one to two and three spatial dimensions (1-D, 2-D and 3-D). Straightforward 2-D implementations of FE and FD formulations have not delivered the excellent results observed in 1-D models. The problem is attributed to crosswind diffusion that occurs when the advective direction is not parallel with the gridlines (Hughes and Brooks, 1979; Westerink and Cantekin, 1988; Cantekin and Westerink, 1990).

This issue was addressed with the streamline-upwind/Petrov-Galerkin (SU/PG) method (Hughes and Brooks, 1979). The SU/PG method is an upwinding strategy for 2-D and 3-D transport that curtails crosswind diffusion by using upstream weighting only in the direction of the advective path. This original formulation used N-1 degree upwinding by using the spatial derivatives of the basis functions as weighting functions. This formulation eliminated crosswind diffusion for certain problems, but difficult problems involving sharp fronts in transient and stationary ADR transport have produced overly dispersive and oscillatory solutions (Mizukami and Hughes, 1985; Hughes et al., 1986; Tezduyar and Park, 1986).

Research continues to improve SU/PG model performance with respect to crosswind diffusion problems. Further investigation has examined 'sigma weighting', and 'transport weighting' approaches (Tezduyar and Ganjoo, 1986; Tezduyar et al., 1987). Of special interest are discontinuity capturing methods that modify SU/PG upwinding in response to the concentration in stationary ADR models (Hughes et al., 1986; Tezduyar and Park, 1986). This scheme defines the streamline upwinding formulation as a function of the magnitude and direction of the velocity and concentration gradients as indicated by difference equation analysis.

Linear triangular elements have also been incorporated into SU/PG models for stationary ADR transport with promising results (Mizukami, 1985). This approach continued with a modification that involved describing an optimal upwinding direction that does not follow the streamlines (Mizukami and Hughes, 1985). In this case, the component

vectors of the upwinding direction are modified by constants that are a function of the advective vector in order to make the advective coordinate matrices satisfy the discrete maximum principle. Other investigators have examined optimal upwinding directions that are not aligned with the streamlines (Galeão and Dutra do Carmo, 1988; Dutra Do Carmo and Galeão, 1991). While these methods have performed well for the stationary case, transient ADR problems are not as well behaved (Tezduyar and Ganjoo, 1986). Tezduyar and Ganjoo have sought to improve modeling of transient ADR problems by making the weighting functions a function of spatial and temporal discretization (Tezduyar and Ganjoo, 1986).

Limiting artificial diffusion to the advective direction in the manner of SU/PG methods is thought to be ineffective at eliminating the phase lag and numerical dispersion frequently found in 2-D transient ADR FE models (Cantekin and Westerink, 1990; de Sampaio, 1990). To address this problem, three non-SU/PG methods were compared by Cantekin and Westerink in 1990. In one, the amount of N+1 degree upwinding applied to bilinear quadrilateral elements is a function of the cosine of the angle between the velocity vector and the element side. This makes the artificial diffusion matrix invariant with the direction of the flow direction, thereby curtailing artificial crosswind diffusion. Another approach uses N+2 degree upwinding without the cosine multiplication scheme. The crosswind upwinding parameters in the this scheme are derived by multiplying the element side parameters. The third method extends the N+2 method to use N+2 degree upwinding along the element sides and N+5 degree upwinding for the cross product terms. This last method was shown to be more accurate, as the crosswind upwinding parameters could be adjusted independently of the element side parameters. In all three cases, optimal parameters were derived from numerical experiment, as well as Fourier and Taylor series analysis.

Sun and Yeh proposed a transient ADR PG method in 2-D that uses N degree upwinding adjusted as a function of Péclet number and advective direction in conjunction with linear triangular elements (Sun and Yeh, 1983). This model appears to be effective, but depends on upwinding parameters that are derived for an undefined range of problems in a trial and error manner that is not documented. This method was extended to 3-D with linear triangular prism elements in 1986 (Wang et al., 1986).

Research on solutions of the transient ADR equation with non-upwinded models has also been directed at improving time integration, as difficult temporal discretizations also degrade model performance. Among these are: Taylor-Galerkin methods that expand the

time derivative term to include second and third-order derivatives (Donea et al., 1984), as well as the use of finite elements in space and time (Wiberg, 1988).

The notion of PG finite elements in space and time was developed by Yu and Heinrich, using linear elements in one dimension and N-1 upstream weighting with a quadratic variation in time (Yu and Heinrich, 1986). Optimal upwinding was defined through the use of Fourier and Taylor series analysis. This method was then extended to two and three spatial dimensions (Yu and Heinrich, 1987).

2.2.4.5 Variants

A few variants of the PG method have been produced by other investigators. High order basis functions have been used in conjunction with linear weighting functions to model advective-dominated flow with the Navier Stokes equations (Leonard, 1979a; Steffler, 1989). The 'optimal test (weighting) function' or local adjoint methods derive weighting functions that are considered to be optimal since they satisfy local adjoint conditions. This method produced results that were similar to those from the uniform PG method used in this work, a PG method with exponential weighting functions, as well as from SU/PG for 1-D transient and stationary ADR problems (Bouloutas and Celia, 1988). Local adjoint methods have been extended to multi-dimensional problems (Neuman, 1990; Russell and Trujillo, 1990).

2.2.4.6 Applications

While the focus of this work has been ADR transport, it is worthwhile to note the variety of other problems PG upwinding has been applied to. Some of these problems are similar to ADR transport, while others are very different. Advective-dominated flow described by nonlinear Burgers' equations (Demkowicz and Oden, 1986a; Hughes, 1987), heat convection in solidification of metallic alloys (Adornato and Brown, 1987), and temperature distributions in combustion problems (Ramos, 1990) are similar to the ADR groundwater contaminant transport problem. Unrelated problems such as turbulent flow in annular exhaust diffusers of gas turbines (Baskharone, 1991), turbulent swirling flows (Benim, 1990), steady viscoelastic flow (Rajagopalan et al., 1990a, 1990b), viscoelastic flow through corrugated tubes (Burdette et al., 1989), two-phase immiscible flow (Espedal and Ewing, 1987), Bradshaw-Ferris-Atwell turbulent boundary layers (Stewart and Unsworth, 1988), electrochemical processes of electrophoretic separation techniques (Ganjoo and Tezduyar, 1987), temperature distributions in deep-well wet oxidation reactors (Liou et al., 1990; Mittal et al., 1991), electromagnetic eddy currents (Marechal and Meunier, 1990),

electrostatic potential and carrier current continuity for semiconductor device simulation (Sharma and Carey, 1989), and evaporation of polydisperse aerosols (Tsang and Huang, 1990) have also been addressed with PG FE methods.

2.2.5 Adaptive Methods

Adaptive methods are known to be effective in reducing oscillations and dispersion in FE solutions of the ADR equation (Thompson, 1985). Numerical methods are called adaptive when they modify their operational parameters in response to error or anticipated error in the solution in such a way to reduce or minimize that error. Three basic strategies are applied to FE modeling: *h*-methods, *r*-methods and *p*-methods. The *h*-method refines grid spacing in the vicinity of the error by adding nodes. The *r*-method also refines grid spacing, but does so by redistributing a fixed number of nodes. The *p*-method adds nodes by substituting higher-order basis functions in elements that contain the error. Since the degrees of freedom that these methods add or redistribute are only applied to areas where they are needed, adapted solutions can be much more efficient than a solution with increased spatial resolution over the entire domain and time span of the model. The *h*- and *p*- methods have matured to the point that they are now featured in commercial general purpose FE packages for personal computers (Cohen, 1992).

Adaptive method research focuses on two central issues: error evaluation or adaptive decision making, and the algorithms that implement the adaptive decisions.

2.2.5.1 Error Evaluation

Truncation error is the main cause of inaccuracy in numerical methods. Since error in FD and FE methods is a function of how accurately partial derivatives are represented, numerical solutions are referred to as being accurate up to the lowest order partial derivative that is correctly described. Truncation error arises from the numerical method's inherent inability to represent higher-order terms, and therefore represents the method's inability to accurately solve the equations at hand. Truncation error is not to be confused with round-off error, which results from the binary numerics used by computers, as well as their limited ability to handle all the digits of floating point decimal numbers. Round-off error can be reduced through the use of proper programming techniques, and is usually a minor contributor to overall error in properly programmed models.

When error in numerical solutions is known before a realization of the solution, it is classified as a priori error, and a posteriori when it is known afterward. Analytical solutions

may provide the value of these errors, but if an analytical solution can be evaluated, the need for a numerical solution vanishes. Similarly, the computational overhead involved in evaluating an error or overall adaptive algorithm may be in excess of the overhead needed to evaluate the problem at the same degree of refinement or order of interpolation as the adapted region over the entire domain.

A priori error is the more useful of the two, as it allows the adaptive decision to be made in advance of any solution. Exact values of a priori error are not easily derived, but an estimate of a priori error magnitude or its bounds is still of use for adaptive methods (Demkowicz and Oden, 1986b). Knowledge of the circumstances under which error occurs is an informal form of a priori error. Sharp fronts are known to generate error and are easily detected in ADR FE models, so their presence alone is a valid trigger for adaptive operations (Arney and Flaherty, 1989).

A posteriori error can be used to validate a solution at a given time level so that the solution at the next time point may proceed on a solid foundation. If the accuracy of the solution is not satisfactory, a posteriori error can guide the adaptive process to produce a better solution after repeating it at that time level.

The goal of adaptive methods is to minimize an error measure, so formal error measures are generally used that are based on model output (Devloo et al., 1987). Error measures that are useful for adaptive decision making must be able to indicate where to add, remove, or place nodes. Estimates of truncation error based on observed spatial partial derivatives have been used as adaptive criteria (de Oliveira and Oliveira, 1988), as well as from FE interpolation theory (Demkowicz et al., 1985; Sharma and Carey, 1989). Many other a posteriori error estimates have been derived for adaptive methods, with varying degrees of absolute accuracy (Bieterman and Babuska, 1982; Oden et al., 1989). These estimates may require multiple FE solution realizations, making them computationally expensive (Kelly et al., 1983). The energy norm has been shown to be an accurate representation of truncation error in FE models (Babuska and Szabo, 1982), and is one of the more common error measures used to drive adaptive model decisions (Kelly et al., 1983; Gui and Babuska, 1986b; Rank and Werner, 1986; Zienkiewicz and Zhu, 1987).

2.2.5.2 Algorithms

A major problem in *h*- and *p*- adaptive methods is the management of the degrees of freedom added to or removed from the FE matrices. Mesh refinement and increased basis

function order both may result in additional nodes. An adaptive procedure should generate adapted matrices that are properly configured for efficient matrix solution techniques.

Refined areas are handled in various ways. The matrices for the entire problem may be reassembled to accommodate the additional nodes (Demkowicz et al., 1989). Decoupling strategies are frequently used that solve for concentrations in the adapted areas outside of the global matrices (Yeh, 1988; Allen and Curran, 1989; Yeh, 1990). A global solution is derived, the adapted areas are located and solved for with their own matrices, and the new information is incorporated into the global solution. This process continues iteratively until the two solutions agree on their interfacial boundaries (Berger and Oliger, 1984). The iterative process is necessary for ADR problems since Neuman boundary conditions must be applied to portions of the interfacial boundaries. Another approach uses a third grid that is a composite of the global and refined areas, and coordinates the behavior of the grids from the global and refined portions of the problem (Bramble et al., 1988). Independent refined area grids may involve a fair number of redundant nodes, as grid overlap between the refined and unrefined areas may be required, or the refined grid may need to extend significantly away from regions that contain error. These requirements may be necessary to ensure convergence between the solutions in the refined and unrefined areas.

Two dimensionless parameters govern accurate FE ADR modeling. As mentioned earlier, the Cr must be less than one. A second dimensionless grouping, the mesh Péclet number (Pe), arises from the product of the nodal spacing and the pore velocity divided by the hydrodynamic dispersion coefficient. This number must be less than two if a FE ADR model is to yield accurate solutions. The Cr is inversely proportional to nodal spacing, so its maximal value of one poses an upper limit on refinement. The Pe is directly proportional to nodal spacing, so the smaller elements that result from refinement result in smaller Pe values in refined elements. Of these two, the Cr limit is the most problematic, and has been addressed by methods that use smaller time steps for the refined areas. The solution proceeds in the adapted area with smaller time increments until the next global timepoint is reached (Berger and Oliger, 1984).

Floating nodes are a problem that occurs in 2-D and 3-D *h*- and *p*-method formulations. These nodes arise on the interface between elements that are adapted to differing degrees. They are present on the margins of the adapted portions of the domain, but are not represented in matrices that correspond to adjoining elements that are not adapted, or adapted to a lesser degree. The solution of the problem shown in Figure (2-1) requires concentration values for the nodes on the interface between the unrefined element on the left

and the refined element on the right. While the finite element formulation provides a good interpolated value at these points, alternative methods for deriving these values have been explored (Carey and Seager, 1985; Demkowicz and Oden, 1986a). Furthermore, inappropriate combinations of boundary conditions and continuity levels may arise on the borders of refined areas and problem variables may result in "poorly posed problems" (Bramble et al., 1988; Demkowicz et al., 1989). This condition arises if the adaptive algorithm solves for concentrations in refined elements of the global problem when the concentrations on the borders are held constant (Dirichlet boundaries). These are issues that can be handled, but at the expense of increased computational cost.

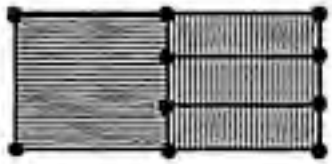

Fig. 2-1. Floating nodes in 2-D grid refinement.

In 2-D and 3-D problems, *h*-refined grids may be aligned with the global grids, or oriented in more appropriate ways (Arney and Flaherty, 1989). Aligned grids require less interpolation effort since more nodes are in common between the refined and global elements, while nonaligned grids add fewer nodes overall, as the refined subdomain may precisely encircle the area requiring refinement.

These problems can also be avoided by progressive refinement over several elements with triangular elements (Bramble et al., 1988; Rivara, 1989), but a larger number of refined elements are needed to obtain the desired level of refinement in a target element, as the refinement progression is carried out over several elements. Solutions from *r*-methods are also not affected by these problems, as nodes are not inserted into their meshes. They do, however, require design of optimal meshes that equidistribute and minimize error, which is a problem of greater theoretical complexity (Thompson, 1985; Adjerid and Flaherty, 1986; Kikuchi, 1986).

The bulk of the adaptive literature relates to *h*-methods, as the *p*-method is a more recent development (Dorr, 1984). The *p*-methods have been shown to provide excellent results for certain problems and have great theoretical appeal, due to their robustness and efficiency They are considered to converge at a faster rate than *h*-methods for most problems (Babuska and Szabo, 1982; Basu and Peano, 1983) which means that *p*-methods can attain

the same degree of accuracy as *h*-methods while using fewer degrees of freedom. More concisely, *p*-methods may offer higher quality solutions at lower computational cost than *h*-methods.

There are drawbacks to *p*-methods, however, as increased basis function order may re-introduce oscillations in some ADR models (Yeh, 1988), and cannot model sharp fronts as well as mesh refining schemes (Basu and Peano, 1983; Gui and Babuska, 1986a). The two methods have been combined to produce *h-p* adaptive methods, which have been shown to have faster convergence rates than either of the individual methods (de S.R. Gago et al., 1983; Gui and Babuska, 1986a). Work is in progress to describes optimal levels of mesh refinement and basis function order in *h-p* method models for a given level of error in the energy norm (Rachowicz et al., 1989; Zienkiewicz et al., 1989).

3 MODEL DEVELOPMENT AND VALIDATION

Eulerian methods do not perform well when they model advective-dominated contaminant transport problems with sharp fronts. Sudden concentration changes produce artificial dispersion, phase lag, and up-gradient oscillations in both FD and FE solutions as shown for finite elements in Figure (3-1). The numerical methods described here attempt to eliminate these problems by using two techniques: adaptive methods and PG upwinding. Two finite element codes were developed: QPG uses quadratic basis functions, while LPG uses linear basis functions.

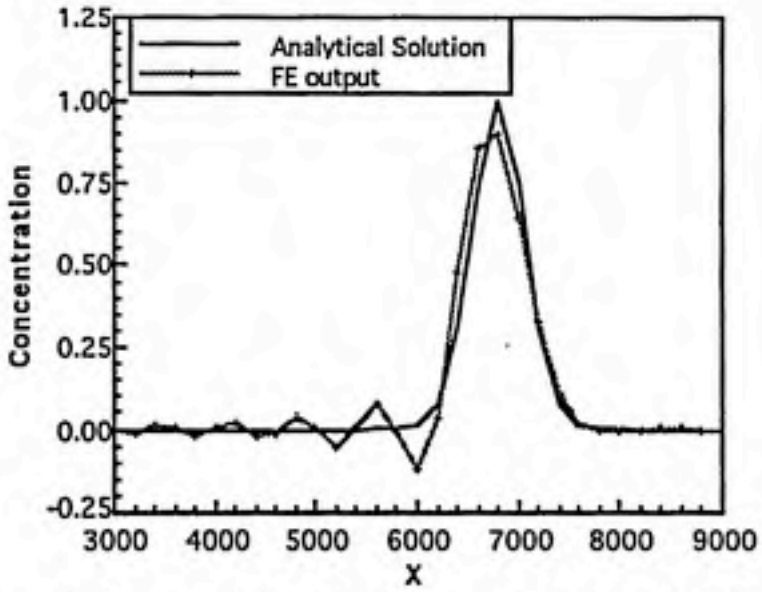

Fig. 3-1. Dispersion and oscillation in a finite element solution at Cr=0.24, Pe=∞, and 100 timesteps.

3.1 Finite Element Formulation

The development of PG FE transport models begins with the ADR equation in one dimension, presented in Equation (3-1), with concentration C, hydrodynamic dispersion coefficient D_h, advective velocity v_x, and first-order decay coefficient k_1. The spatial and

temporal dimensions are indicated by x and t, respectively. Linear local equilibrium (LLE) sorption can be easily included by dividing D_h, v_x, and k_1 by R_f, the retardation factor.

$$\frac{\partial C}{\partial t} = D_h \frac{\partial^2 C}{\partial x^2} - v_x \frac{\partial C}{\partial x} - k_1 C \tag{3-1}$$

The following weighted residual expression results from applying weighting functions W_i and integrating over the domain **D**, which extends from zero to x_L with n_n nodes:

$$\int_{\mathbf{D}} D_h \left[\frac{\partial W_i}{\partial x} \sum_{j=1}^{n_n} \frac{\partial N_j}{\partial x} C_j + W_i \left(v_x \sum_{j=1}^{n_n} \frac{\partial N_j}{\partial x} C_j + k_1 \sum_{j=1}^{n_n} N_j C_j + \sum_{j=1}^{n_n} N_j \frac{\partial C_j}{\partial t} \right) \right] dx$$

$$= D_h W_i \frac{\partial C}{\partial x}\Big|_0^{x_L} \qquad \text{for } i=1,\ldots,n_n \tag{3-2}$$

Zero-order continuous basis functions are used, so the derivative in the diffusive term is reduced from second- to first-order by Green's theorem. This is a valid operation if the spatial derivative of D_h is small in comparison to the spatial derivative of the concentration, which is generally true for this class of problems. A Dirichlet boundary is located at $x=0$, and a Neuman boundary makes $\partial C/\partial x = 0$ at $x=x_L$.

The temporal derivative in Equation (3-2) is then resolved with a Crank-Nicolson finite difference scheme, to yield:

$$\int_{\mathbf{D}} \left[D_h \frac{\partial W_I}{\partial x} \sum_{j=1}^{n_n} \frac{\partial N_j}{\partial x} \frac{C_j^{l+1} + C_j^l}{2} + W_I \left(v_x \sum_{j=1}^{n_n} \frac{\partial N_j}{\partial x} \frac{C_j^{l+1} + C_j^l}{2} + k_1 \sum_{j=1}^{n_n} N_j \frac{C_j^{l+1} + C_j^l}{2} + \sum_{j=1}^{n_n} N_j \frac{C_j^{l+1} - C_j^l}{\Delta t} \right) \right] dx = 0 \tag{3-3}$$

The superscripts l and $l+1$ indicate the known and unknown time levels, respectively, W_I is a shorthand notation that represents all n_n weighting functions, and Δt is the timestep length. Equation (3-3) can be rearranged and expressed in matrix notation as:

$$\left[[\mathbf{A_m}] + \tfrac{1}{2}([\mathbf{A_D}] + [\mathbf{A_v}] + [\mathbf{A_k}]) \right] \{C\}^{l+1} = \left[[\mathbf{A_m}] - \tfrac{1}{2}([\mathbf{A_D}] + [\mathbf{A_v}] + [\mathbf{A_k}]) \right] \{C\}^{l} \tag{3-4}$$

The coefficient matrices in Equation (3-4) correspond to mass $[\mathbf{A_m}]$, hydrodynamic

dispersion [A_D], advection [A_v], and first-order decay [A_k]. The sum of [A_D] and [A_v] is sometimes referred to as the stiffness matrix. These matrices are derived from the portions of Equation (3-3) that relate to each process, and will be described after the definition of the basis and weighting functions in the next section.

3.2 Basis and Weighting Functions

Finite element formulations use basis functions to interpolate the dependent variable, and weighting functions to minimize the difference between the exact and approximated solutions over each element. The traditional BG FE formulation uses identical basis and weighting functions, while PG upwinded FE formulations use different weighting and basis functions. The codes presented here use N+1 and N+2 degree upwinding - the weighting functions have components that are one and two polynomial orders higher than the basis functions.

The PG weighting functions used here are composed of the basis functions and modifying functions that furnish higher-order components. The modifying functions are multiplied by dimensionless parameters that control the contributions of the N+1 and N+2 degree portions of the upwinding functions. While PG upwinding has been demonstrated to produce excellent results when applied to sharp-front problems, relatively little information is available regarding the optimal values of the upwinding parameters α and β for transient ADR models involving sharp fronts.

Linear Lagrange polynomial basis functions ($N_i(\xi)$) may be expressed in terms of natural coordinates (ξ):

$$N_1(\xi) = \frac{1 - \xi}{2} \tag{3-5}$$

$$N_2(\xi) = \frac{1 + \xi}{2} \tag{3-6}$$

For N+1 and N+2 degree PG upwinding of linear elements, the weighting functions ($W_i(\xi)$) contain quadratic ($M_2(\xi)$) and cubic ($M_3(\xi)$) modifying functions in addition to the basis functions.

$$W_1(x) = N_1(\xi) - \alpha M_2(\xi) - \beta M_3(\xi) \tag{3-7}$$

$$W_2(x) = N_2(\xi) + \alpha M_2(\xi) + \beta M_3(\xi) \tag{3-8}$$

The dimensionless upwinding parameter α regulates the amount of N+1 degree upwinding, and β controls N+2 degree upwinding. Therefore, if α and β are set to zero, the model is

equivalent to the standard BG formulation. The following quadratic and cubic modifying functions used here were proposed by Dick (1983) and further studied by Westerink and Shea (1989).

$$M_2(\xi) = \frac{3}{4}(-\xi+1)(\xi+1) \tag{3-9}$$

$$M_3(\xi) = \frac{5}{8}\xi(\xi+1)(\xi-1) \tag{3-10}$$

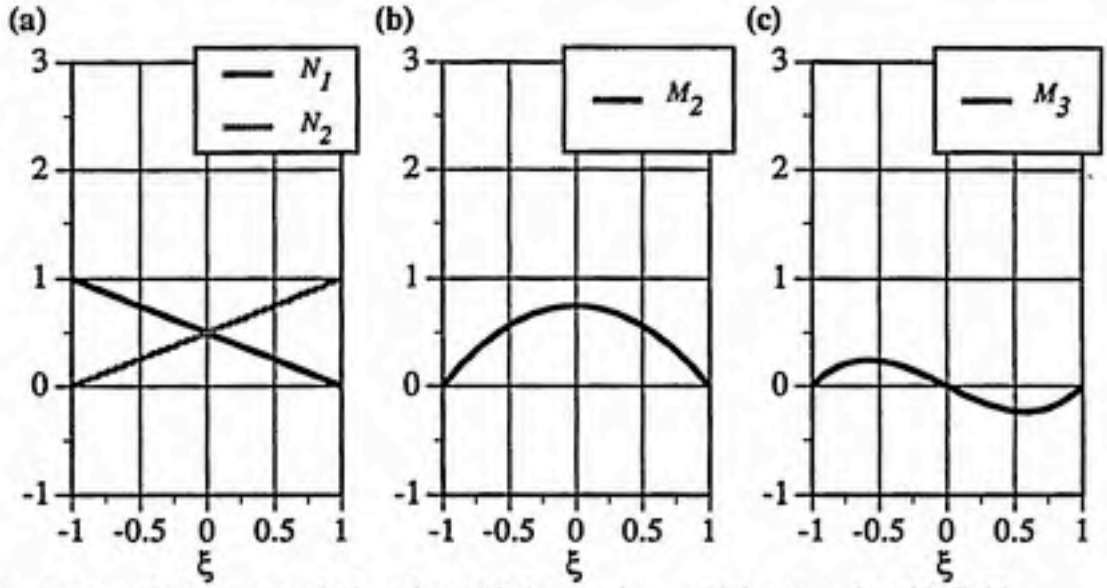

Fig. 3-2. (a) Linear basis functions (b) Quadratic modifying function (c) Cubic modifying function.

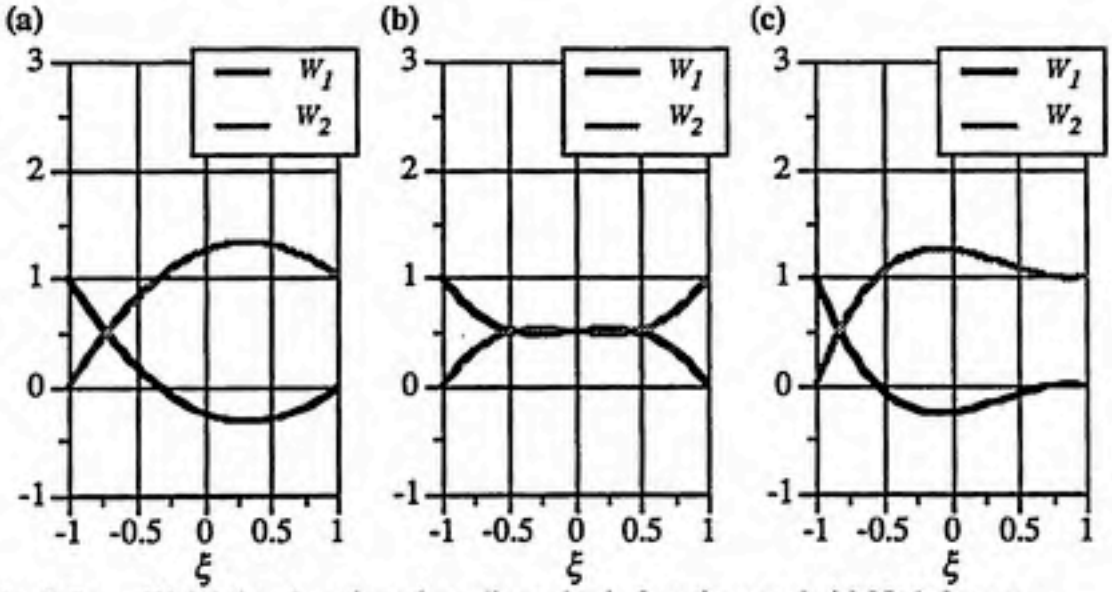

Fig. 3-3. Weighting functions from linear basis functions and: (a) N+1 degree upwinding: α=1, β=0 (b) N+2 degree upwinding: α=0, β=1 (c) N+1 and N+2 degree upwinding: α=1, β=1.

The linear basis functions presented in Equations (3-5) and (3-6) are graphed in Figure (3-2(a)) over the range of natural spatial coordinates that span one element. The quadratic modifying function from Equation (3-9) and the cubic modifying function from Equation (3-10) are also graphed in this figure. The resulting weighting functions for various levels of N+1 and N+2 degree upwinding are graphed in Figure (3-3).

Quadratic elements are composed of three quadratic Lagrange polynomial basis functions - two for the corner nodes at the ends of each element, and one for the mid-element node.

$$N_1(\xi) = \frac{\xi^2 - \xi}{2} \tag{3-11}$$

$$N_2(\xi) = -\xi^2 + 1 \tag{3-12}$$

$$N_3(\xi) = \frac{\xi^2 + \xi}{2} \tag{3-13}$$

Three weighting functions composed of basis functions and modifying functions are also required. For the upwinding formulation, cubic and quartic modifying functions are used, since second-order basis functions are being upwinded by one and two degrees respectively. Four upwinding parameters are used, α_c and β_c for corner nodes and α_m and β_m for mid-element nodes. As for the linear formulation, α_c and α_m affect N+1 upwinding, while β_c and β_m control N+2 upwinding.

$$W_1(\xi) = N_1(\xi) - \alpha_c M_3(\xi) - \beta_c M_4(\xi) \tag{3-14}$$

$$W_2(\xi) = N_2(\xi) + 4\,\alpha_m M_3(\xi) + 4\,\beta_m M_4(\xi) \tag{3-15}$$

$$W_3(\xi) = N_3(\xi) - \alpha_c M_3(\xi) - \beta_c M_4(x\xi) \tag{3-16}$$

In the above weighting functions, $M_3(\xi)$ is the cubic modifying function from Equation (3-10), and $M_4(\xi)$ is the quartic modifying function introduced by Westerink and Shea (1989).

$$M_4(\xi) = \frac{21}{16}\left(-\xi^4 + \xi^2\right) \tag{3-17}$$

The quadratic basis functions from Equations (3-11) (3-12) and (3-13) are graphed in Figure (3-4), as is the cubic modifying function from Equation (3-10), and the quartic modifying function from Equation (3-17). Weighting functions for various combinations of N+1 and N+2 degree upwinding are graphed in Figure (3-5).

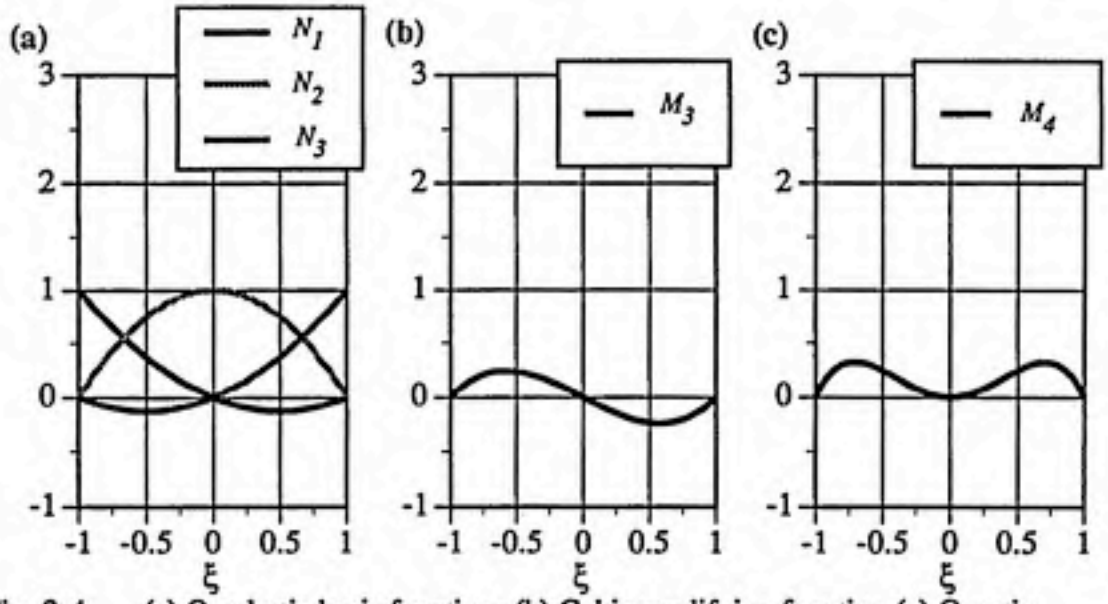

Fig. 3-4. (a) Quadratic basis functions (b) Cubic modifying function (c) Quartic modifying function.

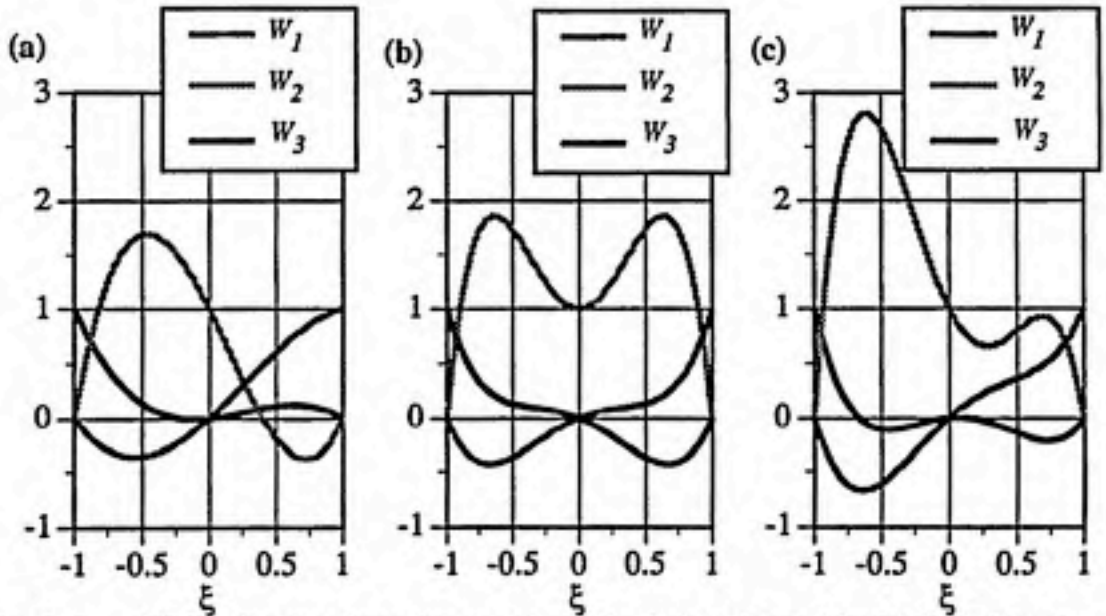

Fig. 3-5. Weighting functions from quadratic basis functions with: (a) N+1 degree upwinding: $\alpha_c=\alpha_m=1$, $\beta_c=\beta_m=0$, (b) N+2 degree upwinding: $\alpha_c=\alpha_m=0$, $\beta_c=\beta_m=1$ (c) N+1 and N+2 degree upwinding: $\alpha_c=\alpha_m=1$, $\beta_c=\beta_m=1$.

3.3 Coefficient matrices

Coefficient matrices are assembled from the basis and weighting functions by using the differential and integral expressions that appear in Equation (3-3). The coefficient matrices for linear elements can be derived by substituting Equations (3-5) through (3-10) into (3-3) to produce:

$$[A_m] = \frac{\Delta x}{\Delta t}\begin{bmatrix} \frac{1}{3} - \frac{\alpha}{4} - \frac{\beta}{24} & \frac{1}{6} - \frac{\alpha}{4} + \frac{\beta}{24} \\ \frac{1}{6} + \frac{\alpha}{4} + \frac{\beta}{24} & \frac{1}{3} + \frac{\alpha}{4} - \frac{\beta}{24} \end{bmatrix} \tag{3-18}$$

$$[A_k] = \Delta x\, k_1\begin{bmatrix} \frac{1}{3} - \frac{\alpha}{4} - \frac{\beta}{24} & \frac{1}{6} - \frac{\alpha}{4} + \frac{\beta}{24} \\ \frac{1}{6} + \frac{\alpha}{4} + \frac{\beta}{24} & \frac{1}{3} + \frac{\alpha}{4} - \frac{\beta}{24} \end{bmatrix} \tag{3-19}$$

$$[A_v] = \frac{v_x}{2}\begin{bmatrix} -1 + \alpha & 1 - \alpha \\ -1 - \alpha & 1 + \alpha \end{bmatrix} \tag{3-20}$$

$$[A_D] = \frac{D_h}{\Delta x}\begin{bmatrix} 1 & -1 \\ -1 & 1 \end{bmatrix} \tag{3-21}$$

The internodal spacing Δx should not be confused with element length. Quadratic elements contain an internal node, so Δx is one half of the element length. The coefficient matrices for quadratic elements in the following equations arise from substituting equations (3-10) through (3-17) into (3-3).

$$[A_m] = \frac{\Delta x}{\Delta t}\begin{bmatrix} \frac{4}{15} - \frac{\alpha_c}{12} - \frac{3\beta_c}{40} & \frac{2}{15} - \frac{\beta_c}{5} & -\frac{1}{15} + \frac{\alpha_c}{12} - \frac{3\beta_c}{40} \\ \frac{2}{15} + \frac{\alpha_m}{3} + \frac{3\beta_m}{10} & \frac{16}{15} + \frac{4\beta_m}{5} & \frac{2}{15} - \frac{\alpha_m}{3} + \frac{3\beta_m}{10} \\ -\frac{1}{15} - \frac{\alpha_c}{12} - \frac{3\beta_c}{40} & \frac{2}{15} - \frac{\beta_c}{5} & \frac{4}{15} + \frac{\alpha_c}{12} - \frac{3\beta_c}{40} \end{bmatrix} \tag{3-22}$$

$$[A_k] = k_1\Delta x\begin{bmatrix} \frac{4}{15} - \frac{\alpha_c}{12} - \frac{3\beta_c}{40} & \frac{2}{15} - \frac{\beta_c}{5} & -\frac{1}{15} + \frac{\alpha_c}{12} - \frac{3\beta_c}{40} \\ \frac{2}{15} + \frac{\alpha_m}{3} + \frac{3\beta_m}{10} & \frac{16}{15} + \frac{4\beta_m}{5} & \frac{2}{15} - \frac{\alpha_m}{3} + \frac{3\beta_m}{10} \\ -\frac{1}{15} - \frac{\alpha_c}{12} - \frac{3\beta_c}{40} & \frac{2}{15} - \frac{\beta_c}{5} & \frac{4}{15} + \frac{\alpha_c}{12} - \frac{3\beta_c}{40} \end{bmatrix} \tag{3-23}$$

$$[A_V] = 2v_x \begin{bmatrix} -\frac{1}{4} + \frac{\alpha_c}{12} + \frac{7\beta_c}{80} & \frac{1}{3} - \frac{\alpha_c}{6} & -\frac{1}{12} + \frac{\alpha_c}{12} - \frac{7\beta_c}{80} \\ -\frac{1}{3} - \frac{\alpha_m}{3} - \frac{7\beta_m}{20} & \frac{2\alpha_m}{3} & \frac{1}{3} - \frac{\alpha_m}{3} + \frac{7\beta_m}{20} \\ \frac{1}{12} + \frac{\alpha_c}{12} + \frac{7\beta_c}{80} & -\frac{1}{3} - \frac{\alpha_c}{6} & \frac{1}{4} + \frac{\alpha_c}{12} - \frac{7\beta_c}{80} \end{bmatrix} \quad (3\text{-}24)$$

$$[A_D] = \frac{2D_h}{\Delta x} \begin{bmatrix} \frac{7}{12} + \frac{7\beta_c}{40} & -\frac{2}{3} - \frac{7\beta_c}{20} & \frac{1}{12} + \frac{7\beta_c}{40} \\ -\frac{2}{3} - \frac{7\beta_m}{10} & \frac{4}{3} + \frac{7\beta_m}{5} & -\frac{2}{3} - \frac{7\beta_m}{10} \\ \frac{1}{12} + \frac{7\beta_c}{40} & -\frac{2}{3} - \frac{7\beta_c}{20} & \frac{7}{12} + \frac{7\beta_c}{40} \end{bmatrix} \quad (3\text{-}25)$$

3.4 Adaptive Method

The adaptive method used in this work is derived from a 1-D *h*-method proposed by G.T. Yeh (1988). The advantage in this approach lies in that the additional nodes produced by mesh refinement are placed in matrices that are isolated from the unrefined global matrix. This results in code that is less complex than what would result from renumbering and reassembling the global matrices, as fewer operations are required, and less computer memory is needed. Soon after its introduction, this method was extended to 2-D in the form of an Eulerian-Lagrangian hybrid in which advection is modeled with the Lagrangian single-step reverse particle tracking method, and the other processes in the problem are handled with an Eulerian (FE) method (Yeh, 1990).

In the 1-D method, spatial elements are uniformly subdivided into smaller subelements for the solution at the next timepoint if a sharp front is detected within the element at the current solution level. Other elements may also be subdivided, depending on user-definable parameters that allow mesh refinement to be projected along the advective path, permitting refinement of elements that are expected to contain the front at the next solution level. The degree of refinement is also user-defined. The LPG code can subdivide elements by any positive number, while QPG is restricted to even positive numbers of subelements by constraints imposed by the adaptive algorithm.

Global matrices contain rows that represent concentrations at nodes from the initial unrefined mesh. Nodes from the subdivided elements are represented by separate matrices that are manipulated in a way that allows the contribution of subdivision on the global matrices to be determined. Once this contribution is determined, the global matrices are

adjusted and solved. This method results in solutions that are exactly the same as if all nodes had been represented by a single matrix.

The Yeh method starts with the node numbering scheme shown in Figure (3-6). In this example, the element bounded by global nodes three and four is refined into eight subelements. Matrix row numbers correspond to node numbers, so this arrangement allows an optimal global numbering pattern throughout the modeled timespan, as the global numbering will not change during element refinement. Renumbering global matrices to accommodate additional nodes is straightforward in the 1-D example shown here, but renumbering nodes so as to generate easily solved matrices is a formidable problem in higher dimensions. Even optimally configured matrices for 2-D and 3-D problems may be very sparse and have large bandwidths. These characteristics tend to bog down matrix solution procedures and require a great deal of computer memory. Inserting nodes into an optimal global matrix requires careful consideration of the numbering scheme so as to increase matrix bandwidth and sparseness as little as possible. The Yeh method addresses this issue by assigning individual matrices to each refined element, thus reducing bandwidth effects and sparseness that arise from refinement.

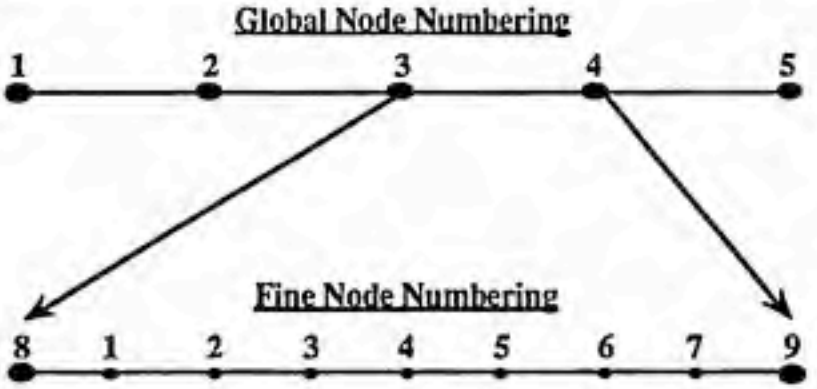

Fig. 3-6. Node numbering used for unrefined global elements and a refined element.

This refined element numbering scheme results in refined element matrices of the form shown in Figure (3-7). A pair of matrices are created that correspond to the left-hand-side (LHS) and the right-hand-side (RHS) of equation (3-4). The populated entries are indicated with diagonal hatching, and the rows that correspond to nodes that appear in global matrices are located at the bottom of the matrices and are framed with a heavy border. As the solution proceeds, concentration values at the current time level are obtained from the refined element matrices if the element was refined at the last time level, or by basis function interpolation if it was not.

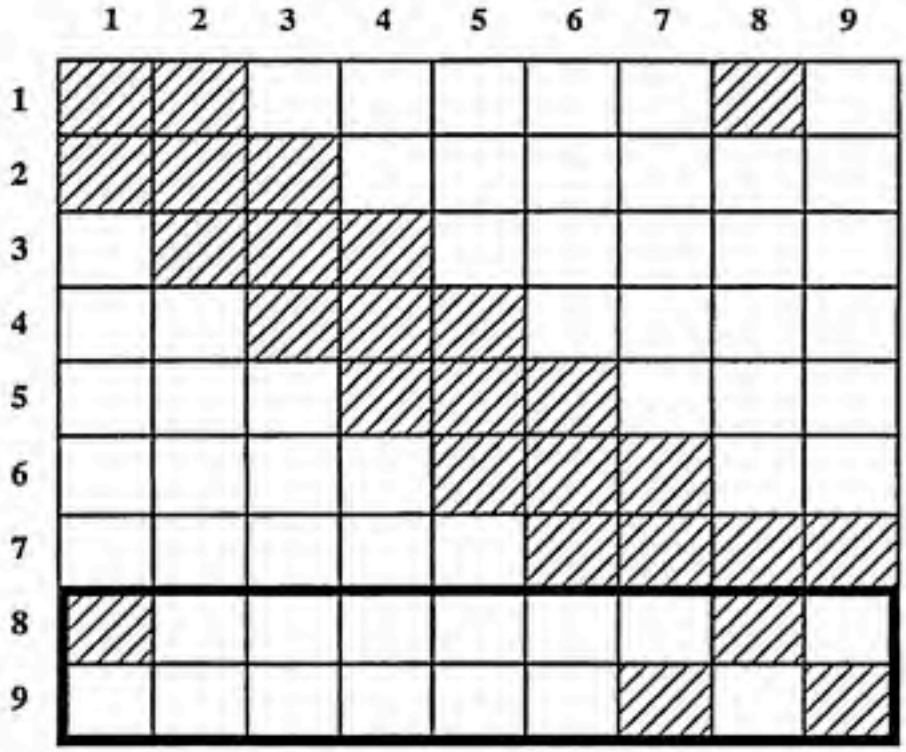

Fig. 3-7. Refined element submatrix composed with numbering from Figure (3-6).

In Figure (3-8a), the refined element matrices have been reduced by Gauss elimination, which has the effect of expressing the global node rows solely as a function of information from global nodes. Fine node rows eight and nine contain entries only in columns eight and nine, which are also indicated with a heavy border. These entries may now be assembled into the global matrix in Figure (3-8b), since they correspond to global nodes three and four. This results in entries for the rows in the global matrices that are identical to those that would be present if the fine nodes had been incorporated in the global matrices. The global matrices may then be manipulated in the customary fashion to derive the solution vector at the global nodes at the next time level.

3.5 Validation

All models were validated by comparison with analytical solutions (Bear, 1979) and independently derived finite element solutions. Solutions involving mesh refinement were compared at various discretizations with output from finite element codes that did not use the adaptive method, but did use identical discretization patterns as those used by the adapted models. Upwinded solutions were compared to published results (Westerink and Shea, 1989).

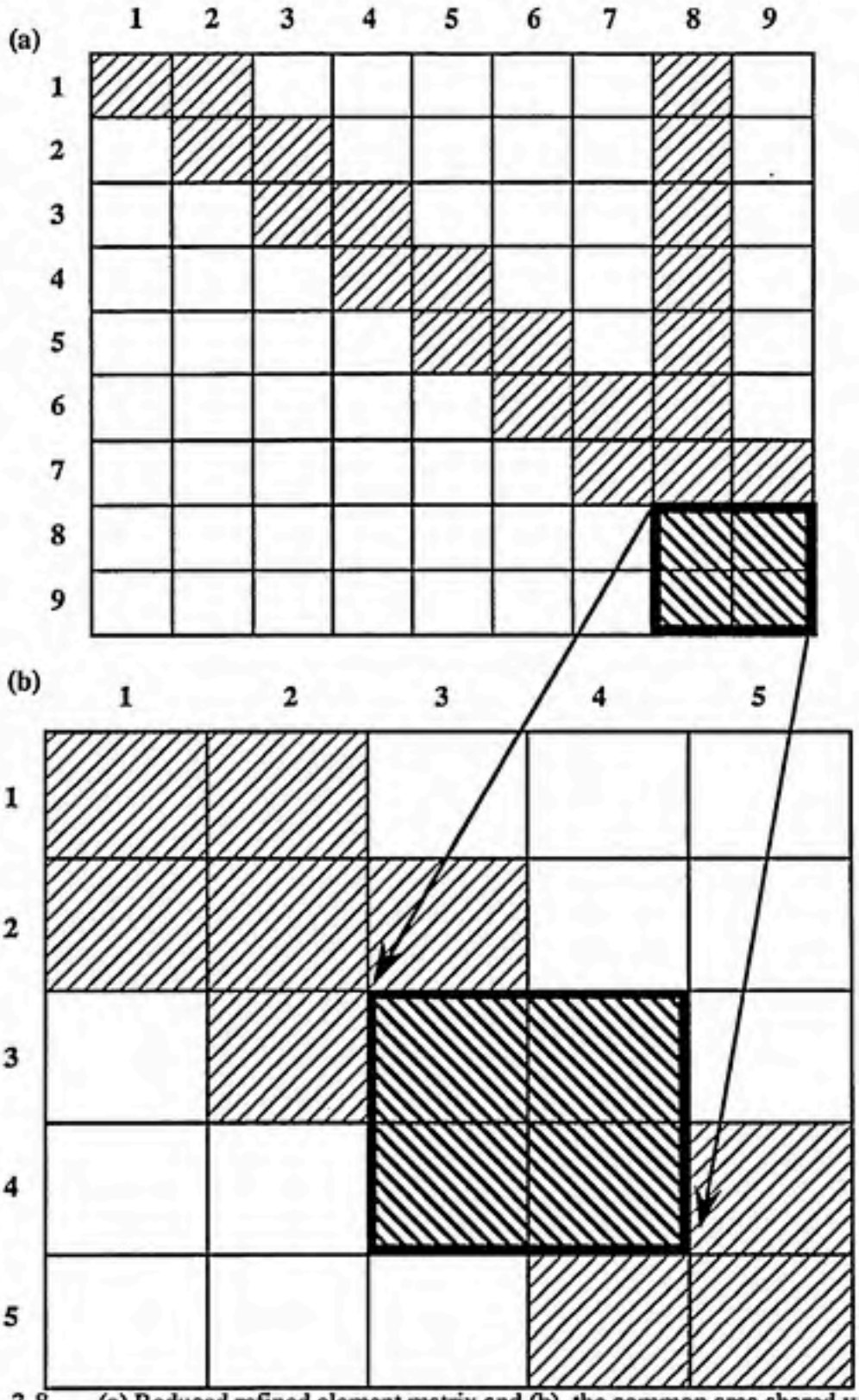

Fig. 3-8. (a) Reduced refined element matrix and (b), the common area shared with the global matrix.

3.6 Features

All reactive processes in these models are linear in nature, so direct solution methods were applied to the finite element matrices. Gauss elimination was enhanced with an upper/lower decomposition technique in order to make the solution process more efficient (Pinder and Gray, 1977; Cornew and Miller, 1990). This method factors LHS matrices outside of the timestepping loop. The elimination factors are stored, and are then used to solve for concentration with RHS matrices within the timestepping loop. As long as the matrices are not altered, this method places many redundant operations outside of the timestepping loop.

A final enhancement to the adaptive algorithm was the implementation of a system that only refactors the global matrix entries that require it. Upper/lower decomposition requires that the matrices be refactored if they are altered in any way. This refactoring is only required for the rows that represent the nodes that bound the refined element as well as all higher numbered rows. Refactoring is not needed for rows with lower index numbers than the refined area, and was therefore not performed.

The complementary error function subroutine used for step source analytical solutions is based on a Chebyshev fit to an "inspired guess" of the functional form of the error function (Press et al., 1989).

3.7 Computing Environment

Program development and execution was performed on Apple Macintosh computers (Plus and IIfx models). Execution times are from the 7.8 MHz MC 68000 based Macintosh Plus. All programs were written and compiled with the 1978 ANSI implementation of the FORTRAN language (Absoft, Inc. Rochester Hills, MI), and the *Mathematica* interpreted computing language for symbolic mathematics (v. 2.03, Wolfram Research, Champaign, IN)

4 MATHEMATICAL ANALYSIS AND RESULTS

Results! Why, man, I have gotten a lot of results. I know several thousand things that won't work. - Thomas A. Edison

4.1 Adaptive Method Results

The adaptive method is demonstrated using the analytical step source shown in Figure (4-1), which is an ideal step that has been aged by 20 time steps with the parameters presented in Table (4-1).

Parameter	Value
Cr	0.1000
Dh	0.0125
kl	0.0
Pe	200
Rf	1.0
v_x	0.5
Δt	1.0
Δx	5.0

Table 4-1. Default parameters for adapted models.

The concentration profile shown in Figure (4-2) is generated when the source is modeled with a fixed FE mesh of 40 elements over 230 timesteps. The defects in the solution are remedied by the adaptive method as shown in Figure (4-3). In this case, elements were refined into eight subelements when the change in concentration across an element exceeded 0.005. Refining the elements to this extent decreases the Pe but increases the Cr by a factor of eight in the adapted area. This changes the Cr from 0.1 to 0.8, and the Pe from 200 to 25. The Pe is greater than two in this case, but the numerical solution is

accurate due to the predispersion of the step source, so that it does not contain an infinite gradient or singularity at the start of the numerical solution.

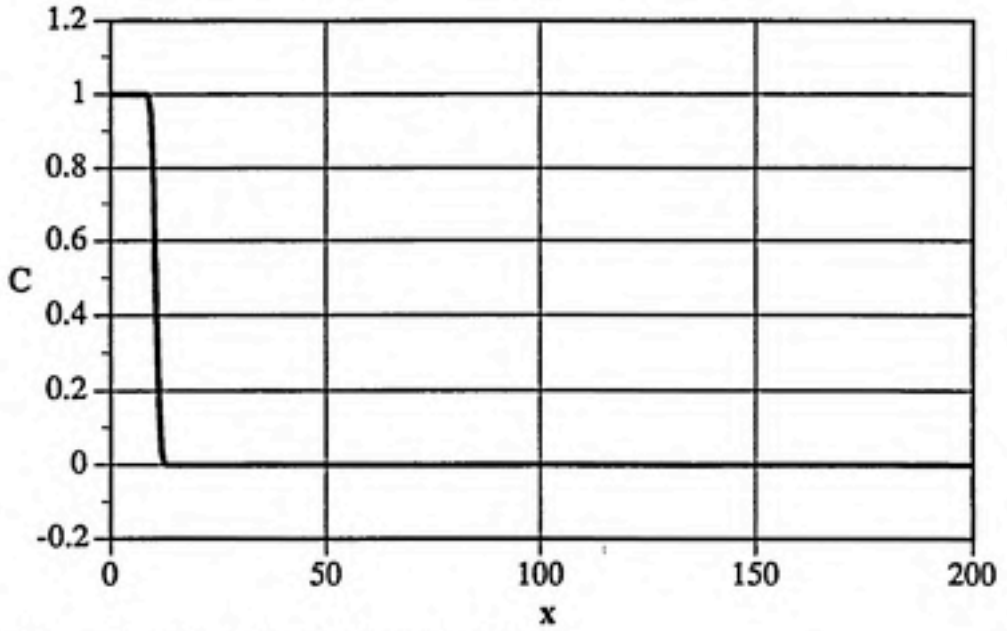

Fig. 4-1. Step source for adaptive examples.

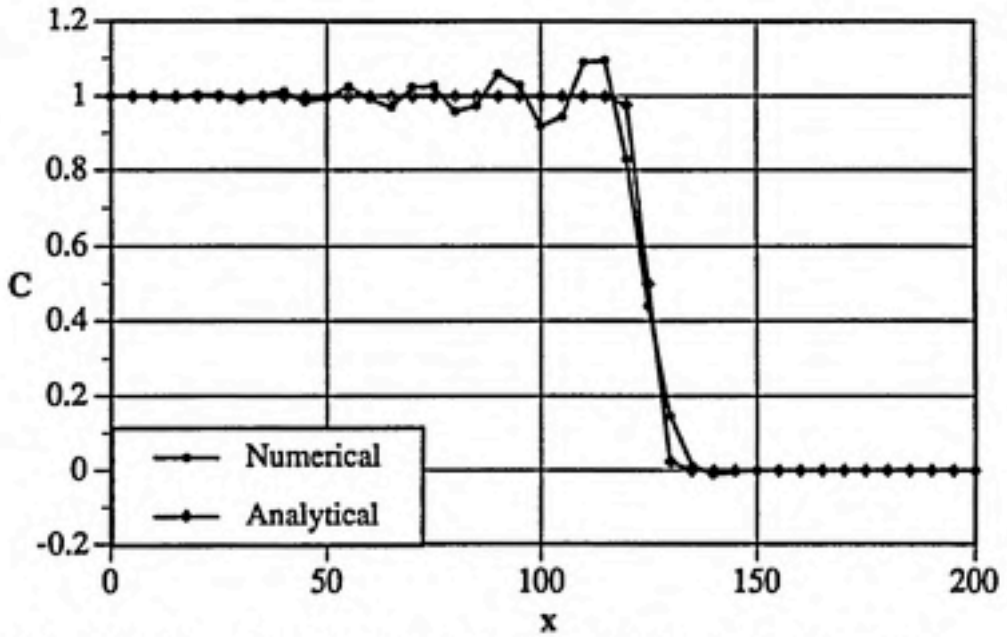

Fig. 4-2. Step source modeled with linear elements at Cr=0.1 and Pe =200.

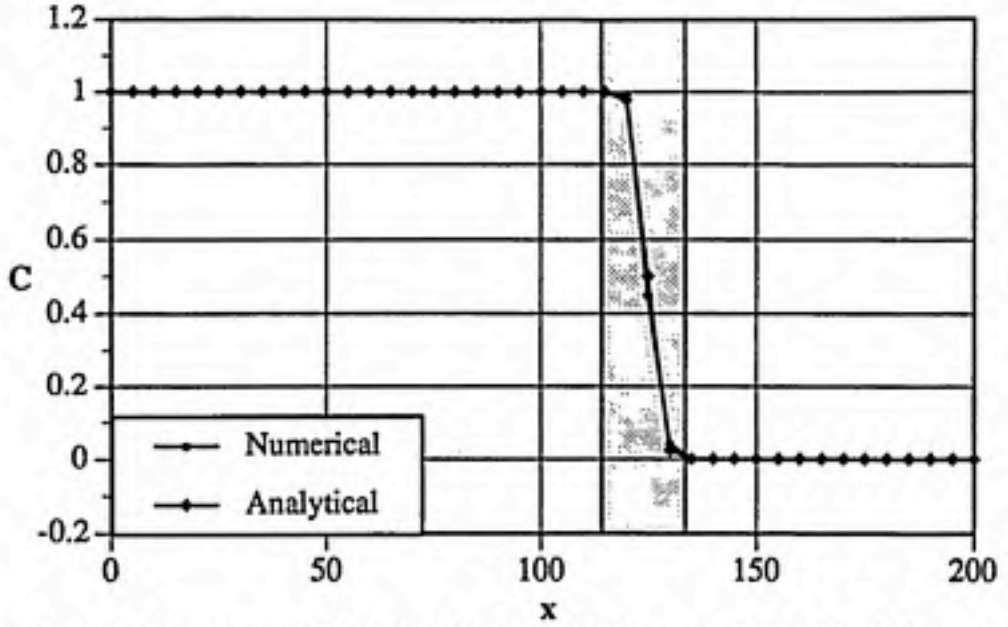

Fig. 4-3. Step source modeled with adapted linear elements. The refined elements indicated with shading have Cr=0.8 and Pe=25, while the unrefined elements have Cr=0.1 and Pe=200.

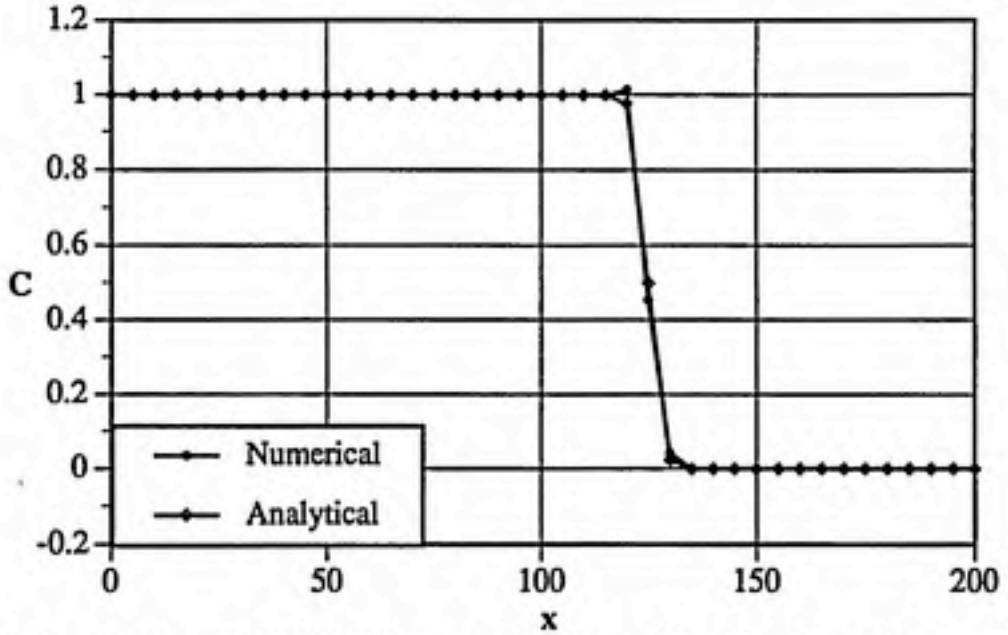

Fig. 4-4. Step source modeled with linear elements at Cr=0.8 and Pe =25.

The unrefined model required 216 seconds to execute, while the adapted results were obtained in 273 seconds, an increase of only about 26%. Changing the global discretization to be equivalent to the refined area produces the solution profile shown in Figure (4-4). This solution took 1621 seconds to evaluate, or 493% longer than the adaptive method which

produced similar excellent results, and 650% longer than the unrefined model. For clarity, only every eighth node is plotted in Figure (4-4). Timing results for this section are collected in Table (4-2)

The unrefined solution from quadratic elements shown in Figure (4-5) is an improvement over its counterpart for linear elements in Figure (4-2), but it still suffers from the same flaws. The unadapted quadratic solution was produced in 269 seconds, and the adapted solution in Figure (4-6) took 412 seconds, or 53% longer to execute. The quadratic adapted solution was produced in the same way as the linear case, by refinement by a factor of eight. Note that in this case, the adapted solutions are of similar quality and the refined quadratic solution took 51% longer than its linear counterpart. Execution of the unrefined quadratic solution took 24% longer than the unrefined linear solution.

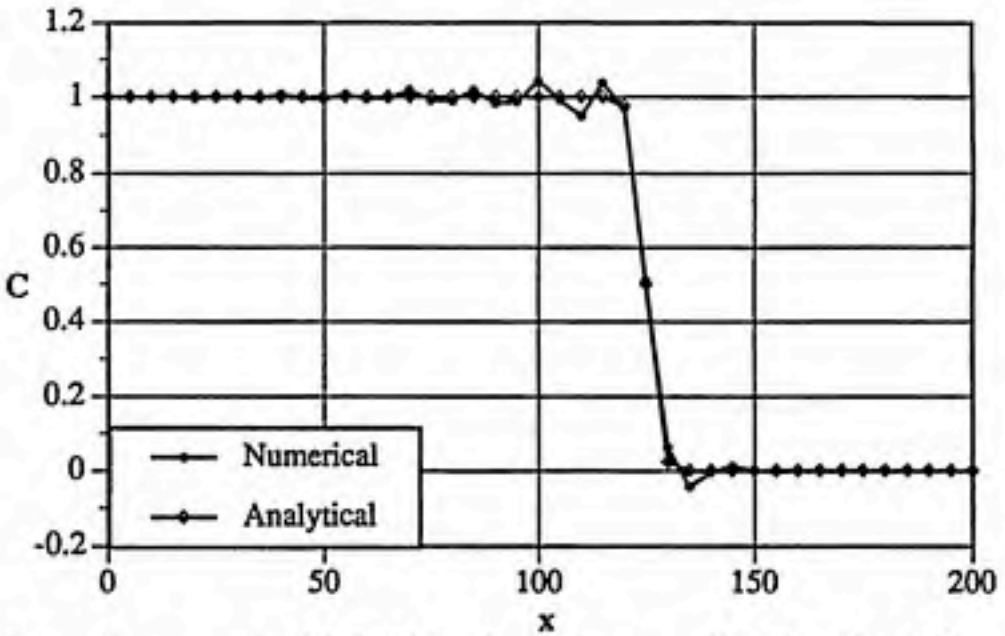

Fig. 4-5. Step source modeled with quadratic elements at Cr=0.1 and Pe =200.

Finally, in Figure (4-7), the solution performed with global parameters set to those of the refined case required 2022 seconds to execute, or about 390% longer to run than the 412 seconds required by the equivalent adapted solution. While these timing figures are impressive, it is important to note that factors such as domain length, model time and adaptive sensitivity affect the relative efficiency of the solutions.

Model	Configuration	Seconds
Linear	Unrefined	216
	Adapted	273
	Refined	1621
Quadratic	Unrefined	269
	Adapted	412
	Refined	2022

Table 4-2. Execution times for adapted models.

Quadratic elements were expected to provide better solutions than linear ones, but the additional computational expense was not expected to be so high. Note that the quadratic solutions all had longer execution times than their linear counterparts, despite using half as many elements. Both solutions used identical node spacing, so they both used the same number of nodes. The larger bandwidth of the quadratic matrices must therefore be responsible for the increased execution times. The linear adapted method not only produced a better solution than the unadapted quadratic model, but did so in roughly the same amount of time: 273 sec. for the linear adapted method and 269 sec. for the unadapted quadratic solution.

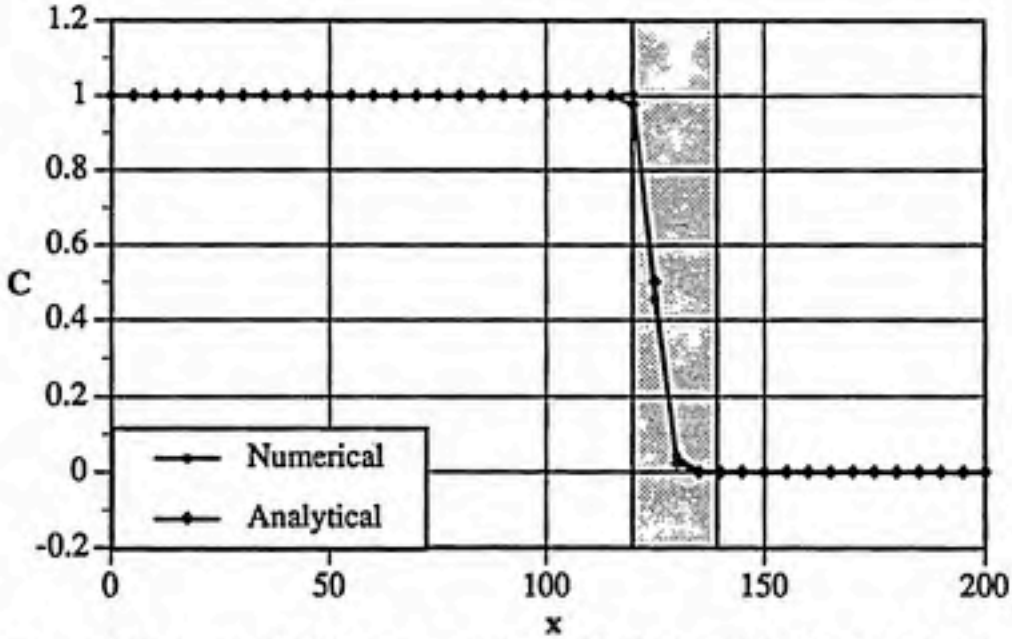

Fig. 4-6. Step source modeled with adapted quadratic elements. The refined elements indicated with shading have Cr=0.8 and Pe=25, while Cr=0.1 and Pe=200 for unrefined elements.

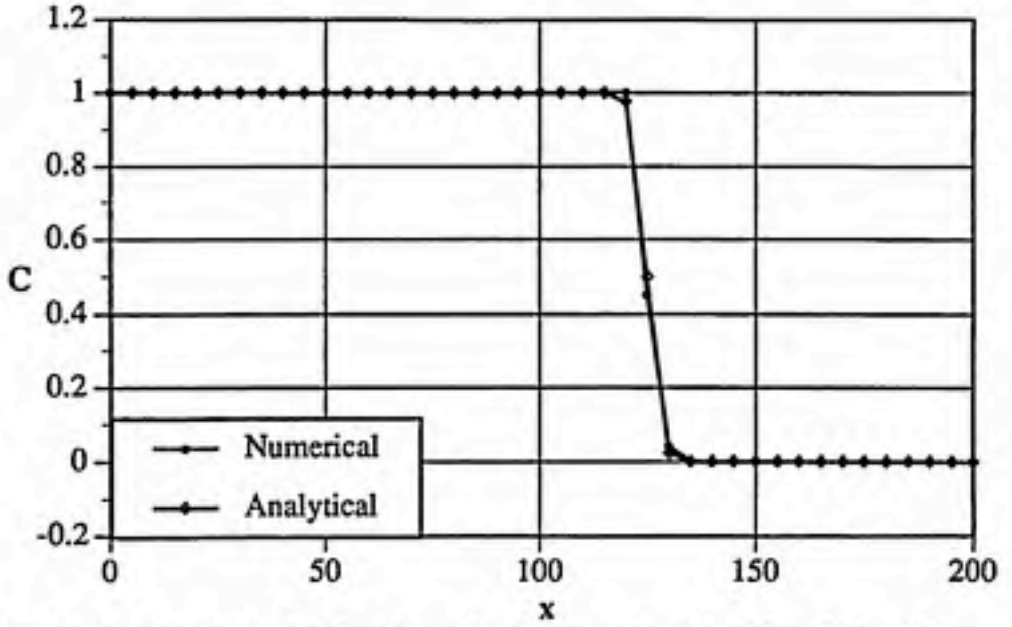

Fig. 4-7. Step source modeled with quadratic elements at Cr=0.8 and Pe =25.

The above examples demonstrate that element refinement improves the quality of the solutions. The small inaccuracies observed in the step source examples at Pe=25 may be acceptable for some applications, but the larger errors at Pe=200 are not. The *h*-method removes these inaccuracies by shortening elements, which reduces the value of the Pe, but only to a point, as element length reduction also has the effect of increasing the Cr, which reintroduces error.

The Gaussian source defined in Equation (4-1) is a common test problem for numerical transport models. Its standard deviation σ_x, dimensionless standard deviation $\overline{\sigma_x}$, and peak location μ are defined in Equations (4-2), (4-3), and (4-4), respectively.

$$C_x^t = \frac{1}{\sigma_x\sqrt{2\pi}} exp\left(\frac{-(x-\mu)^2}{2\,\sigma_x^2} - k_1 t\right) \tag{4-1}$$

$$\sigma_x = \sqrt{2D_h t} \tag{4-2}$$

$$\overline{\sigma_x} = \sigma_x/\Delta x \tag{4-3}$$

$$\mu = v_x t \tag{4-4}$$

Linear FE models of Gaussian source with $\overline{\sigma_x}$ =1.32 at t=0 appear in Figures (4-8) and (4-9). The peak amplitude of the sources was normalized to unity. Model conditions are identical to the step source solutions, save for a shift in the starting point of the source in order to separate the peak from either boundary by at least five standard deviations.

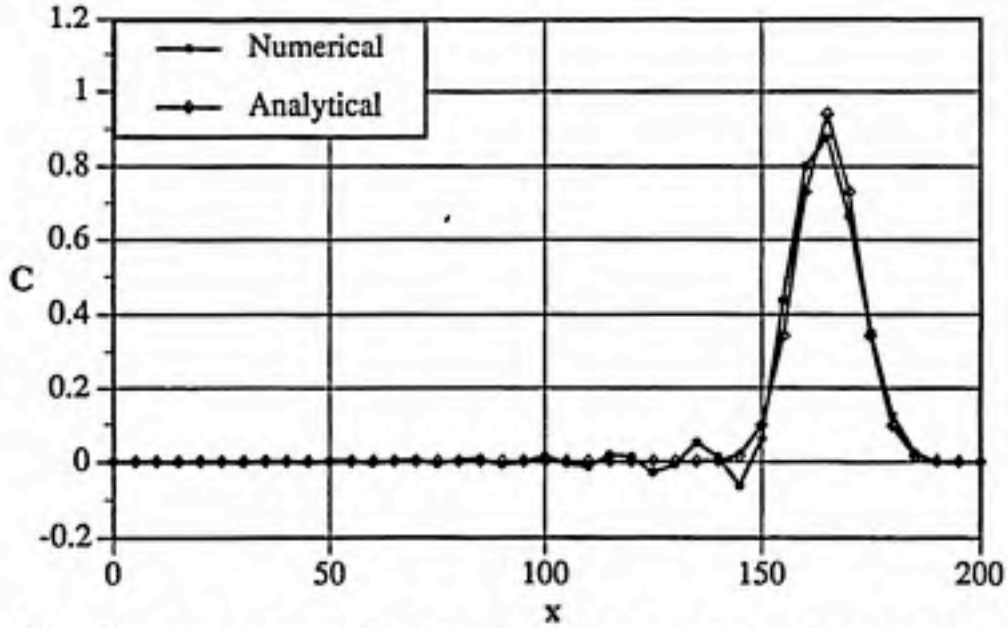

Fig. 4-8. Gaussian source modeled with linear elements at Cr=0.1 and Pe=200.

Gaussian sources were also well modeled by the adaptive method, as shown in Figure (4-9) which uses the same model configuration for step sources used to model the step source shown in Figure (4-3). Results from a model with global refinement equivalent to the adapted region of Figure (4-9) are shown in Figure (4-10). As in figures (4-4) and (4-7), only every eighth node is plotted for Figure (4-10).

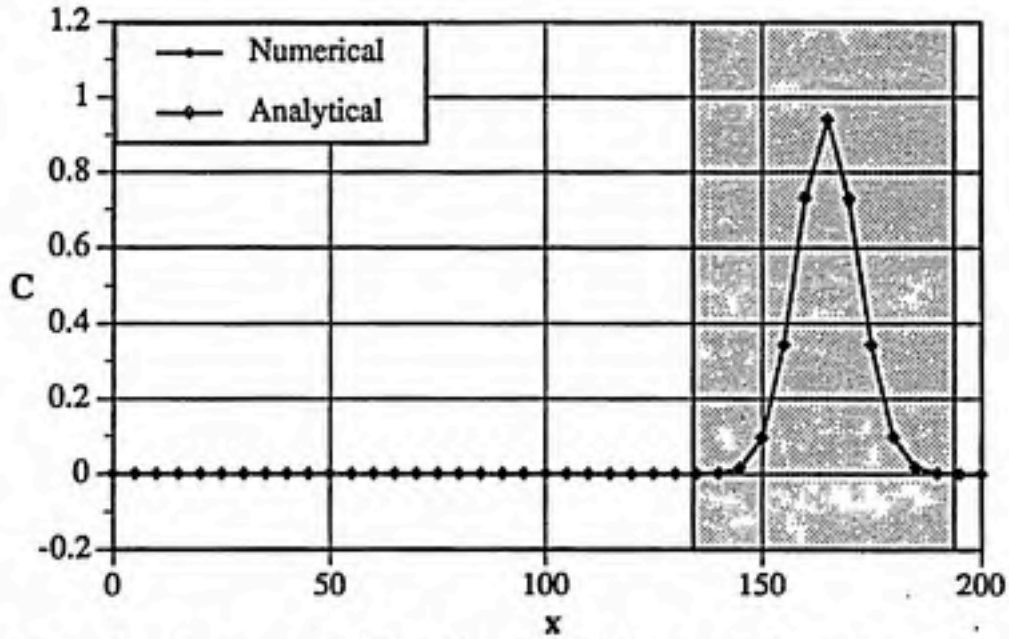

Fig. 4-9. Gaussian source at $\overline{\sigma_x}$ =1.32 modeled with adapted linear elements. The refined elements indicated with shading have Cr=0.8 and Pe=25, while Cr=0.1 and Pe=200 for unrefined elements.

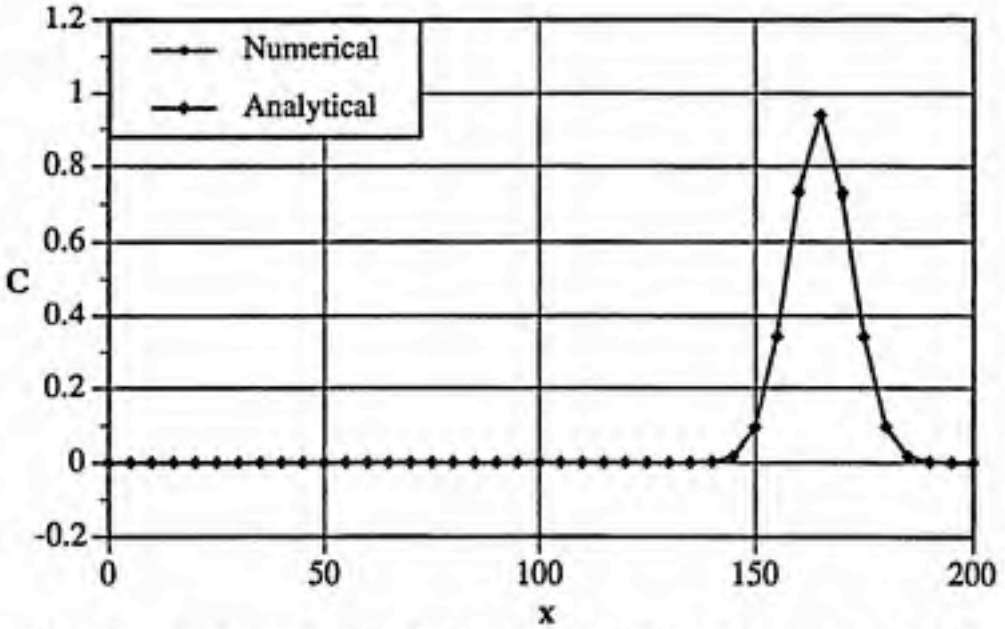

Fig. 4-10. Gaussian source at $\overline{\sigma_x}$ =1.32 modeled with linear elements at Cr=0.8 and Pe=25.

In this case, the quality of the solution was very sensitive to the magnitude of the adaptive criterion. Increasing the criterion magnitude resulted in severe peak depression of the concentration profile. This is probably due to the lack of adapted elements in the peak zone of the profile when the peak lies between nodes. This results in deceptively small differences in the concentrations at the nodes that saddle the peak, and a concomitant lack of refined elements. Lower values of the criterion resulted in the good results presented in Figure (4-9), but also increased the number of adapted elements and execution time. The quality of step source solutions was not observed to be as sensitive to the magnitude of the adaptive criterion.

The adaptive method performed as anticipated for 1-D problems. Matrix manipulations were entirely transparent, and adaptive solutions were identical to FE solutions performed on fixed grids with identical discretization patterns. Adapted models provided nearly identical solutions to fixed grid models in significantly less time than the fixed grid models required when their global element length was set to the refined element length used in the adapted models.

A final comment on this method relates to extending it to higher dimensions. As mentioned before, Yeh has applied his method to 2-D problems in the context of an Eulerian-Lagrangian model (Yeh, 1990). This model employs Eulerian methods to model

the dispersive and other nonadvective components of the ADR equation. The specific means by which the adapted method was applied to this portion of the model were not published, so the following observations are the result of a fully Eulerian 2-D implementation performed by C.T. Miller and E. Nelson in the spring of 1990.

An attractive feature of the Yeh method is its clean isolation of the refined elements from the global matrices. As mentioned in the introduction, 2-D and 3-D problems have floating nodes on the interfaces between refined and nonrefined regions. These nodes require concentration values and must conform to appropriate boundary conditions. A "poorly posed problem" results when a domain is encircled with first type or Dirichlet boundaries. This situation arises when all of the floating node values are fixed, so second type or Neuman boundaries must be used on some of the interfacial boundaries. This condition requires an iterative solution process to make concentration values on the Neuman boundaries agree between refined and nonrefined areas, since a Neuman boundary fixes the first spatial partial derivative of C, but not the value of C.

The isolation provided by the adaptive method breaks down at this point, as the solution is no longer identical to what would be produced by a method that incorporated the refined elements into the global matrices. The concise simplicity demonstrated for 1-D models is lost in higher dimension applications of the method. The interfaces between refined elements compound this problem, since each refined element is an independent subdomain. The problems mentioned above for interfacing between refined and unrefined elements are still in effect, and individual refined elements cannot be formed into a single refined region.

This may be the motivation for using this method in the context of an Eulerian-Lagrangian approach. The dispersive components only have to be modeled in the vicinity of sharp fronts, so the Eulerian grids would be much smaller in this case than for a full Eulerian model where they must extend over the entire spatial domain. The need to renumber the global matrices is still eliminated, but the complexity introduced by higher dimensional implementations reduces the attractiveness of the method.

4.2 Petrov Galerkin Upwinding Analysis and Results

The effectiveness of PG upwinding and its dependence on optimal upwinding parameters are shown in Figures (4-11), (4-12) and (4-13). The Gaussian sources and modeling conditions presented in these figures are described in Table (4-3).

Parameter	Value
Cr	0.24
D_h	0.0
$k1$	0.0
Pe	∞
Rf	1.0
starting point	3000
v_x	0.5
x_L	22000
α	0.0
β	0.0
Δt	96
Δx	200
σ_x	264
$\bar{\sigma}_x$	1.32

Table 4-3. Default parameters for models of Gaussian sources.

In Figure (4-11a), the nonupwinded BG solution on the left contains significant oscillations, phase error and peak depression. The N+1 degree solution in Figure (4-11b) attenuates the oscillations and phase error, but the peak is also damped. In Figure (4-12a), N+2 upwinding also attenuates some of the inaccuracies in the nonupwinded solution, as does the combined N+1 and N+2 degree solution in Figure (4-12b).

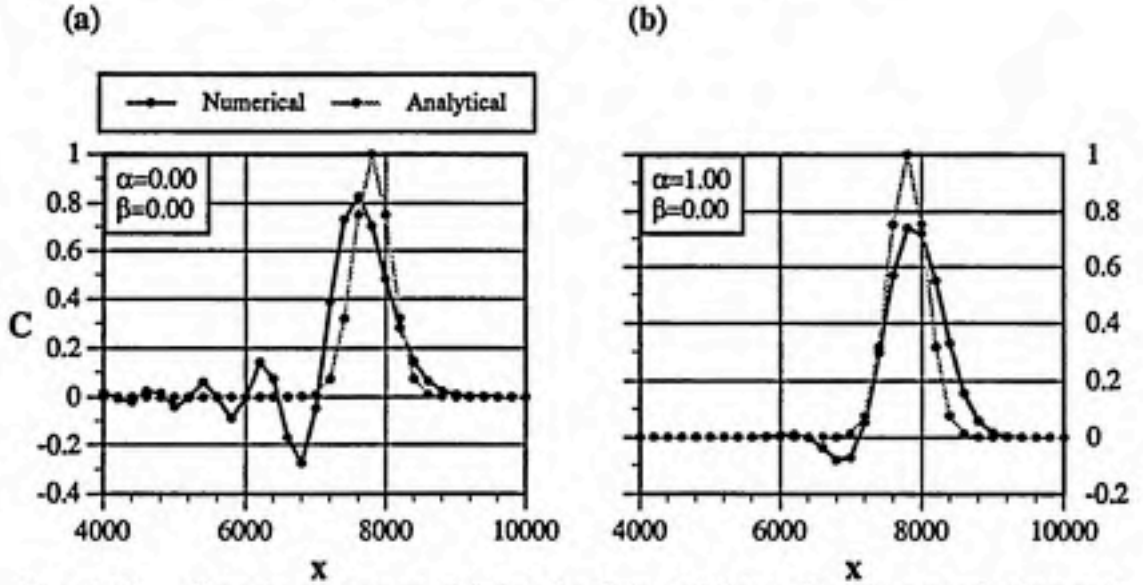

Fig. 4-11. Gaussian source modeled at Cr=0.24 and Pe=∞ for (a) no upwinding and (b) N+1 degree upwinding.

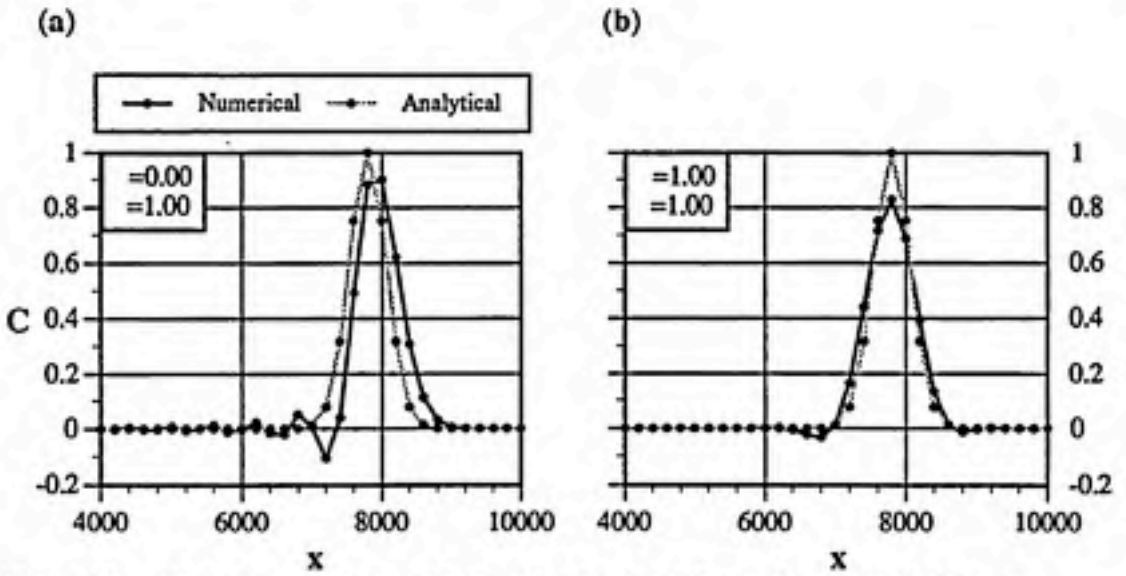

Fig. 4-12. Gaussian source modeled at Cr=0.24 and Pe=∞ for (a) N+2 degree upwinding and (b) simultaneous N+1 and N+2 degree upwinding.

Up to this point, the values of α and β have been set to zero or unity, but when optimal upwinding parameters are used, better solutions are possible, as shown in Figure (4-13). Different values of α and β may improve or degrade model output relative to the nonupwinded solution, so the ability of this method to produce near perfect solutions at infinite Pe is balanced by the possibility of solutions that are worse than those from nonupwinded models.

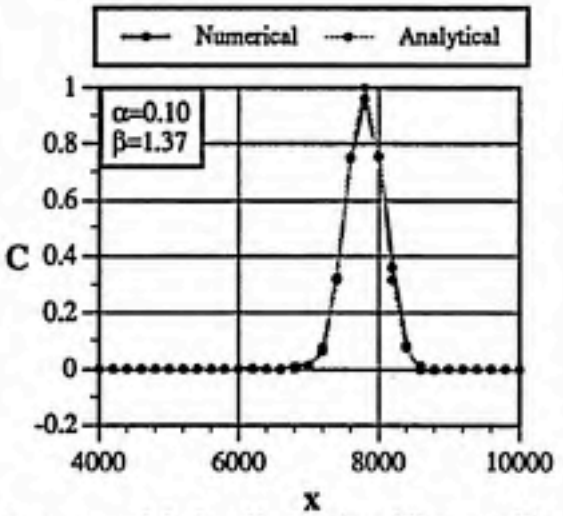

Fig. 4-13. Gaussian source modeled at Cr=0.24 and Pe=∞ with optimal N+1 and N+2 degree upwinding parameters.

In the following sections, Taylor series and Fourier analyses as well as numerical experimentation are performed with the goal of describing optimal upwinding parameters for N+1 and N+2 degree upwinded linear and quadratic elements.

4.2.1 Taylor Series Analysis

The motivation behind this Taylor series analysis was to represent the truncation error in a form that would be amenable to computerized optimization. The intent was to find upwinding parameters that minimized this error at specific values of mesh Courant ($Cr=v_x\Delta t/\Delta x$), Péclet ($Pe=v_x\Delta x/D_h$), and Damköhler numbers ($Da=k_1\Delta x/v_x$), and then describe the upwinding parameters as a function of these dimensionless problem variables. The functional relationship between the dimensionless variables and the observed optimal upwinding parameters could then be approximated with curve fitting techniques.

The truncation error can be described as a function of problem-specific variables and the upwinding parameters by Taylor series analysis. The series expansion of the nodal concentration specified by $C_{x+\Delta x}^{t+\Delta t}$ about C_x^t is defined as:

$$C_{x+\Delta x}^{t+\Delta t} = \sum_{i=0}^{\infty} \sum_{j=0}^{i} \frac{\Delta x^{i-j}\,\Delta t^{j}}{(i-j)!\,j!} \frac{\partial^i C_x^t}{\partial x^{(i-j)}\partial t^j} \tag{4-5}$$

where the superscripts of C indicate time level, and the subscripts reflect the spatial location.

Concentrations at time level $t+\Delta t$ will contain temporal partial derivatives in their series expansions about a concentration at time level t. These temporal partial derivatives may be expressed entirely in terms of spatial partial derivatives by using the ADR equation (Equation (3-1)). For instance, differentiation of the ADR equation with respect to time results in:

$$\frac{\partial^2 C}{\partial t^2} = D_h \frac{\partial^3 C}{\partial x^2 \partial t} - v_x \frac{\partial^2 C}{\partial x \partial t} - k_1 \frac{\partial C}{\partial t} \tag{4-6}$$

The temporal partial derivatives on the right hand side may then be substituted with higher-order spatial derivatives of the ADR equation, yielding an expression for the second temporal derivative that does not involve temporal partial derivatives:

$$\frac{\partial^2 C}{\partial t^2} = D_h^2 \frac{\partial^4 C}{\partial x^4} - 2D_h v_x \frac{\partial^3 C}{\partial x^3} + (v_x^2 - 2D_h k_1)\frac{\partial^2 C}{\partial x^2} + 2k_1 v_x \frac{\partial C}{\partial x} + k_1^2 C \qquad (4\text{-}7)$$

Further differentiation and substitution can be used to eliminate all temporal partial derivatives in the Taylor series.

For linear basis functions, the coordinate matrices described in Equations (3-18) through (3-21) are assembled and multiplied by the concentration vectors as described in Equation (3-4). After some rearranging, a difference equation for $C_x^{t+\Delta t}$, the concentration at the spatial solution point x and time level $t+\Delta t$, can be derived, as shown in Equation (4-8).

$$\begin{aligned}
&\left[C_{x-\Delta x}^{t}\left(\frac{-1}{6\Delta t} - \frac{\alpha}{4\Delta t} - \frac{\beta}{24\Delta t} - \frac{D_h}{2\Delta x^2} - \frac{v_x}{4\Delta x} - \frac{\alpha v_x}{4\Delta x} + \frac{k_1}{12} + \frac{\alpha k_1}{8} + \frac{\beta k_1}{48}\right) + \right. \\
&\quad C_x^{t}\left(\frac{-2}{3\Delta t} + \frac{\beta}{12\Delta t} + \frac{D_h}{\Delta x^2} + \frac{\alpha v_x}{2\Delta x} - \frac{k_1}{3} - \frac{\beta k_1}{24}\right) + \\
&C_{x+\Delta x}^{t}\left(\frac{-1}{6\Delta t} + \frac{\alpha}{4\Delta t} - \frac{\beta}{24\Delta t} - \frac{D_h}{2\Delta x^2} + \frac{v_x}{4\Delta x} - \frac{\alpha v_x}{4\Delta x} + \frac{k_1}{12} - \frac{\alpha k_1}{8} + \frac{\beta k_1}{48}\right) + \\
&C_{x-\Delta x}^{t+\Delta t}\left(\frac{1}{6\Delta t} + \frac{\alpha}{4\Delta t} + \frac{\beta}{24\Delta t} - \frac{D_h}{2\Delta x^2} - \frac{v_x}{4\Delta x} - \frac{\alpha v_x}{4\Delta x} + \frac{k_1}{12} + \frac{\alpha k_1}{8} + \frac{\beta k_1}{48}\right) + \\
&\left. C_{x+\Delta x}^{t+\Delta t}\left(\frac{1}{6\Delta t} - \frac{\alpha}{4\Delta t} + \frac{\beta}{24\Delta t} - \frac{D_h}{2\Delta x^2} + \frac{v_x}{4\Delta x} - \frac{\alpha v_x}{4\Delta x} + \frac{k_1}{12} - \frac{\alpha k_1}{8} + \frac{\beta k_1}{48}\right)\right] \\
&\qquad \left(\frac{2}{3\Delta t} - \frac{\beta}{12\Delta t} - \frac{D_h}{\Delta x^2} + \frac{\alpha v_x}{2\Delta x} + \frac{k_1}{3} - \frac{\beta k_1}{24}\right)^{-1} = C_x^{t+\Delta t}
\end{aligned} \qquad (4\text{-}8)$$

$$
\begin{aligned}
\Bigg[\, C^{t}_{x-\Delta x}\left(\frac{-2}{15\Delta t}-\frac{\alpha_m}{3\Delta t}-\frac{3\beta_m}{10\Delta t}-\frac{2D_h}{3\Delta x^2}-\frac{7\beta_m D_h}{10\Delta x^2}-\frac{v_x}{3\Delta x}+\right.\\
\left.\frac{\alpha_m v_x}{3\Delta x}-\frac{7\beta_m v_x}{20\Delta x}+\frac{k_1}{15}+\frac{\alpha_m k_1}{6}+\frac{3\beta_m k_1}{20}\right)+\\
C^{t}_{x}\left(\frac{-16}{15\Delta t}-\frac{4\beta_m}{5\Delta t}+\frac{4D_h}{3\Delta x^2}+\frac{7\beta_m D_h}{5\Delta x^2}-\frac{2\alpha_m v_x}{3\Delta x}+\frac{8k_1}{15}+\frac{2\beta_m k_1}{5}\right)+\\
C^{t}_{x+\Delta x}\left(\frac{2}{15\Delta t}+\frac{\alpha_m}{3\Delta t}-\frac{3\beta_m}{10\Delta t}-\frac{2D_h}{3\Delta x^2}-\frac{7\beta_m D_h}{10\Delta x^2}+\frac{v_x}{3\Delta x}-\right.\\
\left.\frac{\alpha_m v_x}{3\Delta x}+\frac{7\beta_m v_x}{20\Delta x}+\frac{k_1}{15}-\frac{\alpha_m k_1}{6}+\frac{3\beta_m k_1}{20}\right)+\\
C^{t+\Delta t}_{x-\Delta x}\left(\frac{2}{15\Delta t}+\frac{\alpha_m}{3\Delta t}+\frac{3\beta_m}{10\Delta t}-\frac{2D_h}{3\Delta x^2}-\frac{7\beta_m D_h}{10\Delta x^2}-\frac{v_x}{3\Delta x}-\right.\\
\left.\frac{\alpha_m v_x}{3\Delta x}-\frac{7\beta_m v_x}{20\Delta x}+\frac{k_1}{15}+\frac{\alpha_m k_1}{6}+\frac{3\beta_m k_1}{20}\right)+\\
C^{t+\Delta t}_{x+\Delta x}\left(\frac{2}{15\Delta t}-\frac{\alpha_m}{3\Delta t}+\frac{3\beta_m}{10\Delta t}-\frac{2D_h}{3\Delta x^2}-\frac{7\beta_m D_h}{10\Delta x^2}+\frac{v_x}{3\Delta x}+\right.\\
\left.\left.\frac{\alpha_m v_x}{3\Delta x}+\frac{7\beta_m v_x}{20\Delta x}+\frac{k_1}{15}-\frac{\alpha_m k_1}{6}+\frac{3\beta_m k_1}{20}\right)\right]\\
\left(\frac{16}{15\Delta t}+\frac{4\beta_m}{5\Delta t}+\frac{4D_h}{3\Delta x^2}+\frac{7\beta_m D_h}{5\Delta x^2}+\frac{2\alpha_m v_x}{3\Delta x}+\frac{8k_1}{15}+\frac{2\beta_m k_1}{5}\right)^{-1}=C^{t+\Delta t}_{x}
\end{aligned}
\tag{4-9}
$$

The coordinate matrices from Equations (3-22) to (3-25) are assembled in the same way to produce similar expressions for quadratic elements for the mid-element nodes as shown in Equation (4-9) as well as for the corner nodes as shown in Equation (4-10). These equations are solved at each node in the system of equations described in the FE matrices, and the difference between the solutions they provide and the exact solution is the truncation error.

Taylor series expansions about C^{t}_{x} are then taken as described in Equation (4-5) in order to describe the truncation error at $C^{t+\Delta t}_{x}$. These expansions are then substituted for the concentrations at the various temporal and spatial locations that appear in Equations (4-8) through (4-10). Once these expansions have been inserted, the temporal partial derivatives are converted to spatial dimensions in the manner described in Equations (4-6) and (4-7). The truncation error T is then expressed in Equation (4-11) as the difference between the known concentration at the next time level ($C^{t+\Delta t}_{x}$) and an infinite sum of products of spatial partial derivatives and coefficients.

$$\left[C^{t}_{x-2\Delta x}\left(\frac{1}{15\Delta t}+\frac{\alpha_c}{12\Delta t}+\frac{3\beta_c}{40\Delta t}+\frac{D_h}{12\Delta x^2}+\frac{7\beta_c D_h}{40\Delta x^2}+\frac{v_x}{12\Delta x}+\right.\right.$$

$$\left.\frac{\alpha_c v_x}{12\Delta x}+\frac{7\beta_c v_x}{80\Delta x}-\frac{k_1}{30}-\frac{\alpha_c k_1}{24}-\frac{3\beta_c k_1}{80}\right)+$$

$$C^{t}_{x-\Delta x}\left(\frac{-2}{15\Delta t}+\frac{\beta_c}{5\Delta t}-\frac{2D_h}{3\Delta x^2}-\frac{7\beta_c D_h}{20\Delta x^2}-\frac{v_x}{3\Delta x}-\frac{\alpha_c v_x}{6\Delta x}+\frac{k_1}{15}-\frac{\beta_c k_1}{10}\right)+$$

$$C^{t}_{x}\left(\frac{-8}{15\Delta t}+\frac{3\beta_c}{20\Delta t}+\frac{7D_h}{6\Delta x^2}+\frac{7\beta_c D_h}{20\Delta x^2}-\frac{\alpha_c v_x}{6\Delta x}-\frac{4k_1}{15}-\frac{3\beta_c k_1}{40}\right)+$$

$$C^{t}_{x+\Delta x}\left(\frac{-2}{15\Delta t}+\frac{\beta_c}{5\Delta t}-\frac{2D_h}{3\Delta x^2}-\frac{7\beta_c D_h}{20\Delta x^2}+\frac{v_x}{3\Delta x}-\frac{\alpha_c v_x}{6\Delta x}+\frac{k_1}{15}-\frac{\beta_c k_1}{10}\right)+$$

$$C^{t}_{x+2\Delta x}\left(\frac{1}{15\Delta t}-\frac{\alpha_c}{12\Delta t}+\frac{3\beta_c}{40\Delta t}+\frac{D_h}{12\Delta x^2}+\frac{7\beta_c D_h}{40\Delta x^2}-\frac{v_x}{12\Delta x}+\right.$$

$$\left.\frac{\alpha_c v_x}{12\Delta x}-\frac{7\beta_c v_x}{80\Delta x}-\frac{k_1}{30}+\frac{\alpha_c k_1}{24}-\frac{3\beta_c k_1}{80}\right)+ \qquad (4\text{-}10)$$

$$C^{t+\Delta t}_{x-2\Delta x}\left(\frac{-1}{15\Delta t}-\frac{\alpha_c}{12\Delta t}-\frac{3\beta_c}{40\Delta t}+\frac{D_h}{12\Delta x^2}+\frac{7\beta_c D_h}{40\Delta x^2}+\frac{v_x}{12\Delta x}+\right.$$

$$\left.\frac{\alpha_c v_x}{12\Delta x}+\frac{7\beta_c v_x}{80\Delta x}-\frac{k_1}{30}-\frac{\alpha_c k_1}{24}-\frac{3\beta_c k_1}{80}\right)+$$

$$C^{t+\Delta t}_{x-\Delta x}\left(\frac{2}{15\Delta t}-\frac{\beta_c}{5\Delta t}-\frac{2D_h}{3\Delta x^2}-\frac{7\beta_c D_h}{20\Delta x^2}-\frac{v_x}{3\Delta x}-\frac{\alpha_c v_x}{6\Delta x}+\frac{k_1}{15}-\frac{\beta_c k_1}{10}\right)+$$

$$C^{t+\Delta t}_{x+\Delta x}\left(\frac{2}{15\Delta t}-\frac{\beta_c}{5\Delta t}-\frac{2D_h}{3\Delta x^2}-\frac{7\beta_c D_h}{20\Delta x^2}+\frac{v_x}{3\Delta x}-\frac{\alpha_c v_x}{6\Delta x}+\frac{k_1}{15}-\frac{\beta_c k_1}{10}\right)+$$

$$C^{t+\Delta t}_{x+2\Delta x}\left(\frac{-1}{15\Delta t}+\frac{\alpha_c}{12\Delta t}-\frac{3\beta_c}{40\Delta t}+\frac{D_h}{12\Delta x^2}+\frac{7\beta_c D_h}{40\Delta x^2}-\frac{v_x}{12\Delta x}+\right.$$

$$\left.\left.\frac{\alpha_c v_x}{12\Delta x}-\frac{7\beta_c v_x}{80\Delta x}-\frac{k_1}{30}+\frac{\alpha_c k_1}{24}-\frac{3\beta_c k_1}{80}\right)\right]$$

$$\left(\frac{8}{15\Delta t}-\frac{3\beta_c}{20\Delta t}+\frac{7D_h}{6\Delta x^2}+\frac{7\beta_c D_h}{20\Delta x^2}+\frac{\alpha_c v_x}{6\Delta x}+\frac{4k_1}{15}-\frac{3\beta_c k_1}{40}\right)^{-1}=C^{t+\Delta t}_{x}$$

$$T = C_x^{t+\Delta t} - \left(F_0 C_x^t + F_1 \frac{\partial C_x^t}{\partial x} + F_2 \frac{\partial^2 C_x^t}{\partial x^2} + F_3 \frac{\partial^3 C_x^t}{\partial x^3} + F_4 \frac{\partial^4 C_x^t}{\partial x^4} + F_5 \frac{\partial^5 C_x^t}{\partial x^5} + F_6 \frac{\partial^6 C_x^t}{\partial x^6} + F_7 \frac{\partial^7 C_x^t}{\partial x^7} + F_8 \frac{\partial^8 C_x^t}{\partial x^8} + F_9 \frac{\partial^9 C_x^t}{\partial x^9} + F_{10} \frac{\partial^{10} C_x^t}{\partial x^{10}} + \ldots + F_{\infty} \frac{\partial^{\infty} C_x^t}{\partial x^{\infty}}\right) \quad (4\text{-}11)$$

In this equation, the F_i variables represent unique coefficients that correspond to *ith*-order partial derivatives. The parenthesized summation of coefficient and partial derivative products in Equation (4-11) is an analytical approximation of the FE model solution, and its accuracy improves as the extent of the series is increased. Coefficients up to fifth-order were derived manually and validated with expressions published by Westerink and Shea (1989).

Past work (Lantz, 1971; Yu and Heinrich, 1986; Westerink and Shea, 1989) has sought to minimize the truncation error by minimizing individual coefficients with greater priority placed on those that correspond to fifth and lower-order derivatives. This is not unreasonable, as the magnitudes of lower-order derivatives are not only much larger than higher-order derivatives, but the magnitude of these partial derivatives falls off rapidly with increased differential order.

The products of these derivatives and their coefficients are not easily evaluated, since the algebraic expressions that describe them become very large with increased differential order. This problem was overcome through the use of Mathematica. This program's ability to perform operations from algebra and calculus on large symbolic expressions allowed the exploration of the Taylor series to far higher orders than has been done in the past.

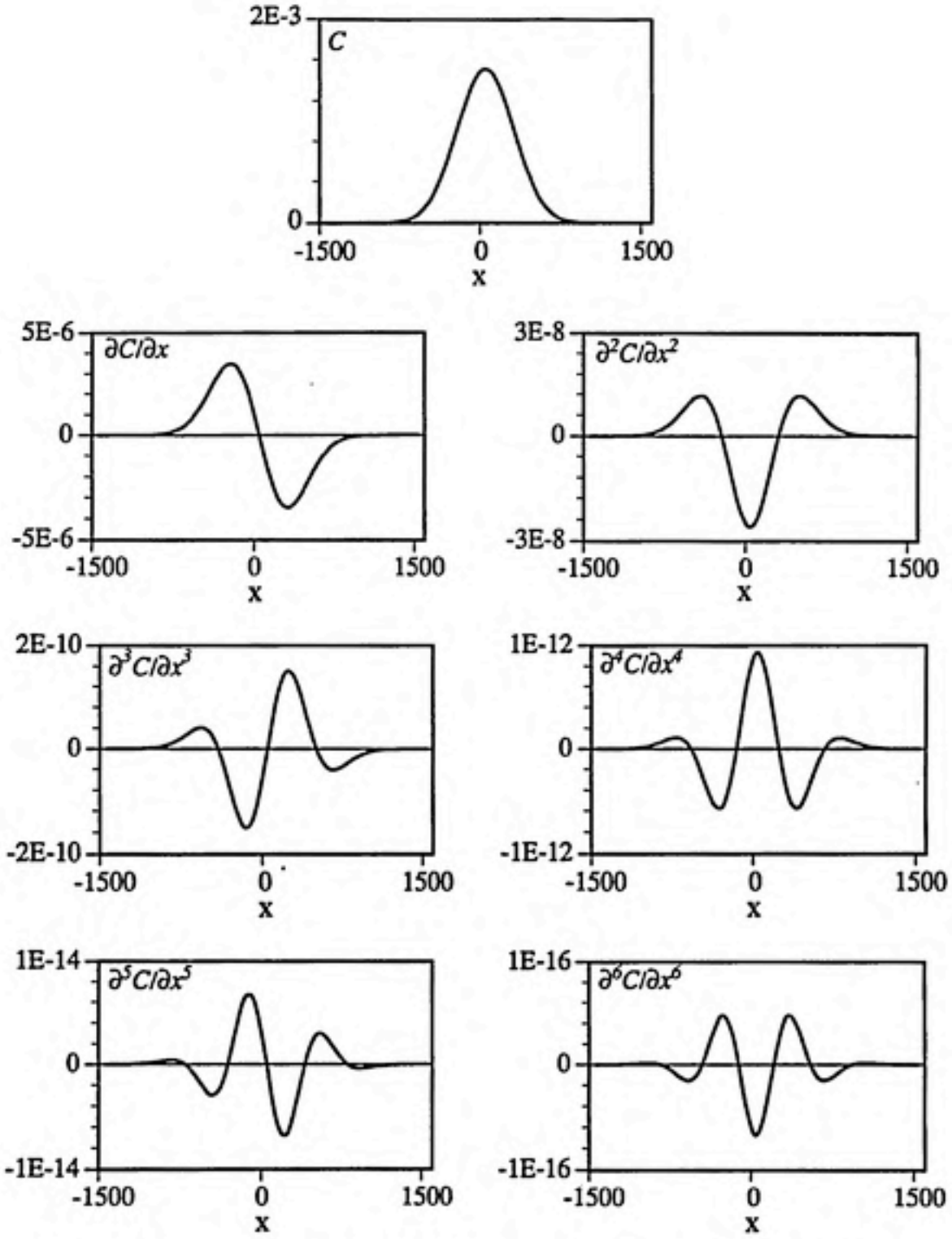

Fig. 4-14. Gaussian source with σ_x =264 (top), and its spatial partial derivatives ranging from first to sixth-order.

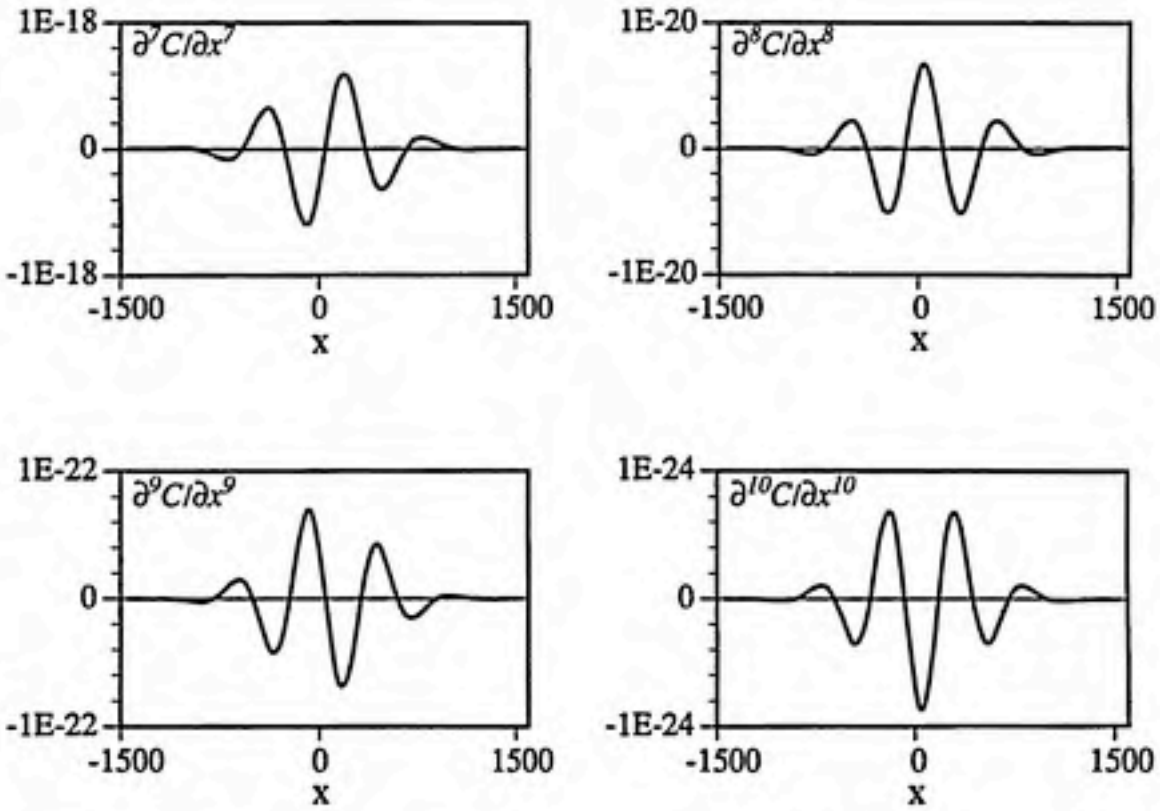

Fig. 4-15. Seventh- through tenth-order partial derivatives of a Gaussian source with σ_x =264.

Figures (4-14 and 4-15) demonstrate this decrease of magnitude with increasing differential order. Since the peak magnitudes of these derivatives drops by about two orders of magnitude for every unit increase in differential order, it should be safe to neglect terms of sixth-order and greater, as was done previously.

This assumption proved to be incorrect. The relative importance of the different order terms for this problem is shown in Figure (4-16). The third-order term is clearly dominant in this case, but the fifth-order term is also important. Other terms provide greater contributions than would be expected from the magnitudes of their corresponding partial derivatives. Based on the definition of T in Equation (4-11), the only possible explanation is that the F_i are large enough to offset the small values of the partial derivatives.

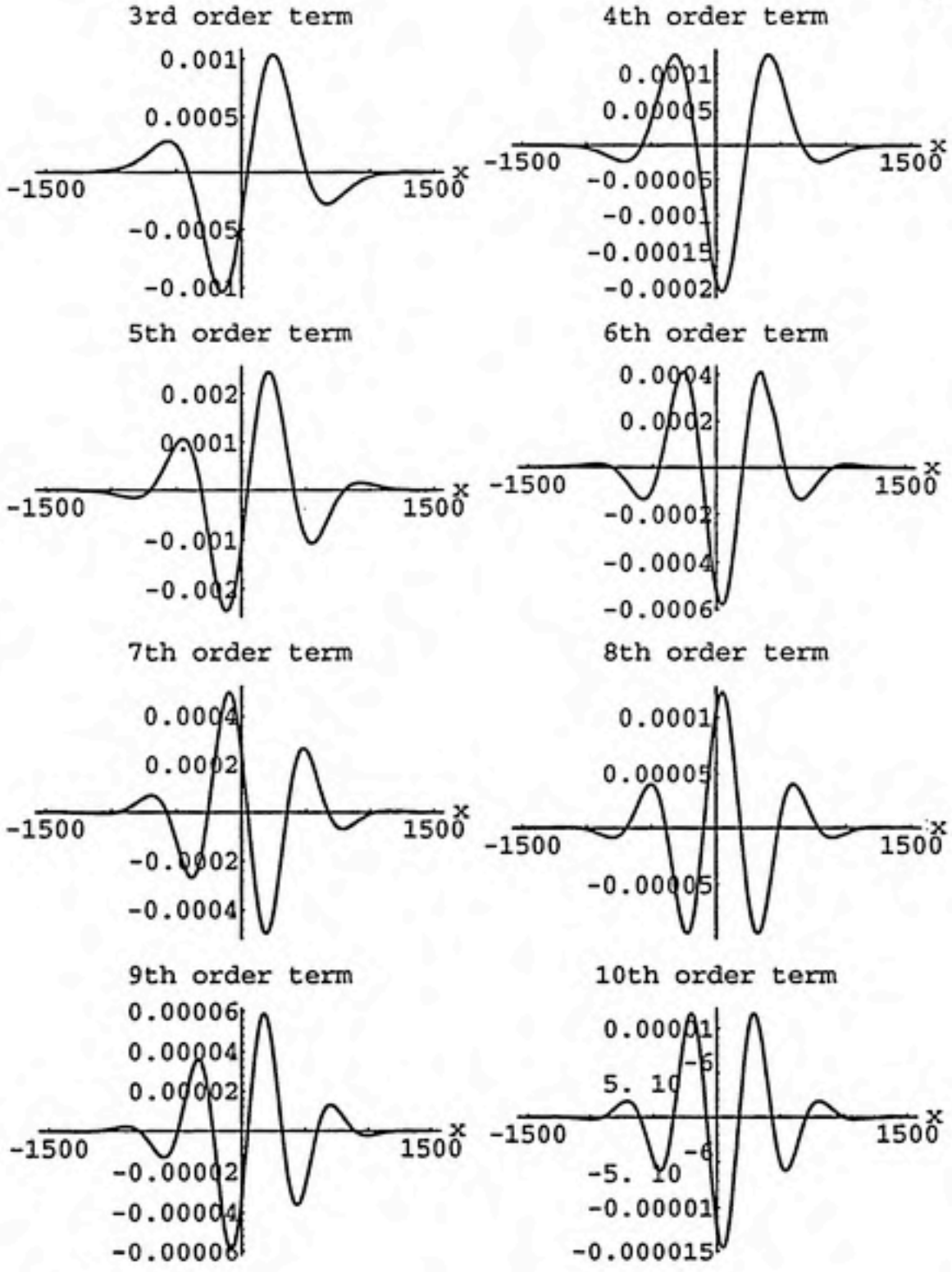

Fig. 4-16. $F_i\partial^i C/\partial x^i$ terms from third- to tenth-order of a Gaussian source with σ_x =1.32, Pe=∞, and Cr=0.24.

The tenth-order Taylor series expansion of the truncation error shown in Figure (4-17) reasonably describes the error observed in the finite element model for a Gaussian source with the characteristics given in Table (4-3).

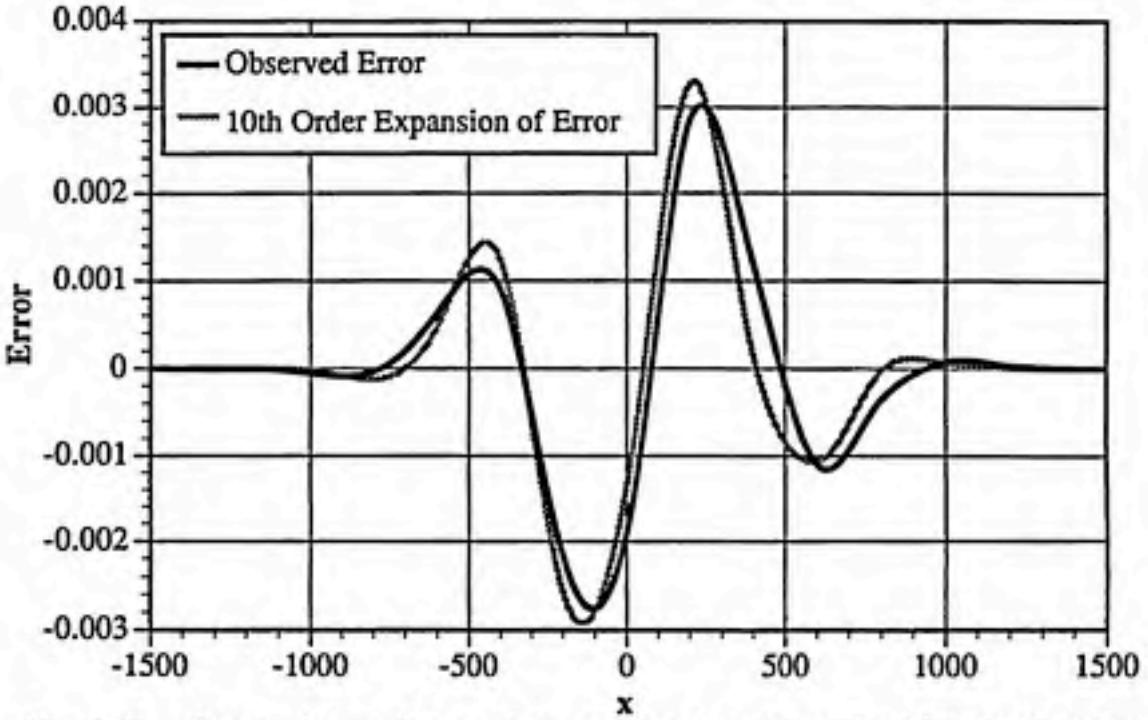

Fig. 4-17. Observed truncation error compared to the error predicted by a tenth-order Taylor series expansion. Model of a Gaussian source with $\overline{\sigma_x}$ =1.32, Pe=∞, and Cr=0.24 after one timestep.

The only difference between the next case and the preceding one is the change in $\overline{\sigma_x}$ from 1.32 to 0.50. The tenth-order Taylor series expansion of the truncation error in Figure (4-18a) does not accurately describe the error observed in the finite element model, and even the fifteenth-order expansion shown in Figure (4-18b) falls short of matching the observed error profile.

The different order terms from this problem are shown in Figure (4-19) The seventh-order term is the largest, but other higher-order terms are of similar magnitude. This is to be expected, since greater than fifteenth-order terms were suggested to be significant by Figure (4-18b).

(a)

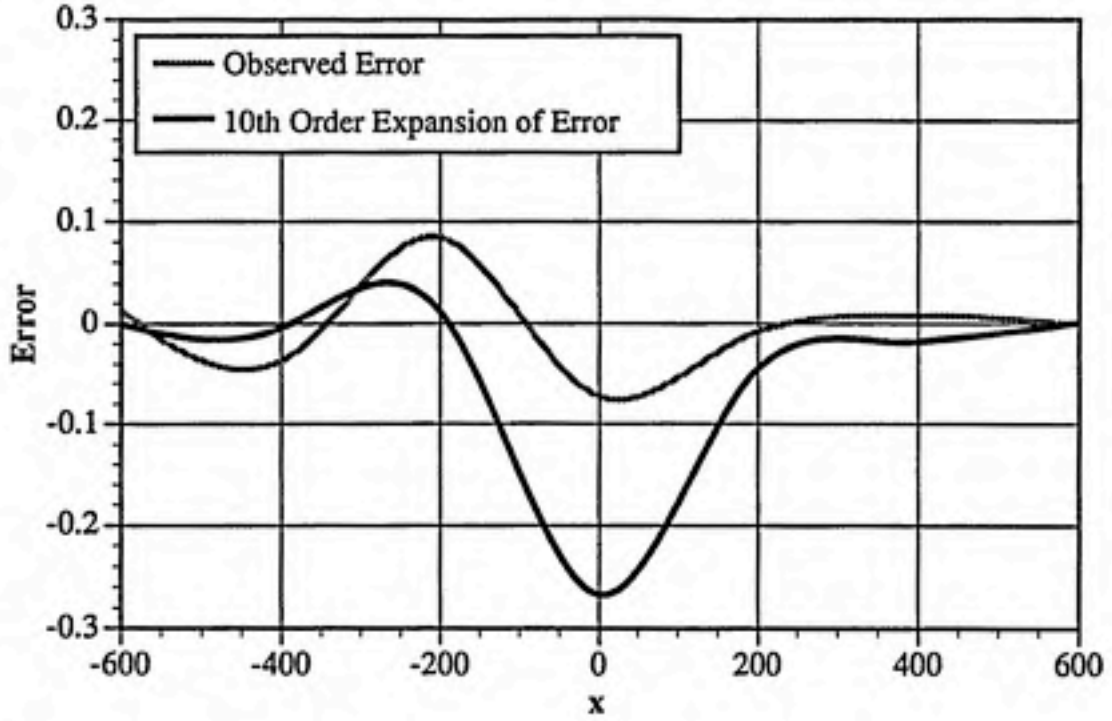

(b)

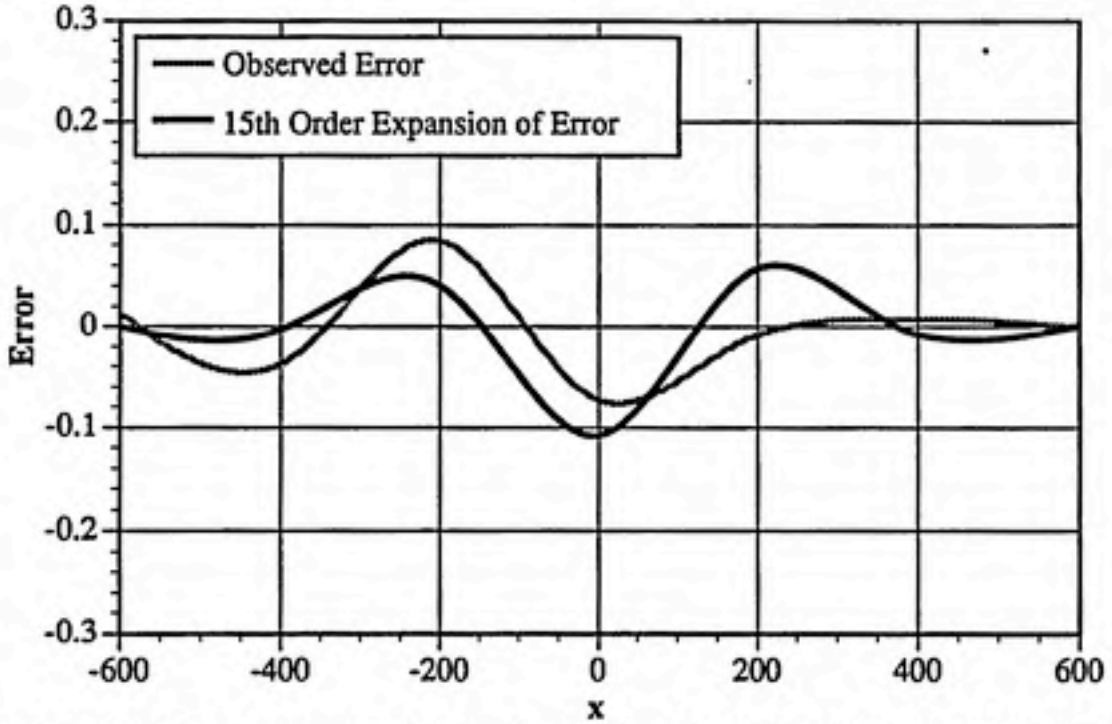

Fig. 4-18. Truncation error of a Gaussian source with $\overline{\sigma_x}$ =0.50, Pe=∞, and Cr=0.24. over one timestep. Comparison of the observed error with: (a) Error predicted by a tenth-order Taylor series expansion. (b) Error predicted by fifteenth-order Taylor series expansion.

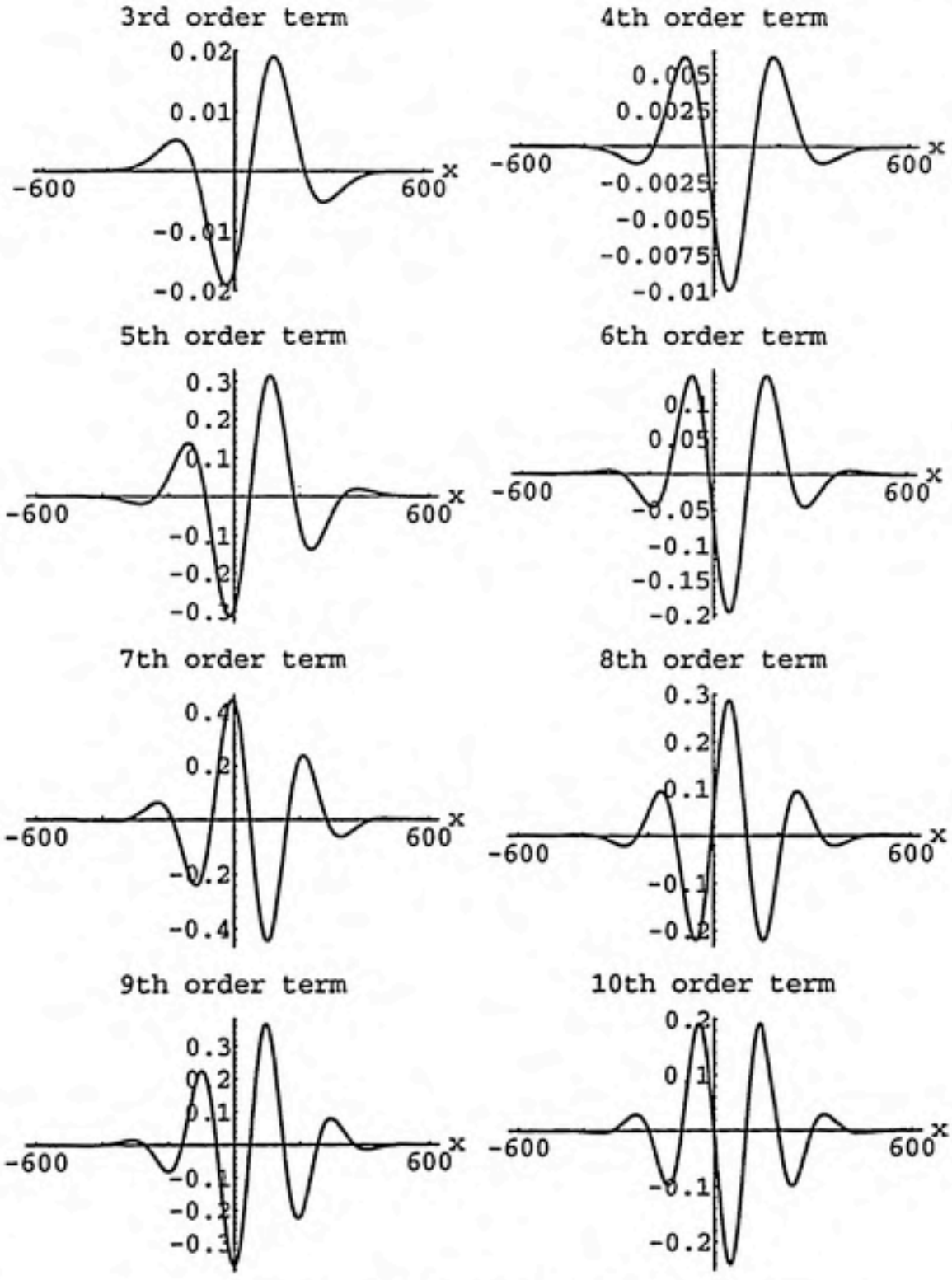

Fig. 4-19. $F_i\partial^i C/\partial x^i$ terms from third to tenth-order of a Gaussian source with $\overline{\sigma_x}$ =0.50, Pe=∞, and Cr=0.24.

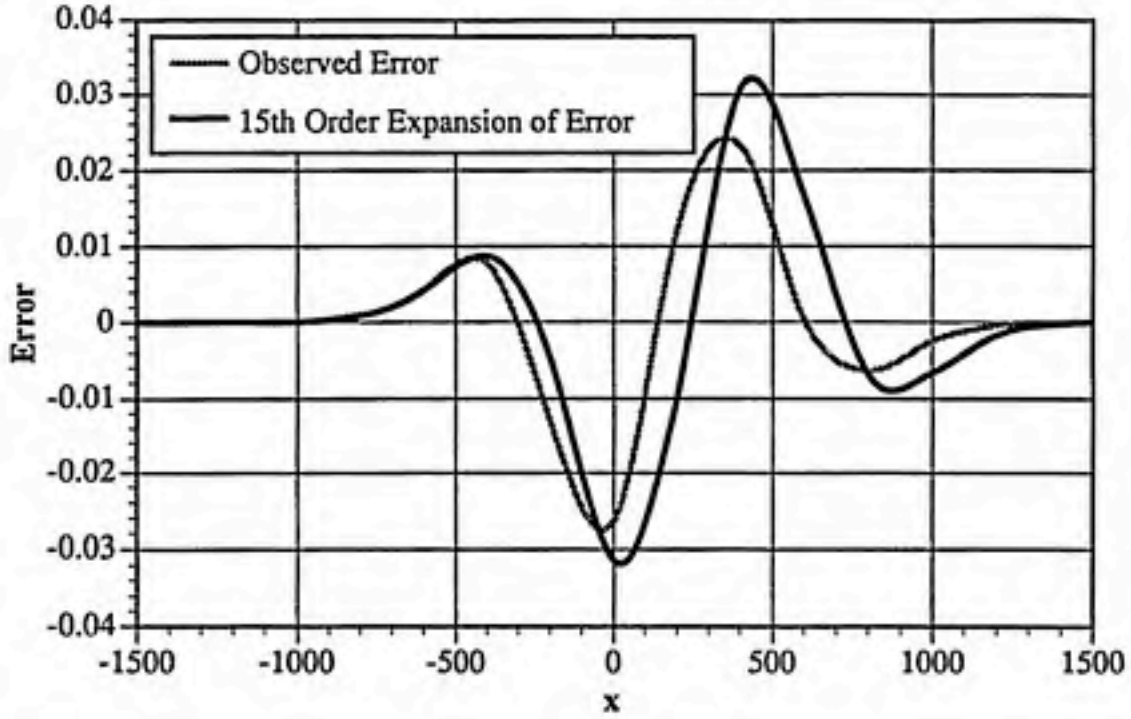

Fig. 4-20. Observed truncation error compared to the error predicted by a fifteenth-order Taylor series expansion. Model of a Gaussian source with $\overline{\sigma_x}$ =1.32, Pe=∞, and Cr=0.80 over one timestep.

In Figure (4-20), the $\overline{\sigma_x}$ is 1.32 again, but the Cr is changed from 0.24 to 0.80 by increasing Δt from 96 to 320. In this case, a fifteenth-order Taylor series fails to accurately describe the observed error.

Higher-order terms may therefore be significant in describing truncation error. While the magnitude of the derivative portion of these terms is extremely small, the values of the corresponding F_i may be large enough to make even tenth-order terms larger than third-order terms. This requires that Taylor series expansions be carried out to even higher orders to accurately describe the truncation error. Sensitivity of the upper limit of the series expansion order required to adequately describe truncation errors was also observed for variations in Pe, and Da. In some cases, even twenty-fifth-order expansions did not adequately represent the observed error.

Figures (4-17) through (4-20) illustrate two major problems with this line of investigation:

a) The order of the most significant terms in the Taylor series expansion of the truncation error is a function of the source condition ($\overline{\sigma_x}$), as well as model parameters such as Cr, Pe, and Da.

b) The upper limit on the order of terms required to accurately describe the truncation error is also a function of these parameters.

As mentioned earlier, prior research carried out Taylor series analysis to fifth-order (Yu and Heinrich, 1986; Westerink and Shea, 1989; Cantekin and Westerink, 1990). It was expected that the ability to evaluate more terms of the Taylor series would improve its ability to describe optimal upwinding parameters. Unfortunately, it was not anticipated that higher than fifteenth-order expansions would be necessary. The algorithm used in the Mathematica code can evaluate the Taylor series expansions from zero-order to as high an order as computer memory and time constraints will allow, but fifteenth-order expansions may require as much as 8Mb of RAM and several minutes to evaluate on a high-performance PC. Many cases of practical concern did not appear to be accurately represented by expansions of up to twenty-fifth-order, which would require far more memory and time to evaluate. The relationship between expansion order and memory/time overhead is roughly geometric, based on the increase in the size of the series coefficient expressions for each increment in order. This problem is compounded by the goal of using the series expansion of the truncation error in concert with optimization techniques to derive optimal upwinding parameters. This would require many error evaluations, and make computing costs prohibitive.

Source dependence of the truncation error is a particularly troublesome observation. The overhead involved in very high order Taylor series analysis could be resolved through the use of bigger and faster computers, but the dependence of the truncation error on $\overline{\sigma_x}$ lessens the utility of this approach. This dependence is the result of the derivatives in the each term of the series expansion. The significance of individual derivatives is directly related to the shape of the source. Any "optimal" parameters derived by this method would therefore be optimal only for specific source conditions. Unfortunately, when dispersion is present, the range of significant derivative terms is in a state of flux, as dispersion alters the concentration profile of the source at each timestep. Furthermore, even for essentially

nondispersive conditions, real world modeling of contaminant transport in groundwater rarely involves well characterized sources.

4.2.2 Fourier Analysis

In brief, Fourier analysis consists of describing a function in terms of infinite sums of sinusoids of varying wavelengths. The Fourier analysis performed by Westerink and Shea (1989) starts with substitution of Equations (4-12), (4-13), and (4-14) into the appropriate difference equations (Equation. (4-8), (4-9), or (4-10)) to express concentrations at time level $t+\Delta t$ in terms of concentrations at time level t.

$$C_{x-\Delta x}^{t+\Delta t} = a_\lambda C_{x-\Delta x}^{t} \tag{4-12}$$

$$C_{x}^{t+\Delta t} = a_\lambda C_{x}^{t} \tag{4-13}$$

$$C_{x+\Delta x}^{t+\Delta t} = a_\lambda C_{x+\Delta x}^{t} \tag{4-14}$$

The variable a_λ is the numerical amplification factor with spatial wavelength λ. The concentrations at $x-\Delta x$ and $x+\Delta x$ are then expressed as a function of C_x^t with Equations (4-15) and (4-16). A more detailed description of Fourier analysis of FE ADR transport models may be found in Pinder and Gray's excellent book on finite element modeling of hydrological problems (1977).

$$C_{x-\Delta x}^{t} = C_{x}^{t} e^{\left(\frac{-2\pi \Delta x\, i}{\lambda}\right)} \tag{4-15}$$

$$C_{x+\Delta x}^{t} = C_{x}^{t} e^{\left(\frac{2\pi \Delta x\, i}{\lambda}\right)} \tag{4-16}$$

$$i = \sqrt{-1} \tag{4-17}$$

The exponential expressions may be converted to trigonometric form with the following Euler formula definition.

$$e^{\left(\frac{-2\pi \Delta x\, i}{\lambda}\right)} = \cos\left(\frac{2\pi \Delta x}{\lambda}\right) - i \sin\left(\frac{2\pi \Delta x}{\lambda}\right) \tag{4-18}$$

When these substitutions are performed on Equation (4-8), the amplification factor for linear elements may be expressed as:

$$a_\lambda = \frac{\left(4+\beta+6\alpha Cr+\frac{12Cr}{Pe}\right)\cos\left(\frac{2\pi\Delta x}{\lambda}\right)+\left(8-\beta-6\alpha Cr-\frac{12Cr}{Pe}\right)+\left(-6\sqrt{-1}(\alpha+Cr)\sin\left(\frac{2\pi\Delta x}{\lambda}\right)\right)}{\left(4+\beta-6\alpha Cr-\frac{12Cr}{Pe}\right)\cos\left(\frac{2\pi\Delta x}{\lambda}\right)+\left(8-\beta+6\alpha Cr+\frac{12Cr}{Pe}\right)+\left(-6\sqrt{-1}(\alpha-Cr)\sin\left(\frac{2\pi\Delta x}{\lambda}\right)\right)} \tag{4-19}$$

Similar manipulations also result in the analytical amplification factor, $a_{a\text{-}\lambda}$:

$$a_{a\text{-}\lambda} = \left[\cos\left(\frac{2\pi}{\lambda}\Delta x\right) - \sqrt{-1}\sin\left(\frac{2\pi}{\lambda}\Delta x\right)\right]\exp\left[-\left(\frac{Cr}{Pe}\right)\left(\frac{2\pi}{\lambda}\Delta x\right)^2\right] \tag{4-20}$$

Equations (4-21) and (4-22) are then used to describe two different measures of error: the damping ratio and the phase error. In these equations, *Im* and *Re* refer to the imaginary and real parts of their parenthesized arguments, respectively.

$$\text{Damping Ratio} = \left(\frac{|a_\lambda|}{|a_{a\text{-}\lambda}|}\right)^{\frac{\lambda}{\Delta x\, Cr}} \tag{4-21}$$

$$\text{Phase Error} = \frac{\lambda}{\Delta x\, Cr}\tan^{-1}\left(\frac{Im\,(a_\lambda)}{Re\,(a_\lambda)}\right) - 2\pi \tag{4-22}$$

A perfect numerical solution would have a damping ratio of one and a phase error of zero. A damping ratio of one produces solutions with no peak depression relative to an analytical solution. Zero phase error results from accurate propagation of all the component frequencies of the source profile, and would result in solutions that not only had no phase difference relative to analytical solutions in their major features, but were also oscillation-free. In summary, a solution with a damping ratio of one has a correct peak amplitude, and a solution with zero phase error has a correct peak location, as well as no oscillations.

Unfortunately, this method also produces source dependent optimal parameters. While the phase error and damping ratio could be used in order to describe optimal parameters, such parameters would be optimal only for specific wavelengths. The spectrum of wavelengths and their relative contributions present in a source are a function of the shape of that source. This makes description of generalized source independent upwinding parameters a complicated, if not impossible task.

4.2.3 Numerical Experimentation

Numerical experimentation, or a formalized trial and error approach, was then used to describe optimal upwinding parameters. A Levenberg-Marquardt (LM) optimization algorithm was used to estimate upwinding parameters that minimized the Euclidean norm of the numerical solution relative to the analytical solution.

The LMDIF1 minimization routine was obtained from the NETLIB E-Mail software distribution service operated by Oak Ridge National Laboratories (Garbow et al., 1980). (This collection of subroutines and other useful mathematical software may be obtained free of charge by contacting the service at: NETLIB@ORNL.GOV.) LMDIF1 identifies the values of variables that minimize the Euclidean norm of a solution vector of a series of functions of those variables relative to a data vector. The Jacobian matrix required for LM optimization is estimated with a forward difference approximation.

LMDIF1 was incorporated in the linear FE code (LPG), and a data vector consisting of the residuals between the nodal concentrations from the analytical solution and the finite element solution was derived after each realization of the FE solution. The Euclidean norm was computed from this vector of residuals after one timestep, and the upwinding parameters were then adjusted as required by the LM algorithm to minimize this norm. The single timestep realization was then repeated from initial conditions until convergence criteria were satisfied. Convergence was typically considered to be obtained when variations of less than $\sim 1.49 \times 10^{-8}$ were observed in the upwinding parameters. This line of investigation produced upwinding parameters that performed well in comparison to previously published results (Westerink and Shea, 1989).

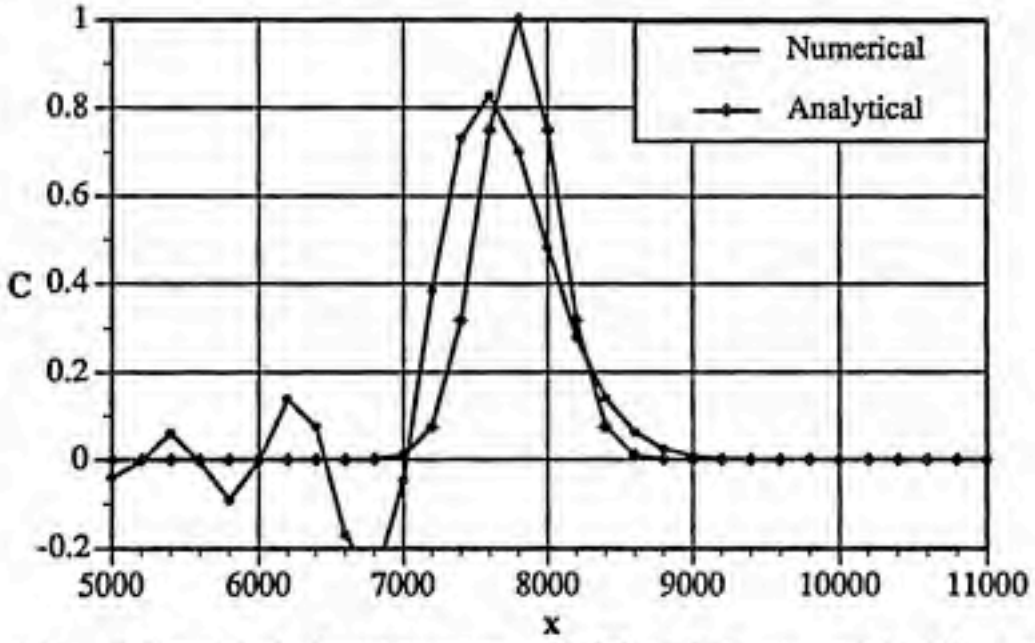

Fig. 4-21. BG model of a Gaussian source with σ_x =1.32, Pe=∞, and Cr=0.8, after 30 timesteps. α=0.0000, β=0.0000.

The example problem is first shown in Figure (4-21) for the case of no upwinding. As mentioned earlier, setting α and β to zero results in the traditional BG solution. The default

parameters from Table (4-3) were used in this case, save for Δt=320, and, consequently, Cr=0.8. After 30 timesteps, the solution suffers from oscillations, phase lag, and peak depression.

The parameters used by Westerink and Shea to produce the results shown in Figure (4-22) were defined by their own numerical experimentation method. In their work, parameters were judged to be optimal when the error between the analytical and FE solutions was minimized as indicated by the majority of six measures of error. These error measures are presented in Equations (4-23) through (4-28) in dimensionless form.

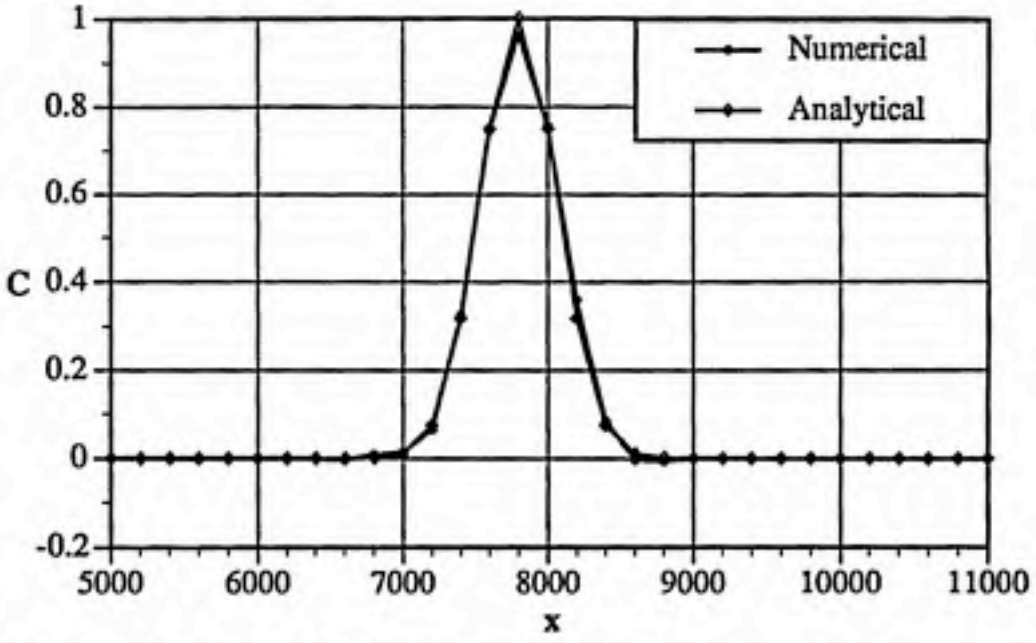

Fig. 4-22. PG model of a Gaussian source with $\overline{\sigma_x}$ =1.32, Pe=∞, and Cr=0.8, after 30 timesteps. α=0.1000, and β=1.3700 from Westerink and Shea (1989).

i) Integral measure of the overall error: E_i

$$E_i = \left(\frac{1}{x_L} \int_0^{x_L} \left(\frac{C_n(x) - C_a(x)}{C^{mo}} \right)^2 dx \right)^{1/2} \tag{4-23}$$

ii) Discrete measure of the overall error: E_d

$$E_d = \left(\sum_i \left(\frac{C_n(x_i) - C_a(x_i)}{C^{mo}} \right)^2 \right)^{1/2} \tag{4-24}$$

iii) Peak depression: E_p

$$E_p = \left| \frac{C_a^m - C_n^m}{C_a^m} \right| \tag{4-25}$$

iv) Maximum oscillation: E_o

$$E_o = \left| \frac{C_n^{m-}}{C_a^m} \right| \tag{4-26}$$

v) Phase shift: E_s

$$E_s = \frac{x_a^m - x_n^m}{x_a^m} \tag{4-27}$$

vi) Mass preservation: E_m

$$E_m = 1.0 - \frac{1}{x_L} \int_0^{x_L} \frac{C_n(x)}{C^{m0}} dx \tag{4-28}$$

When perfect agreement between analytical and FE solutions is attained, E_i, E_d, E_p, E_o, and E_s are equal to zero and E_m is equal to one. The a subscript indicates analytical or exact values, while numerical values are subscripted with n. C^{m0} is the maximum concentration at t=0, while C^m and C^{m-} are the maximum positive and negative concentrations at the current time level. The spatial locations of maximal concentrations are referred to as x^m, and are subscripted with a and n for the analytical and numerical cases, respectively. While all of the above accurately reflect components of the error between the analytical and numerical solutions, the "majority rule" approach imposes a weighting system on a system of six variables with varying degrees of independence. The first two measures, E_i and E_d are closely related, and should react to changes in the upwinding parameters in the same way. They are also the only two criteria that will be zero only when the analytical and numerical solutions are identical. The other criteria may be equal to zero (or one for E_m) when the numerical solution is not accurate. E_m is probably best left out of the analysis, as mass balance does not guarantee accurate model output. E_s and E_o are directly related, as mentioned in the section on Fourier analysis. E_o and E_p are inversely related for the case of N+1 upwinding, as the numerical dispersion it adds to smooth the oscillations also results in peak depression.

The approach used in this work was to minimize a single error measure: the L-2 or Euclidean norm, which is equivalent to minimizing E_d. The only difference between E_d and the L-2 norm is that E_d is normalized by the mass in the system, which is constant in the cases presented here. The results shown in Figure (4-23) reflect this philosophical difference. The parameters derived with LMDIF1 result in better peak representation, but with slightly more oscillation in the upstream tail.

In Figure (4-24), the source dependence of the optimality of the upwinding parameters is demonstrated. A change in $\overline{\sigma_x}$ from 1.32 to 1.00 results in a significant change in solution quality. These observations are all accentuated by extending the modeling runs to 100 timesteps, as presented in Figures (4-25) through (4-28)

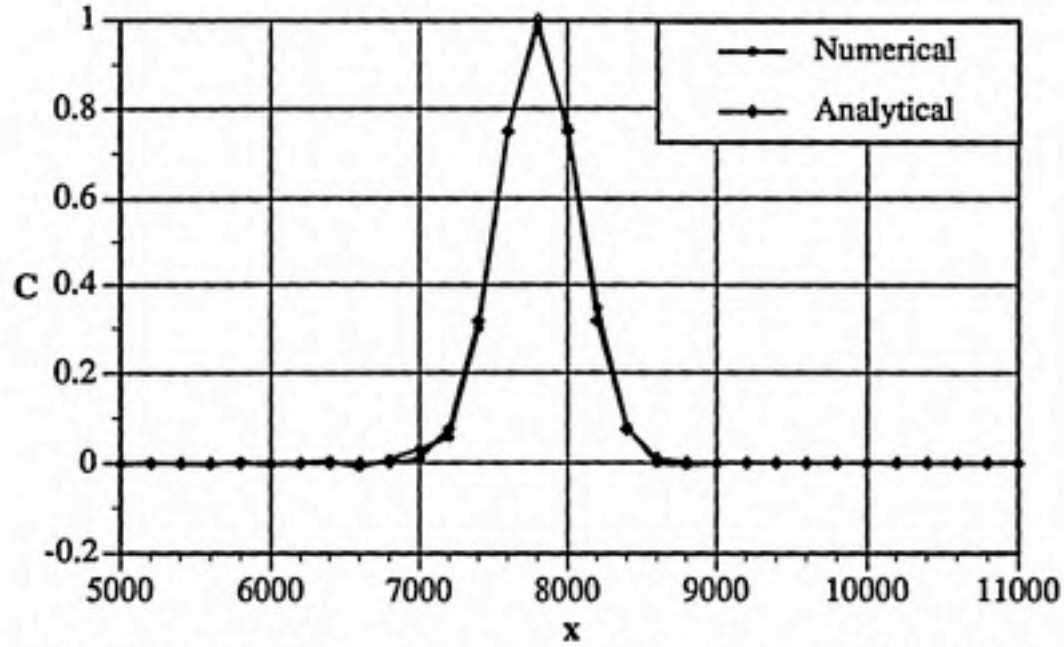

Fig. 4-23. PG model of a Gaussian source with $\overline{\sigma_x}$ =1.32, Pe=∞, and Cr=0.8, after 30 timesteps. α=0.0113, and β=1.3812 from LMDIF1.

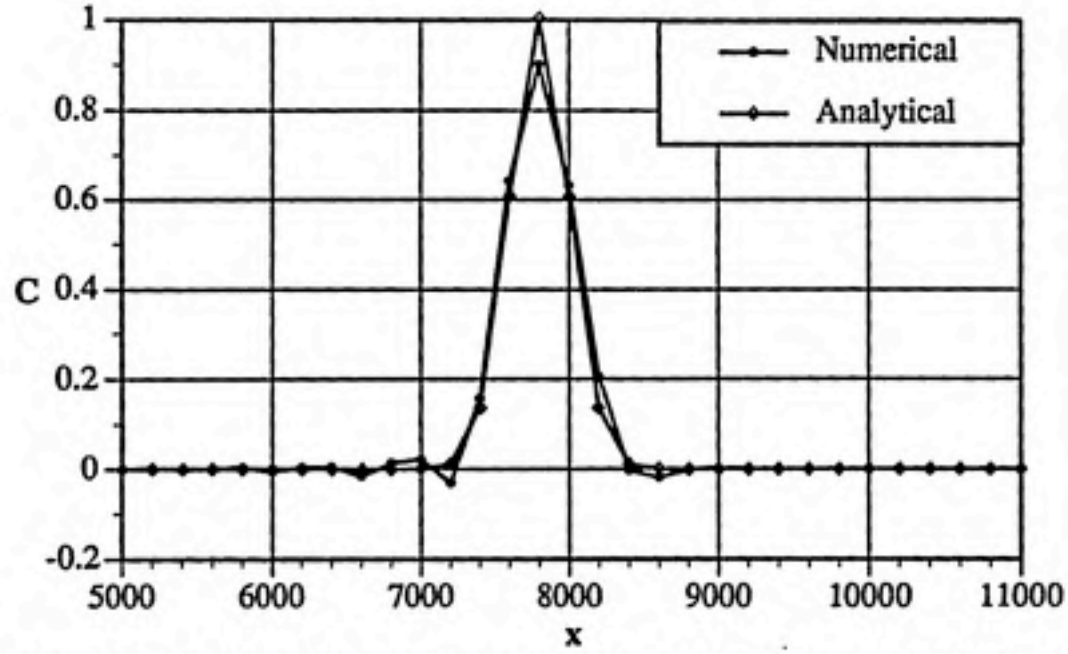

Fig. 4-24. PG model of a Gaussian source with $\overline{\sigma_x}$ =1.00, Pe=∞, and Cr=0.8, after 30 timesteps. α=0.1000, and β=1.3700 from Westerink and Shea (1989).

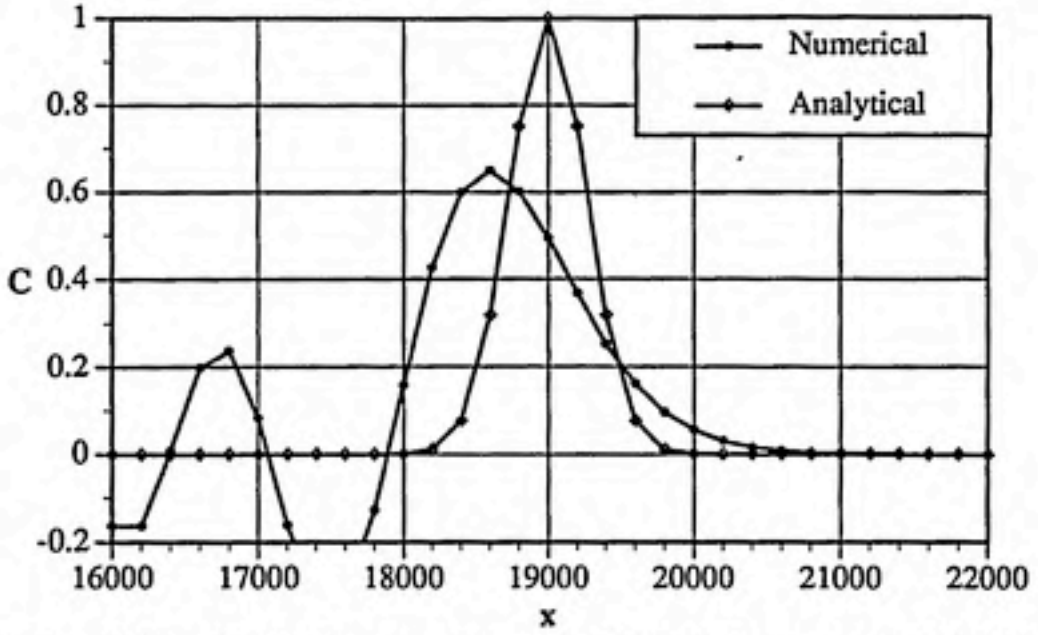

Fig. 4-25. BG model of a Gaussian source with σ_x =1.32, Pe=∞, and Cr=0.8, after 100 timesteps. α=0.0000 and β=0.0000.

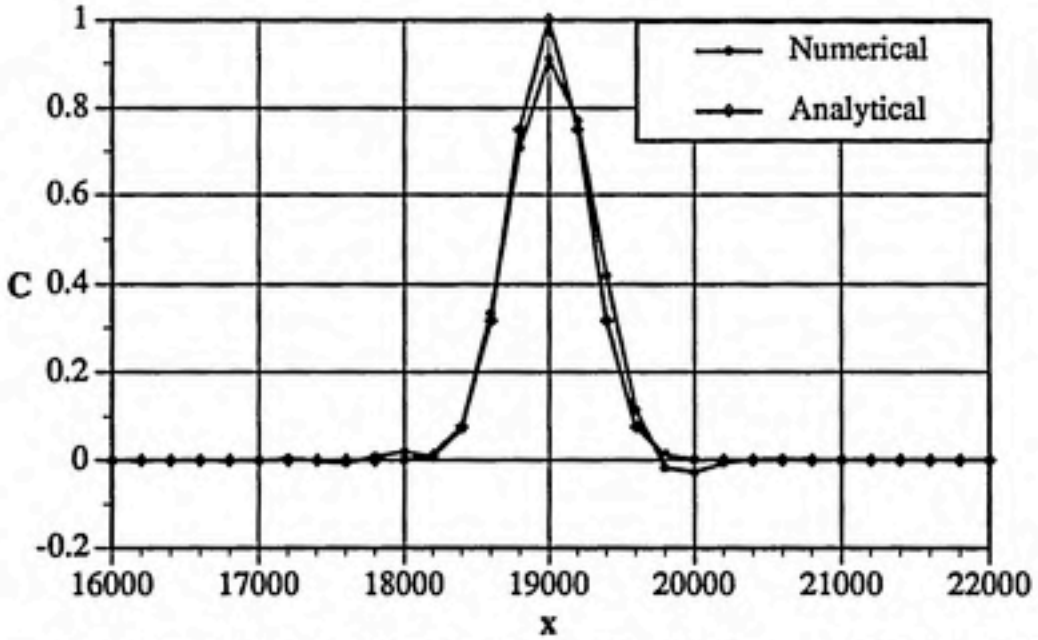

Fig. 4-26. PG model of a Gaussian source with σ_x =1.32, Pe=∞, and Cr=0.8, after 100 timesteps. α=0.1000, and β=1.3700 from Westerink and Shea (1989).

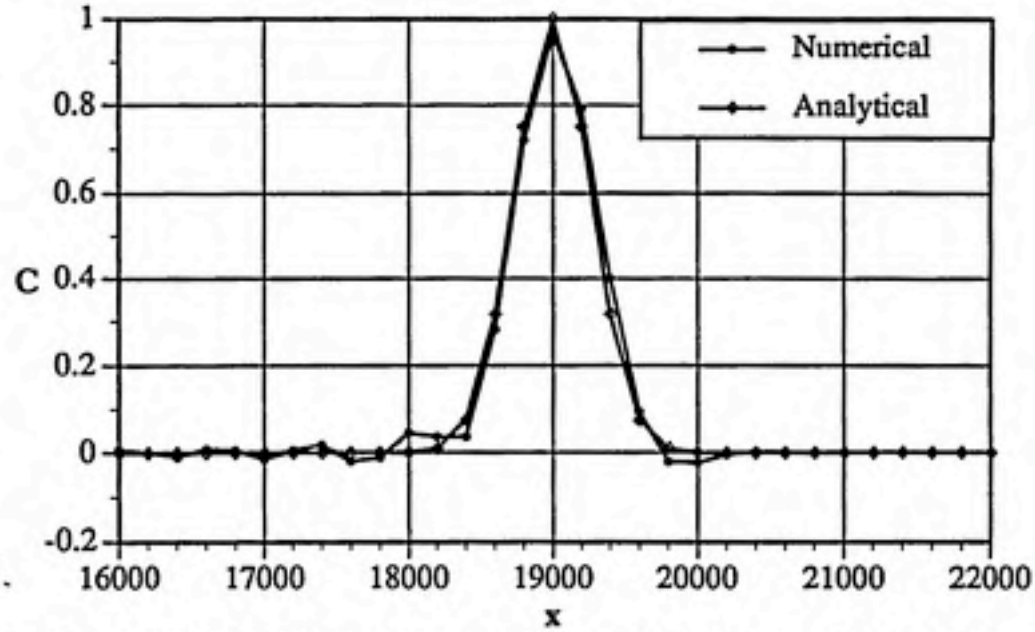

Fig. 4-27. PG model of a Gaussian source with σ_x =1.32, Pe=∞, and Cr=0.8, after 100 timesteps. α=0.0113, and β=1.3812 from LMDIF1.

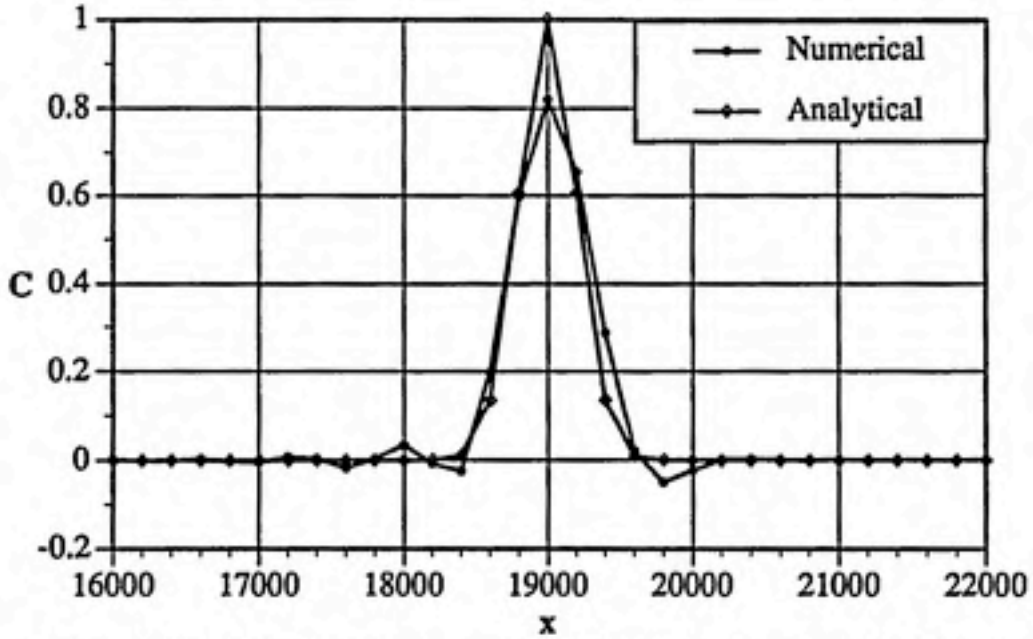

Fig. 4-28. PG model of a Gaussian source with σ_x =1.00, Pe=∞, and Cr=0.8, after 100 timesteps. α=0.1000, and β=1.3700 from Westerink and Shea (1989).

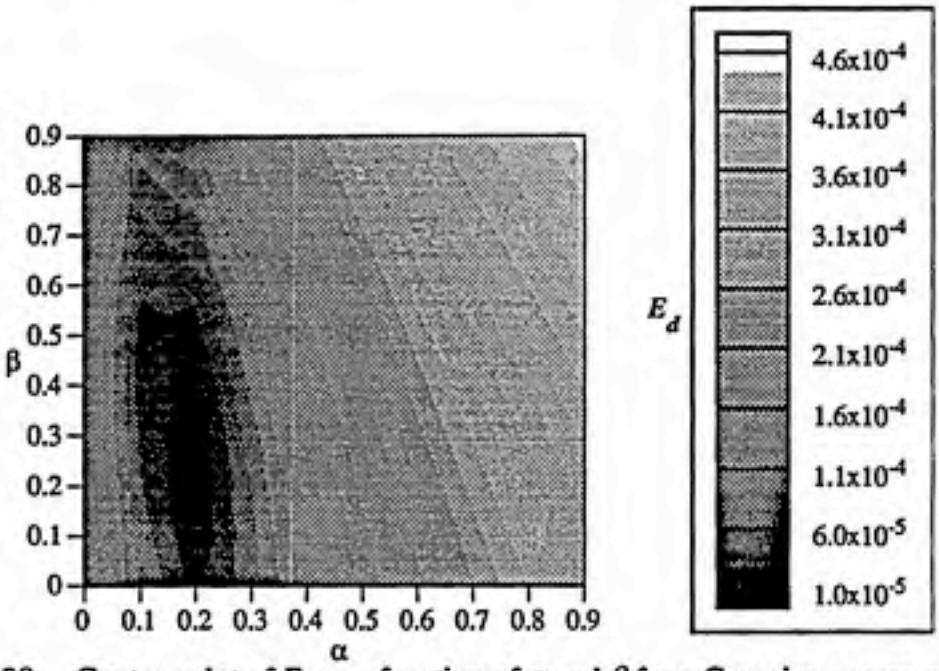

Fig. 4-29. Contour plot of E_d as a function of α and β for a Gaussian source with σ_x =0.66, Pe=∞, and Cr=0.24 after 1 timestep.

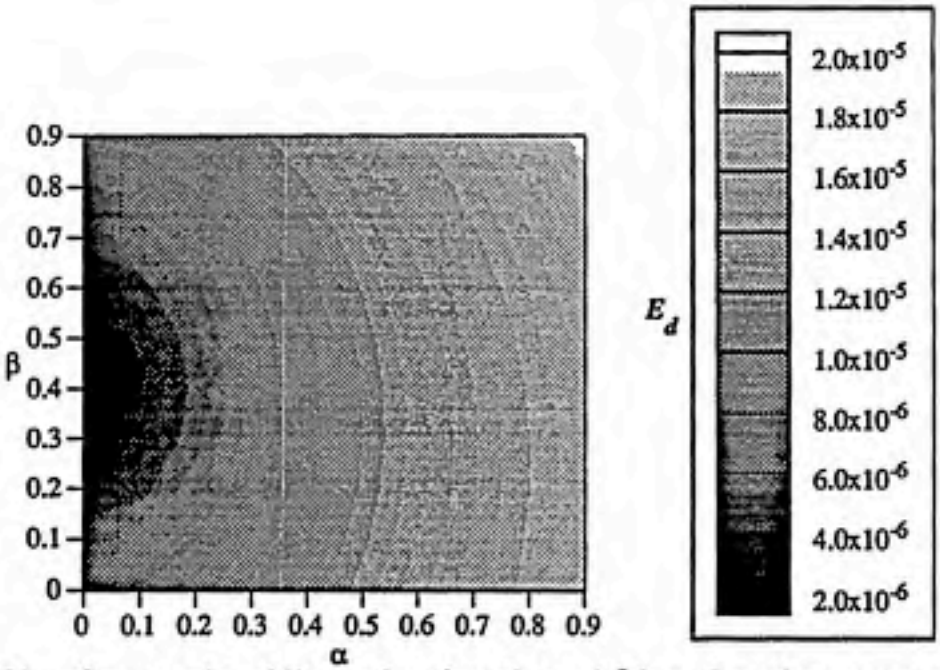

Fig. 4-30. Contour plot of E_d as a function of α and β for a Gaussian source with σ_x =1.32, Pe=∞, and Cr=0.24 after 1 timestep.

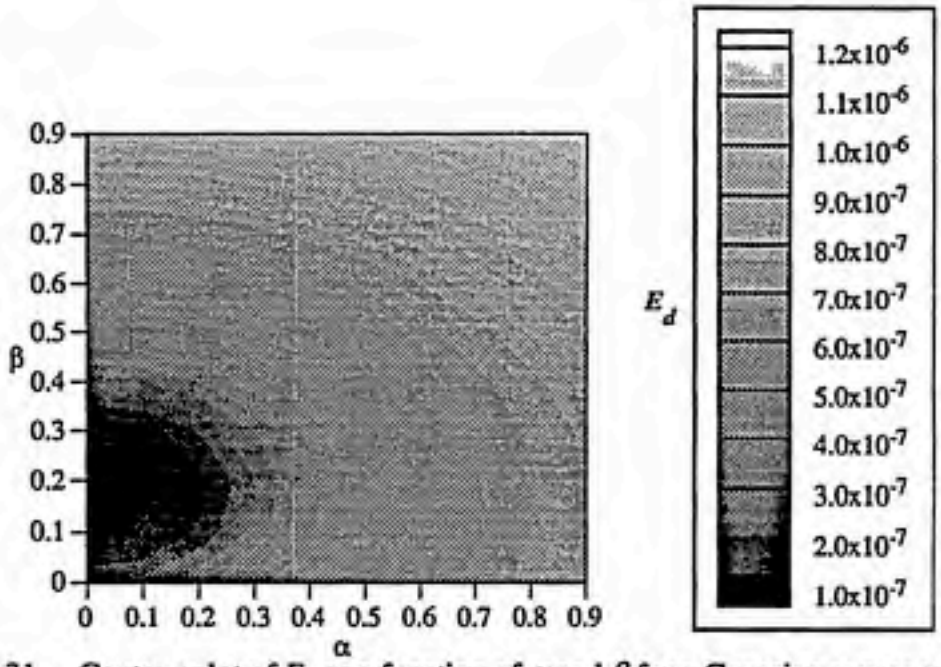

Fig. 4-31. Contour plot of E_d as a function of α and β for a Gaussian source with $\overline{\sigma_x}$ =2.64, Pe=∞, and Cr=0.24 after 1 timestep.

Figures (4-29), (4-30), and (4-31) also demonstrate the dependence of the optimality of upwinding parameters on source conditions. Each plot was generated with the default variables from Table (4-3), save for the standard deviation of the source which is incremented by a factor of two between Figures (4-29) and (4-30), and doubled again between Figure (4-30) and (4-31). The discrete error E_d defined in Equation (4-24) is minimal for different combinations of α and β between these three plots. As mentioned previously, this measure of error is equivalent to the Euclidean norm minimized by LMDIF1. The results in Figure (4-30) are consistent with the α and β values presented by Westerink as well as those derived by LMDIF1 for that specific combination of Cr, Pe, and $\overline{\sigma_x}$ (Westerink and Shea, 1989).

The source dependence of optimum upwinding parameters is clearly related to the upwinding method, and is not an artifact of the analytical techniques used to identify optimal parameters. This dilemma led to the development of a novel upwinding strategy, which is described in the following section.

5 GRADIENT UPWINDING

5.1 Motivation

As seen in the previous section, PG upwinding outperforms traditional BG methods. Upwinded FE models can deliver near perfect results at infinite Pe. Unfortunately, the proper amount of upwinding required to produce these results was also demonstrated to be a function of the source condition, so while impressive results can be obtained, they are restricted to specific problems. Optimal PG upwinding is therefore not easily applied to most real world problems, as these involve a great variety of source conditions. Furthermore, while advective-dominated transport presumes large values of Pe, the presence of dispersion may still be significant at Pe numbers of interest. Dispersion will change the shape of the source from timepoint to timepoint, and upwinding parameters that were optimal at t =0 will not be optimal later in modeling time.

If the upwinding condition is a function of the source, the ability of an individual element to correctly represent the solution at the next time level is a function of the concentration gradient across it at the current time level. The uniform upwinding method presented up to this point imposes an identical level of upwinding on all elements in the domain. In the following section, a method is presented that makes the element specific upwinding condition a function of the gradient across each individual element in the domain.

5.2 Formulation

The finite element method readily accommodates heterogeneity in various physical parameters, so non-uniform upwinding is permissible (Heinrich and Zienkiewicz, 1977; Christie and Mitchell, 1978). The global matrices for the PG method used in this work can be modified to include element specific upwinding parameters as follows: Each row of the finite element matrices represents the equation for the solution at a given node. This row contains terms that describe the contribution from every element involved in the solution at

that node. For one dimensional finite elements, no more than two elements contribute to the solution at a given node. For linear finite elements, the coefficient matrices described in Equation (3-18) to (3-21) can be assigned upwinding parameters α^u and β^u that correspond to the upstream element, as well as α^d and β^d for the downstream element. The following difference equation results after the appropriate substitutions are made.

$$\left[C^t_{x-\Delta x}\left(\frac{-1}{6\Delta t}-\frac{\alpha^u}{4\Delta t}-\frac{\beta^u}{24\Delta t}-\frac{D_h}{2\Delta x^2}-\frac{v_x}{4\Delta x}-\frac{\alpha^u v_x}{4\Delta x}+\frac{k_1}{12}+\frac{\alpha^u k_1}{8}+\frac{\beta^u k_1}{48}\right)+\right.$$

$$C^t_x\left(\frac{-2}{3\Delta t}-\frac{\alpha^u-\alpha^d}{4\Delta t}+\frac{\beta^u+\beta^d}{24\Delta t}+\frac{D_h}{\Delta x^2}+\frac{(\alpha^u+\alpha^d)v_x}{2\Delta x}-\frac{k_1}{3}+\frac{(\alpha^u-\alpha^d)k_1}{8}-\frac{(\beta^u+\beta^d)k_1}{48}\right)+$$

$$C^t_{x+\Delta x}\left(\frac{-1}{6\Delta t}+\frac{\alpha^d}{4\Delta t}-\frac{\beta^d}{24\Delta t}-\frac{D_h}{2\Delta x^2}+\frac{v_x}{4\Delta x}-\frac{\alpha^d v_x}{4\Delta x}+\frac{k_1}{12}-\frac{\alpha^d k_1}{8}+\frac{\beta^d k_1}{48}\right)+$$

$$C^{t+\Delta t}_{x-\Delta x}\left(\frac{1}{6\Delta t}+\frac{\alpha^u}{4\Delta t}+\frac{\beta^u}{24\Delta t}-\frac{D_h}{2\Delta x^2}-\frac{v_x}{4\Delta x}-\frac{\alpha^u v_x}{4\Delta x}+\frac{k_1}{12}+\frac{\alpha^u k_1}{8}+\frac{\beta^u k_1}{48}\right)+ \tag{5-1}$$

$$\left.C^{t+\Delta t}_{x+\Delta x}\left(\frac{1}{6\Delta t}-\frac{\alpha^d}{4\Delta t}+\frac{\beta^d}{24\Delta t}-\frac{D_h}{2\Delta x^2}+\frac{v_x}{4\Delta x}-\frac{\alpha^d v_x}{4\Delta x}+\frac{k_1}{12}-\frac{\alpha^d k_1}{8}+\frac{\beta^d k_1}{48}\right)\right]$$

$$\left(\frac{2}{3\Delta t}+\frac{\alpha^u-\alpha^d}{4\Delta t}-\frac{\beta^u+\beta^d}{12\Delta t}-\frac{D_h}{\Delta x^2}+\frac{(\alpha^u+\alpha^d)v_x}{2\Delta x}+\frac{k_1}{3}+\frac{(\alpha^u-\alpha^d)k_1}{8}-\frac{(\beta^u+\beta^d)k_1}{48}\right)^{-1}=C^{t+\Delta t}_x$$

While this is a valid approach, it also adds many more upwinding parameters, since each element requires its own pair. This problem is resolved by making the upwinding condition in each element a function of the gradient across it:

$$\alpha^e = f(\Delta C_m) \tag{5-2}$$
$$\beta^e = f(\Delta C_m) \tag{5-3}$$

where α^e and β^e are the element specific N+1 and N+2 degree upwinding parameters assigned to individual elements. This general definition of Gradient Upwinding (GU) permits many different relationships between the gradient and the local upwinding parameters. Experiments were performed with various functions in order to identify expressions that resulted in improved performance over the uniform upwinding models. An upwinding function was sought that would involve few input parameters, was as simple as possible, and would perform well over a wide range of concentration magnitudes. With these constraints in mind, the following functions were proposed:

$$\alpha^e = \sum_{i=0}^{n} \alpha_i \left(\frac{\Delta C_m}{\max(|C_{m1}|,|C_{m2}|)} \right)^i \tag{5-4}$$

$$\beta^e = \sum_{i=0}^{n} \beta_i \left(\frac{\Delta C_m}{\max(|C_{m1}|,|C_{m2}|)} \right)^i \tag{5-5}$$

The largest polynomial order desired is represented by n. $C_{m,1}$ and $C_{m,2}$ are the concentrations at the two nodes that delimit element m. The ith-order coefficients that are constant throughout the domain are α_i and β_i. For a linear (or first-order) polynomial, the following expression results:

$$\alpha^e = \alpha_0 + \alpha_1 \frac{\Delta C_m}{\max(|C_{m1}|,|C_{m2}|)} \tag{5-6}$$

$$\beta^e = \beta_0 + \beta_1 \frac{\Delta C_m}{\max(|C_{m1}|,|C_{m2}|)} \tag{5-7}$$

Uniform upwinding results when zero-order expressions are used. This special case was used to validate the GU code by comparing output with uniform upwinding results.

The effect GU has on the weighting functions for linear elements is illustrated in Figures (5-1) and (5-2). The elements labeled (a), (b), and (c) in Figure (5-1) have correspondingly labeled graphs of the weighting functions shown in Figure (5-2). These weighting functions result from a linear upwinding function with α_0=0.034757, α_1=0.2183, β_0=-1.3836, and β_1=-0.00417 as coefficient values. The three sets of weighting functions are distinct, and are clearly affected by local concentration gradients. Figures (5-2b) and (5-2c) form a pair of near mirror images. The gradients across these two elements have the same absolute values and opposite signs.

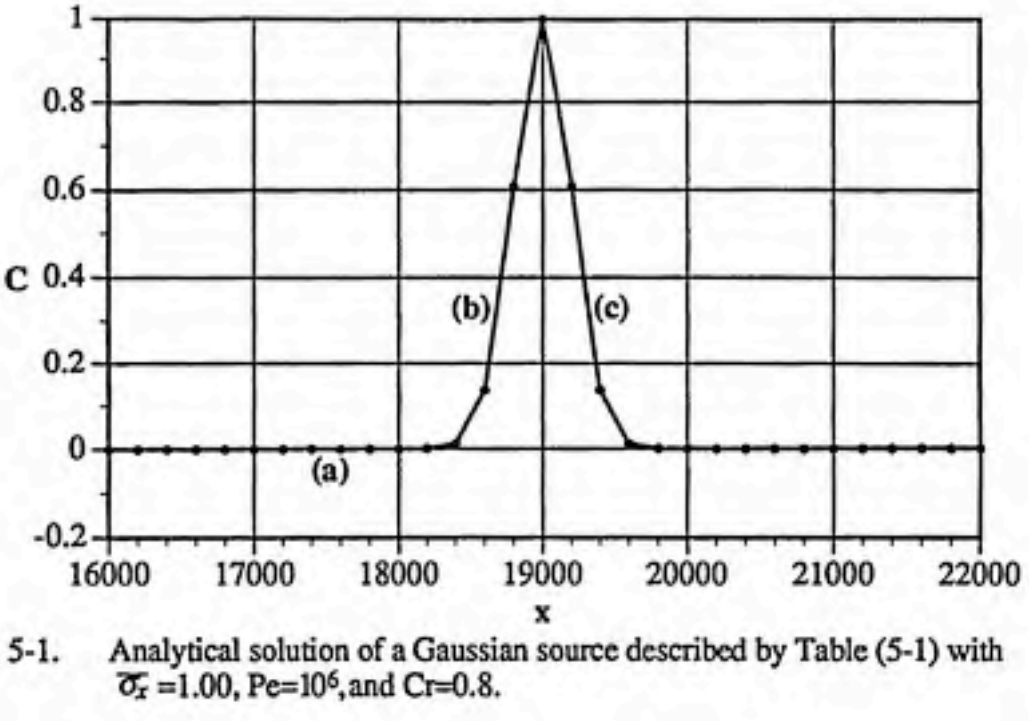

Fig. 5-1. Analytical solution of a Gaussian source described by Table (5-1) with σ_x =1.00, Pe=10^6, and Cr=0.8.

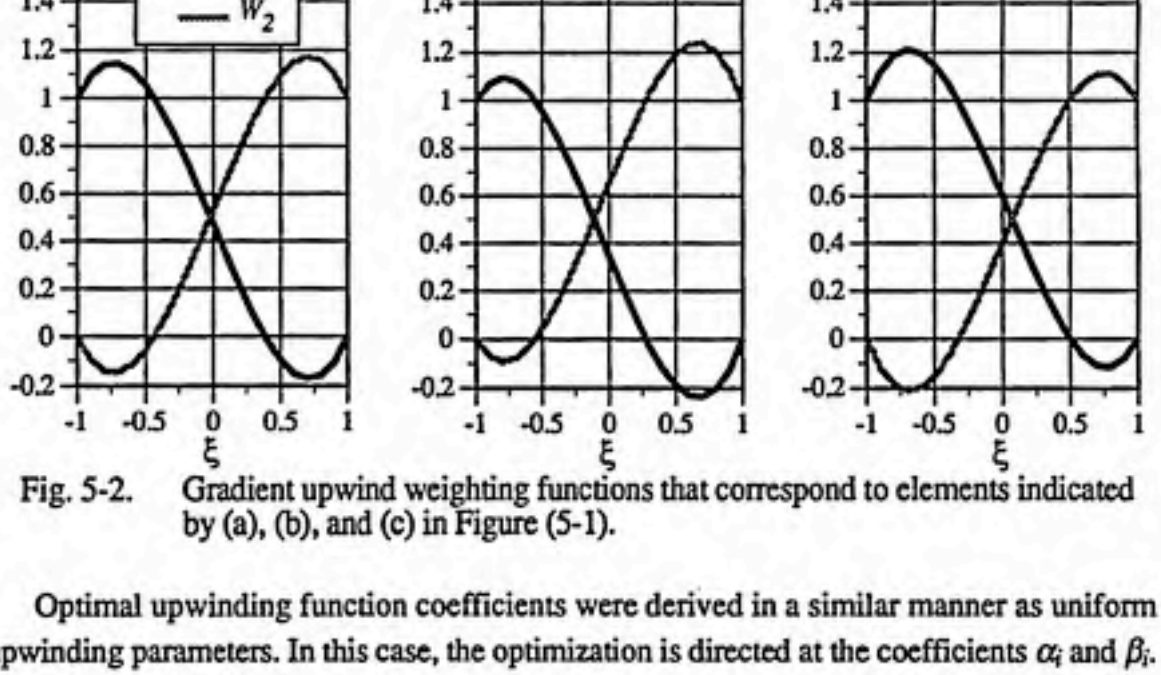

Fig. 5-2. Gradient upwind weighting functions that correspond to elements indicated by (a), (b), and (c) in Figure (5-1).

Optimal upwinding function coefficients were derived in a similar manner as uniform upwinding parameters. In this case, the optimization is directed at the coefficients α_i and β_i. Instead of optimizing over one timestep for one value of σ_x, the FE model is executed for one time step for a variety of σ_x values. The Euclidean norm that LMDIF1 seeks to minimize is a composite of the residuals in all of the solutions. In this manner, a set of

upwinding coefficients is derived that will work well over a range of source conditions. In some cases a set of coefficients is derived for a single σ_x to illustrate the best possible solution obtainable by a given upwinding function.

GU with linear upwinding functions delivered a significant improvement over uniform upwinding. Both linear and quadratic upwinding functions were evaluated, and while the quadratic case provided further improvement, linear functions were used for most of this study. This decision was based primarily on the novelty of the method. It is easier to optimize four coefficients at a time than six, so the insight gained by characterizing the linear case will reduce the effort required to study quadratic and other cases in future. A possible end result may be that the extra computational overhead required by models that use quadratic upwinding functions is not warranted, depending on the marginal improvement in model performance relative to the linear case.

5.3 Results

In the last section, Figures (4-21), (4-22), and (4-23) demonstrated the superiority of PG upwinding over nonupwinded BG solutions. There is room for improvement in those results, especially in the case shown in Figure (4-24) when the modeled source's standard deviation is different from the one for which the upwinding parameters were optimized.

LMDIF1 was used to perform optimizations for several combinations of Cr and Pe for linear upwinding functions and linear finite elements, but most of the model output presented here used the default parameters presented in Table (5-1).

Parameter	Value
Cr	0.8
D_h	0.0001
kJ	0.0
Pe	10^6
Rf	1.0
starting point	3000
v_x	0.5
x_L	22000
Δt	320
Δx	200

Table 5-1. Default parameters for models of Gaussian sources.

The baseline case presented in Figure (5-3) uses uniform upwinding to model the source presented in Figure (5-1) and Table (5-1) after 100 timesteps with little dispersion. Note that the concentration profile and the parameters used are essentially identical to those shown and used in Figure (4-27) for Pe=∞ instead of 10^6. This difference in Pe was judged to be insignificant for these problems.

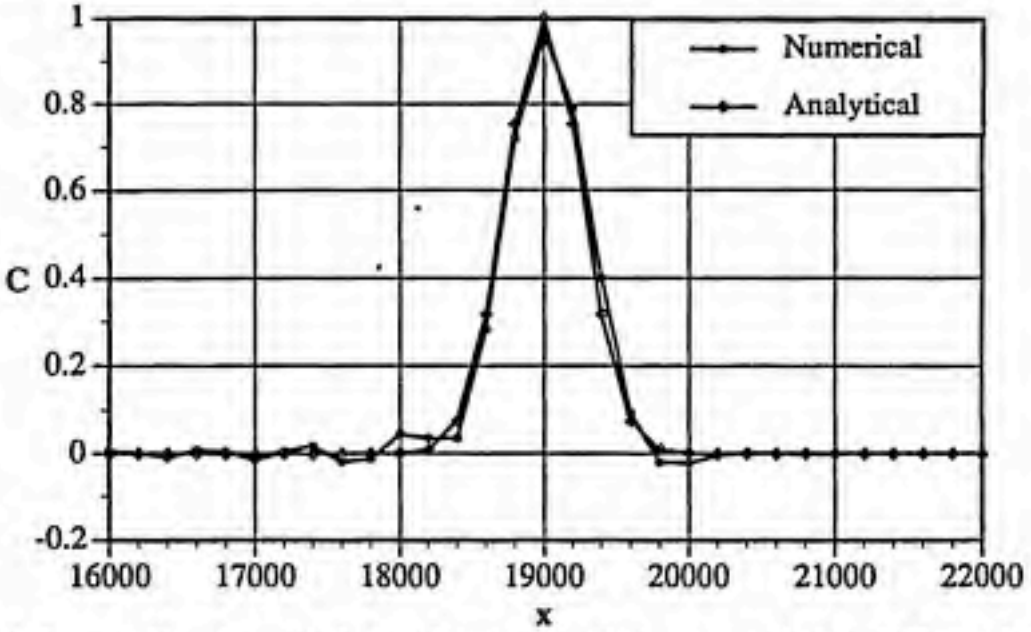

Fig. 5-3. Uniformly upwinded model of a Gaussian source with σ_x =1.32, Pe=10^6, and Cr=0.8, after 100 timesteps. Optimized for σ_x =1.32 with α=0.0113, and β=1.3812 from LMDIF1.

The oscillations and phase shift present in the profile shown in Figure (5-3) are substantially reduced in Figure (5-4). In this case, GU is used with a linear upwinding function. The coefficients used in this example were derived for general problems by using 300 different values of σ_x that lie between 1 and 4 in 0.01 increments. This is a remarkable improvement over the BG solution, which contains substantial oscillations, peak depression and phase shift.

The solution presented in Figure (5-5) does not use a range of σ_x values to derive the upwinding coefficients - they are optimal for a single value of σ_x . This is a better solution than the one in Figure (5-4), and, for non-diffusive problems, indicates the ability of the linear upwinding function to provide an upwinding condition that will accurately model this specific source condition. It also shows to what extent the performance of the general case is compromised for this particular source condition. For this problem, it demonstrates that linear upwinding functions can provide an accurate modeling configuration for this source.

The general case derived in the manner of Figure (5-4) provides a solution of slightly lower quality than the one in Figure (5-5), so there is a loss of accuracy in exchange for the ability to model accurately over a range of source conditions.

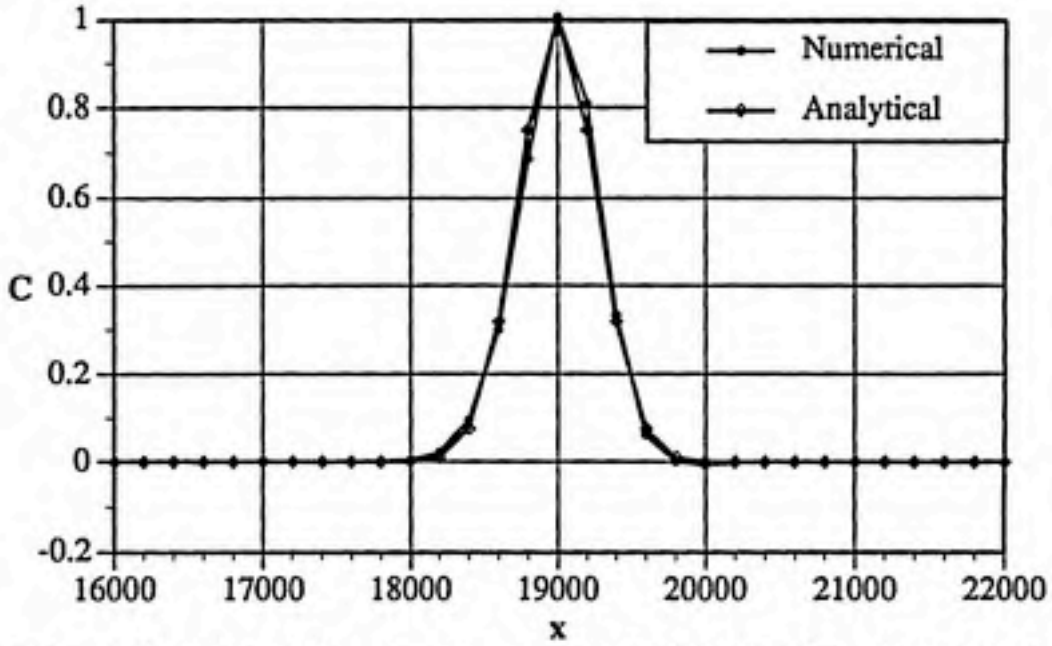

Fig. 5-4. GU model of a Gaussian source with $\overline{\sigma_x}$ =1.32, Pe=10^6,and Cr=0.8, after 100 timesteps. Optimized with $1 \leq \overline{\sigma_x} \leq 4$ in 0.01 increments. α_0=0.03480, α_1=0.22025, β_0=1.38410, and β_1=-0.00452.

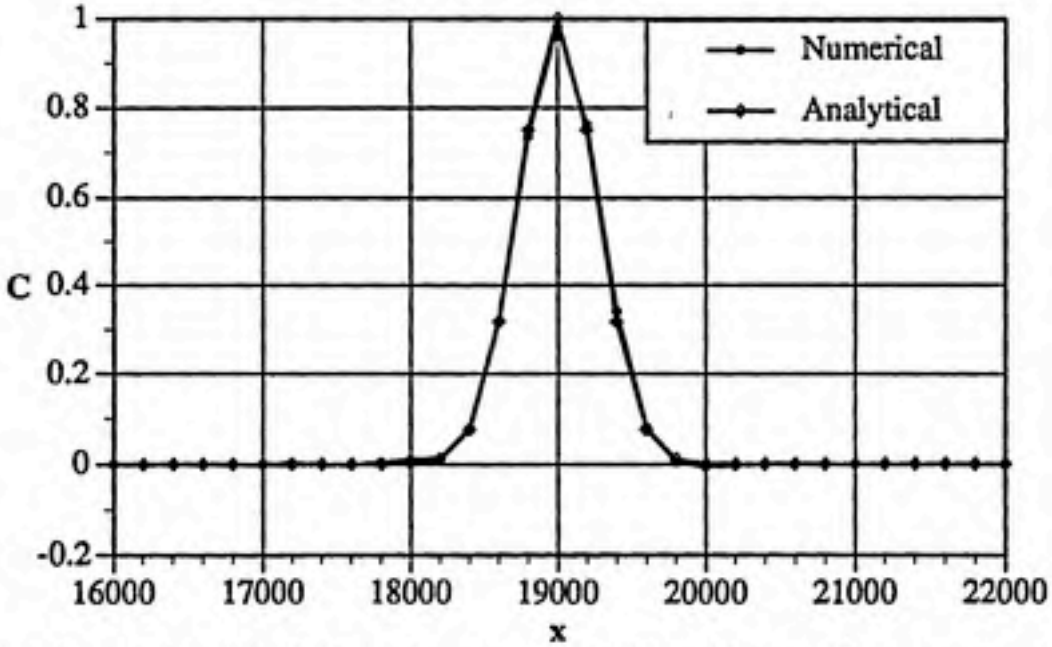

Fig. 5-5. GU model of a Gaussian source with $\overline{\sigma_x}$ =1.32, Pe=10^6,and Cr=0.8, after 100 timesteps. Optimized for $\overline{\sigma_x}$ =1.32 with α_0=0.03186, α_1=0.16249, β_0=1.36040, and β_1=0.00487.

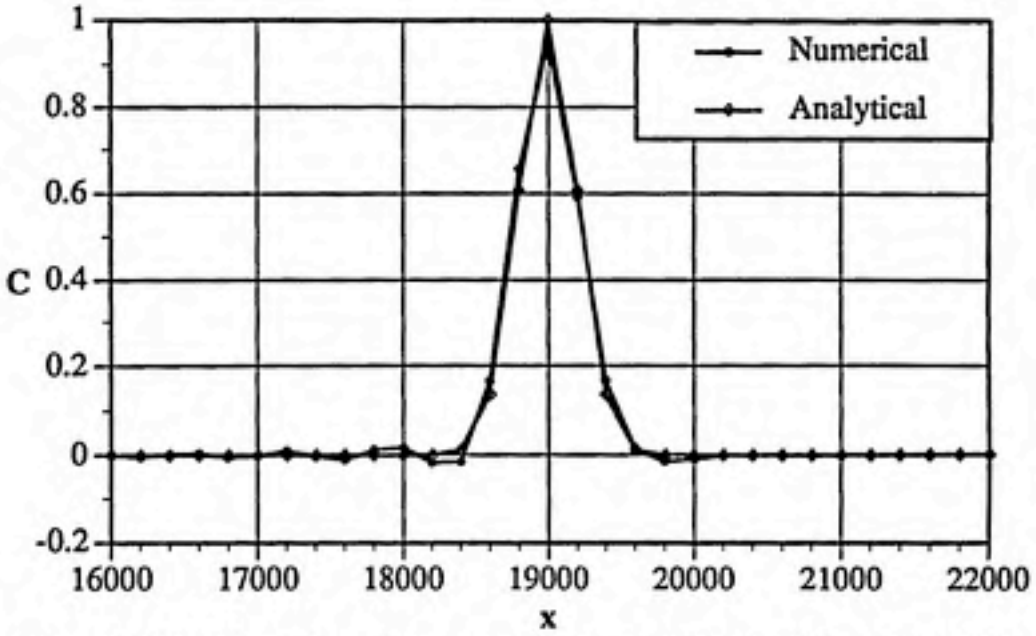

Fig. 5-6. GU model of a Gaussian source with σ_x =1.00, Pe=10^6,and Cr=0.8, after 100 timesteps. Optimized with $1 \leq \sigma_x \leq 4$ in 0.01 increments. α_0=0.03480, α_1=0.22025, β_0=1.38410, and β_1=-0.00452.

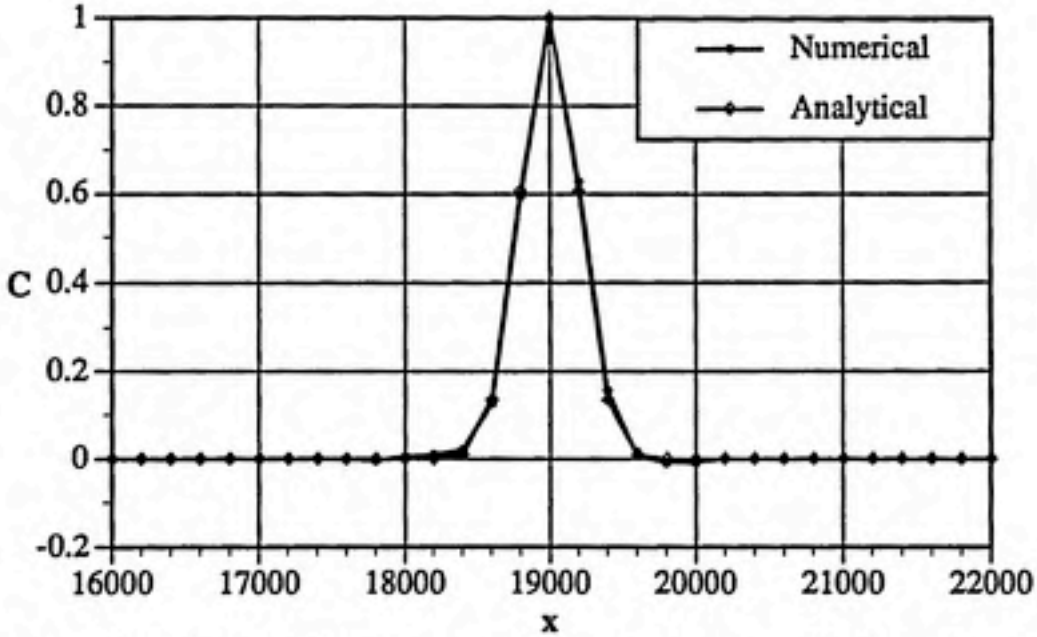

Fig. 5-7. GU model of a Gaussian source with σ_x =1.00, Pe=10^6,and Cr=0.8, after 100 timesteps. Optimized for σ_x =1.00 with α_0=0.03738, α_1=0.24529, β_0=1.42040, and β_1=0.00117.

Figures (5-6) and (5-7) provide similar conclusions for the case when the standard deviation of the source is equivalent to the element length. The quality of the source specific solution is just starting to degrade in this case, and a higher-order upwinding function may be required to provide accurate models of narrower peaks with sharper fronts.

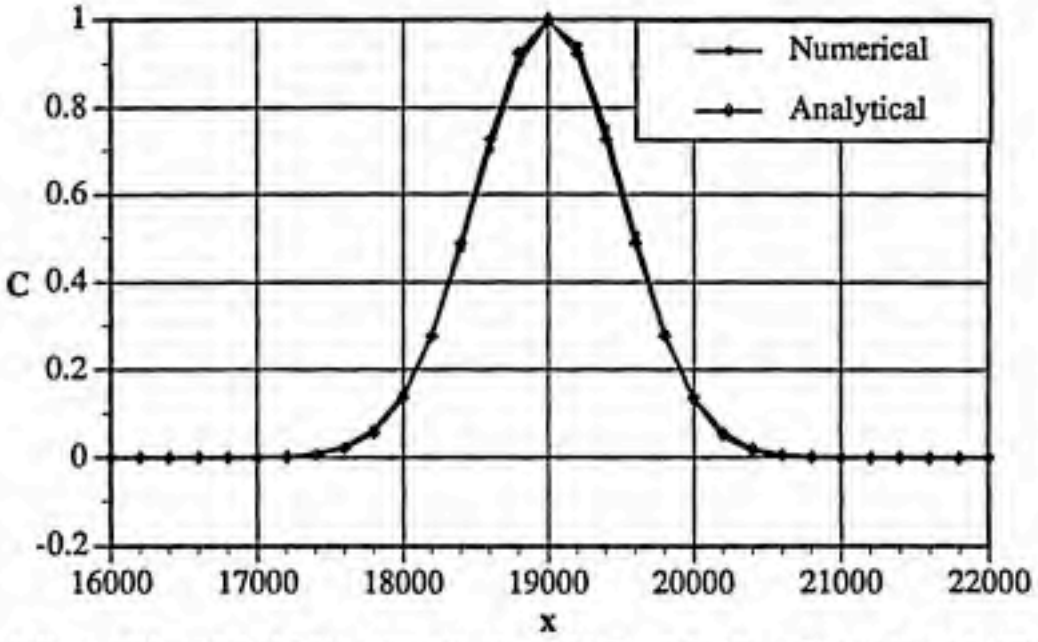

Fig. 5-8. GU model of a Gaussian source with $\bar{\sigma}_x$ =2.50, Pe=10^6,and Cr=0.8, after 100 timesteps. Optimized with $1 \le \bar{\sigma}_x \le 4$ in 0.01 increments. α_0=0.03480, α_1=0.22025, β_0=1.38410, and β_1=-0.00452.

Broader sources such as the one presented in Figure (5-8) are properly modeled by the general case, so sharpening the front is examined in Figure (5-9). In this case, the standard deviation of the source is three-fourths the length of an element, a problem that is not expected to be accurately modeled by a FE formulation, and optimization was carried out for $\bar{\sigma}_x$ =0.75, with a quadratic upwinding function. Linear upwinding functions were not observed to perform at this level of accuracy for this problem.

GU operates on problems that involve dispersion as shown in Figure (5-10). In this case, the source shown in Figure (5-1) is advected with Pe=200 for 375 timesteps, which results in a final normalized standard deviation of 2. Significant improvement is observed over the B-G solution, and the GU solution matches the exact solution nearly perfectly. The normalized standard deviations of the concentration profiles in this problem fall within the envelope that the parameters are optimized for: $1 \le \bar{\sigma}_x \le 2$. This situation is significant, as it demonstrates the ability of the GU method to accurately handle problems that have source conditions that change over time.

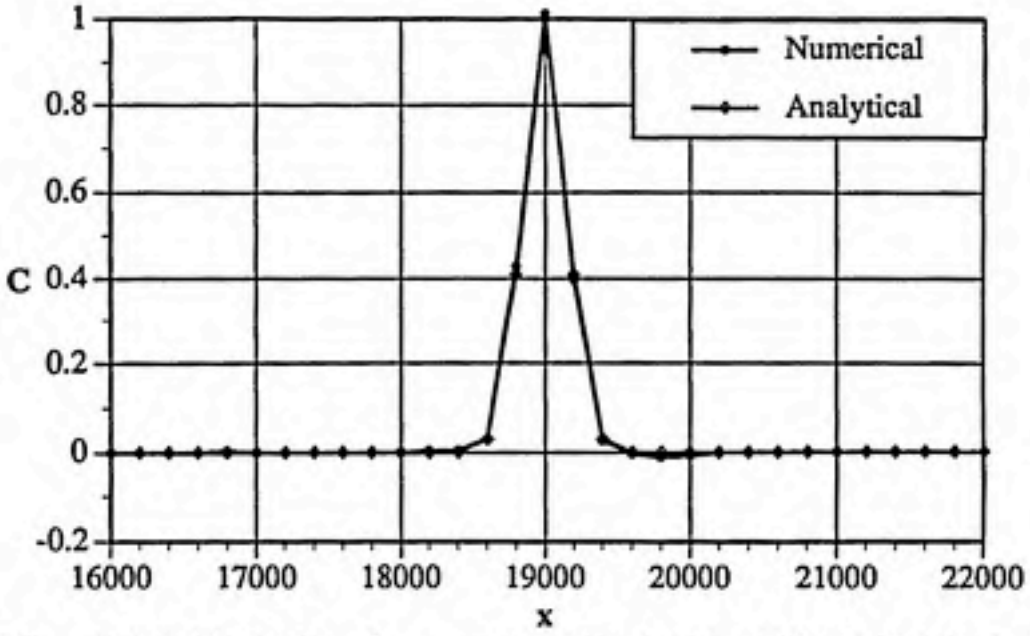

Fig. 5-9. GU model of a Gaussian source with σ_x =0.75, Pe=10^6, and Cr=0.8, after 100 timesteps. Optimized for σ_x =0.75 and a quadratic upwinding function with α_0=0.07743, α_1=0.36326, α_2=0.02873, β_0=1.57340, β_1=0.00236 and β_2=0.09475.

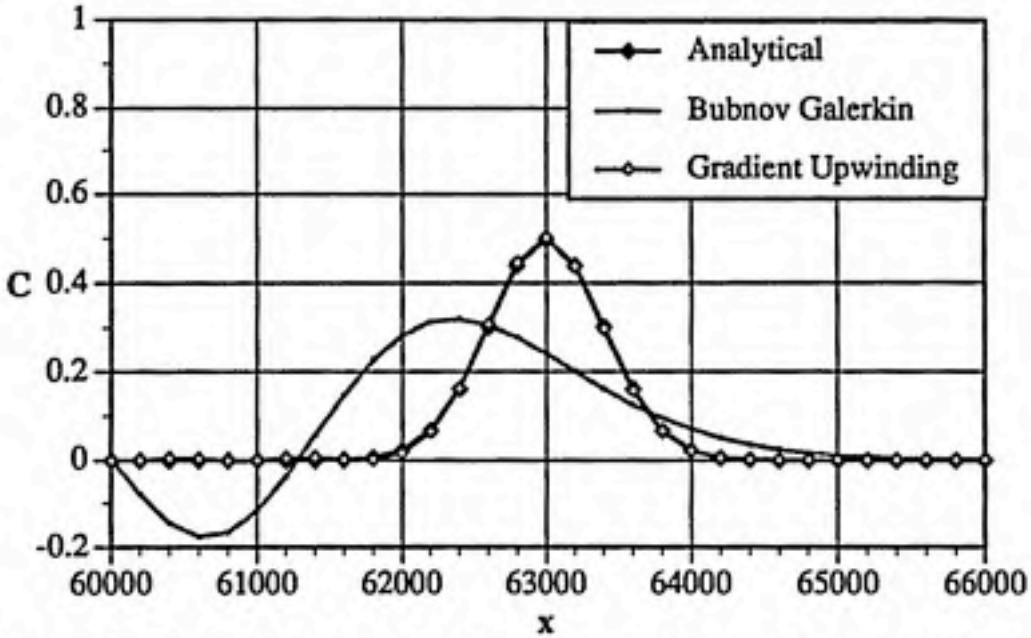

Fig. 5-10. GU model of a Gaussian source with σ_x =1.00, Pe=200, and Cr=0.8, after 375 timesteps. Optimized with $1 \le \sigma_x \le 2$ in 0.01 increments over 5 timesteps. α_0=0.00755, α_1=0.19659, β_0=1.3299, and β_1=-0.00945.

A step source model is presented in Figure (5-11). This is not an ideal step source, as it has been dispersed at Pe=20 for 20 timesteps before it is injected into the FE model as was done for the adapted models. It is important to note this excellent result was obtained with coefficients that were optimized for a Gaussian source, which also demonstrates the source independence of GU method coefficients. The gradients in the face of the step profile used here are similar to those contained in a Gaussian source with $\overline{\sigma_x}$ =2.0

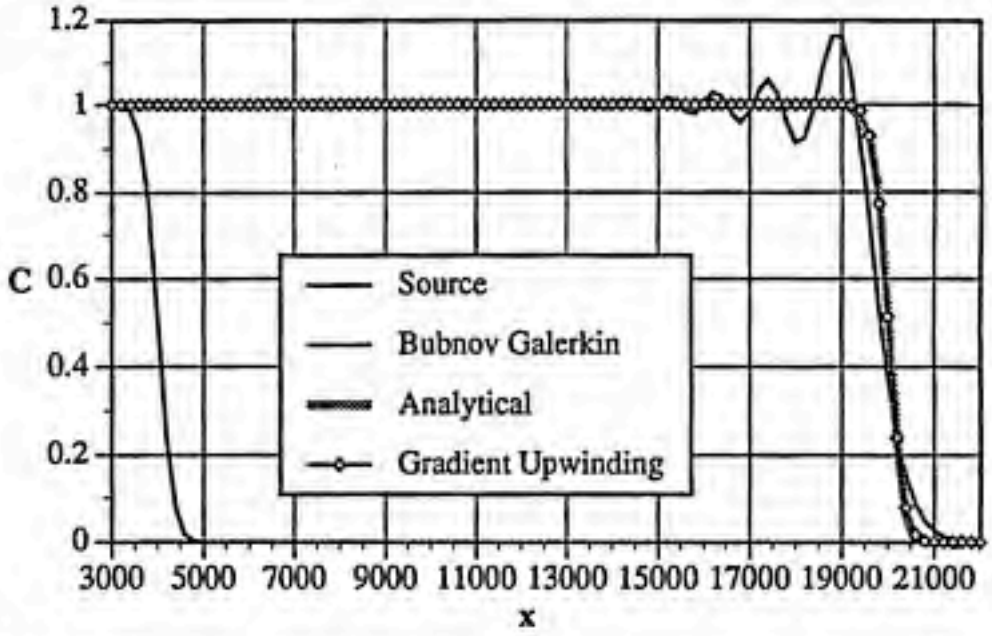

Fig. 5-11. GU model of a predispersed step source. The source is generated from an analytical solution with Pe=20 for 25 timesteps. The FE model continues at Cr=0.8 and Pe=10^6 for 100 timesteps. Parameters were optimized for a Gaussian source with $1 \leq \overline{\sigma_x} \leq 4$ in 0.01 increments. α_0=0.03480, α_1=0.22025, β_0=1.38410, and β_1=-0.00452.

GU models should execute at faster rates than *h*-adapted ones. Both methods generally require matrix refactoring at every timestep, but additional operations required by both methods are far simpler for GU models. It is possible to reduce the amount of refactoring required for either technique, but *h*-adaptive methods will generally require more computing time and space, due to management of the added nodes, which necessitate additional matrix operations. The adaptive method also requires solutions for concentration values in the refined space. Computation of element specific upwinding parameters for GU is a simple task relative to these operations. Comparison of execution times is not performed, as the mechanism that avoids refactoring certain portions of the matrices in the 1-D adaptive solutions was not implemented in the GU codes. While applicable to GU, this feature would

not be effective for 2-D and 3-D FE models, as their matrix hierarchy is not necessarily related to the advective path to the same extent as the 1-D case. In defense of *h*-adaptive methods, they may be more amenable to operating in parallel processing environments, which may provide a substantial increase in efficiency.

The nature of the optimal upwinding coefficients and the upwinding functions used in GU FE models both need to be explored. Problems with extremely sharp gradients such as ideal step sources and Gaussian sources with σ_x <1 either did not produce useful optimal upwinding parameters or simply did not converge. These problems may be addressed with different upwinding functions or alternate optimization strategies. Local minima may impede the optimization process, so different starting points may alleviate these problems. Optimal coefficients may be derived in a sequential fashion. In the case of the linear upwinding functions used here, this would amount to deriving optimal zero-order coefficients first in a two parameter optimization, and then using these values as starting points for zero-order coefficients in the four parameter optimization for linear upwinding functions. Other techniques may be applied to ensure that global minima are obtained at each optimization realization.

It is important that the bounds of applicability of this method be defined. While many of the problems mentioned in the preceding paragraph may be resolved with a more enlightened optimization approach, it is also possible that GU will produce useful enhancement of FE models for specific ranges of Cr, Pe, Da, and concentration gradients. Non-upwinded BG solutions are not as accurate as the GU solutions presented here, but the circumstances under which BG solutions misfire are easily described and are avoidable with an increase in computational overhead. Operation of GU in concert with adaptive methods may result in a significantly larger operational envelope than either of the individual methods.

The final step in this research is to describe optimal upwinding coefficients as a function of dimensionless model parameters such as Cr, Da, and Pe as described in the section on Taylor series analysis. The linear upwinding function applied here produces four coefficients for every combination of Cr, Da, and Pe. If enough of these coefficients are generated at different parameter combinations, they may be fitted to functions of the parameters, which can then be used to provide optimal upwinding coefficients for appropriate values of Cr, Da, and Pe.

6 CONCLUSIONS AND RECOMMENDATIONS

It is possible to improve the performance of FE ADR transport models through the use of higher-order basis functions, adaptive methods, and upstream weighting. These methods improve FE accuracy with different amounts of computational expense and algorithmic complexity. In attempting to enhance FE methods, it is desirable to avoid excessive operational costs or theoretical constraints on the solution relative to the well understood BG method.

As shown in the section on adapted models, FE models with quadratic basis functions can provide an improvement in performance over solutions that use linear basis functions. The accuracy of models that use quadratic basis functions is regulated by the same Pe and Cr limits, however. For this reason, the linear case may be a better option for this class of problems since it can deliver results of similar quality with lower computational overhead than quadratic models when Cr and Pe limits are observed.

Adaptive mesh schemes allow FE models to circumvent the Cr and Pe limits by observing them only in regions of the domain that contain error, or in the case of the ADR equation, sharp fronts. Adaptive 1-D models were developed in this work with linear and quadratic finite elements, and impressive results were obtained from these models. Predispersed step and Gaussian sources were accurately modeled. Quadratic basis function *h*-adaptive models were observed to deliver similar results as those from linear basis functions, with longer execution times and larger memory requirements.

There are two drawbacks with mesh refinement schemes. Shortening element length reduces the Pe, but also increases the Cr. This tradeoff limits the utility of mesh refinement, as the range of applicability of the method is constrained by this relationship. Furthermore, mesh refinement necessitates node renumbering algorithms that significantly increase computational expense. The mesh refinement algorithm explored in this work was selected because of its special handling of the renumbering problem. This advantage was observed to be diminished in 2-D and 3-D implementations, due to consideration of nodes that lie on

interelement boundaries. The relative efficiency of 2-D and 3-D implementations of this adaptive method to general global matrix recomposition and other *h*-adaptive methods were not compared, but it is not unreasonable to assume that these methods would have similar performance levels and computational requirements.

A final issue that was not addressed here relates to error estimation and appropriate response to error in adaptive modeling systems. The location of elements that modify their meshes or basis function order and the degree of such responses are issues that are under active study. Adaptive methods were demonstrated in this work to reduce error through the use of primitive error indicator and response mechanisms. The solution quality was also observed to be sensitive to the magnitude of the error indicator, especially in the case of the Gaussian source. Continuing work in this field is directed at developing more sophisticated adaptive methods that minimize as opposed to simply reducing the error in the solution.

6.1 Uniform upwinding

The starting point of the upstream weighting section of this work was the formulation presented by Westerink and Shea (1989). This method uses weighting functions that are composed of the basis functions as well as two modifying functions that are weighted with dimensionless upwinding parameters. Mathematical analysis of the FE formulation was performed by these investigators to identify optimal upwinding parameters. Taylor series analysis was carried out to the fifth-order term for nondispersed problems, as well as Fourier analysis. These analyses yielded general observations about the nature of optimal parameters, and model output was based on optimal parameters obtained by numerical experimentation.

These optimal parameters were reproduced and possibly improved on in this work with a more formal approach that employed LM minimization of the Euclidean norm of the residuals between the numerical and analytical solutions at each node. The LM derived optimal parameters tended to result in better peak representation of Gaussian sources with a bit more oscillation than did the values provided by Westerink and Shea. Both methods did not perform well when the standard deviation of the source was changed from the value used to optimize the upwinding parameters.

It was hoped that extension of their mathematical analyses with automated techniques provided by Mathematica would provide a description of optimal upwinding parameters in terms of dimensionless model parameters. Taylor series analysis that included fifteenth-order terms showed that these and higher-order terms may be significant

contributors to descriptions of FE model truncation error. It was also noted that the order of the most significant term was a function of problem parameters. Furthermore, both analysis techniques demonstrated that the gradient across each element is an important factor in such descriptions of FE truncation error. This observation, coupled with FE model output demonstrated that optimal upwinding is also a function of this gradient. This observation led to a novel upwinding technique.

6.2 Gradient upwinding

The upwinding parameters used in this method are generated on an element specific level. Upwinding functions use the concentration gradient across the element and predetermined coefficients to determine the upwinding parameter for each element. These coefficients are, in turn, a function of the dimensionless modeling parameters and were determined in this work through the use of LM optimization. Most of the results presented here use a linear upwinding function, which requires four coefficients.

The results indicate that GU is a significant improvement over uniformly applied PG upwinding. Specific problems were modeled more accurately with GU than with uniformly upwinded models, and variations in source conditions were handled without major degradation of solution quality. Extremely sharp front problems were also properly modeled. Correct modelling of dispersive problems demonstrated the adaptability of this method to changing source conditions during model operation. The method appears to be generalizable, as a step source was accurately modeled with optimal upwinding coefficients that were optimized for a Gaussian source.

The next step in this research is to describe optimal upwinding coefficients as a function of model parameters such as Cr, Da, and Pe. The linear upwinding function applied here produces four coefficients for every combination of model parameters. If enough of these coefficients are generated at different combinations of model parameters, and they behave in an amenable fashion, they can be fitted to functions of these parameters. These functions can then be used to provide optimal upwinding coefficients for an appropriate set of model parameters. This is a large, labor intensive problem that will require a significant amount of time to complete. It is therefore advisable to examine some of the following issues first before proceeding with massive numbers of optimization runs and fitting attempts.

There are many directions to be explored in regard to the upwinding functions which guide the upwinding condition in response to gradients. Upwinding functions of the general form presented here as well as others may be applied to this method. The quadratic

upwinding function that provided the results shown in Figure (5-10) requires six coefficients. Producing them for a single set of model parameters requires a significant amount of computer time, and fitting them will require even more. It may be possible to produce the same excellent results without so many coefficients. This is especially desirable for end use applications, as FE models that use this method will be required to calculate upwinding conditions for each element at each timestep, and the simpler these operations are, the lower the computational overhead will be. While the use of other classes of upwinding functions are of interest, alternate basis functions may also provide an interesting line of investigation.

The optimization method used to generate upwinding coefficients for ranges of standard deviations should also be examined. The goal of this process is to optimize the upwinding coefficients for as broad a continuous range of gradients as necessary. This may be a way to make linear upwinding functions competitive with quadratic ones for sharper front problems. Optimization over a range of time steps provides more continuity in the range of gradients, so it should improve the quality of both schemes. Triangular sources may be more appropriate for optimization than the Gaussian ones used up to this point, due to an increase in control over the composition of the scope of gradients that the upwinding coefficients will be optimized for.

The range of model parameters over which the upwinding scheme may provide optimal and useful solutions will have to be defined for each upwinding function. Extremely sharp fronts made optimization convergence unpredictable, and inappropriate coefficients were produced. In these cases, it is entirely possible that the global minimum was not located. Multiple local minima for the L-2 norm of these residuals have been observed in seeking optimal values for coefficients of linear upwinding functions. It is also possible that the limits of applicability of this method or upwinding function have been reached in these cases. Furthermore, it may also be that the limit of accuracy of Eulerian methods in general has been reached for this particular set of modeling parameters. In this case, the combination of GU and adaptive methods may provide a modeling scheme that has a broader range of applicability.

The final step in this process is to accurately express the upwinding coefficients as a function of dimensionless model parameters. Preliminary results indicate that such a relationship is not a simple function of Cr and Pe. In response to this situation, it may be discovered that optimization techniques other than Levenberg-Marquardt may be more appropriate for this problem. Other upwinding functions may provide upwinding

configurations that may not be as powerful as some, but if they are easily described, they may be more useful. An approach that uses a look-up table and interpolation may be a viable alternative for this problem. The range of applicability of an upwinding function is therefore constrained in two places: Can it produce a useful upwinding configuration for a given combination of Cr, Pe, and Da, and then can it then be accurately described by a function of these parameters.

Advection-dominated flow is not the only process that results in sharp fronts in ADR transport. Reaction terms may result in sharp fronts, even in the case when there is no net advection (Tezduyar and Park, 1986; Tezduyar et al., 1987). FE models of highly reactive processes will oscillate in the same way as advection-dominated problems. While this process was not explored in this work, it is a natural extension of this method to describe optimal upwinding parameters in the context of problems involving first order reactions.

Extension of this upwinding method to 2-D and 3-D applications is not a straightforward process. As mentioned earlier, the problems posed by flow that is not aligned with the FE grid results in oscillations and numerical dispersion. This problem has been addressed by a number of investigators. The method proposed by Westerink and Cantekin is an appropriate candidate for the extension of GU to higher dimension problems (Cantekin and Westerink, 1990), as well as the SU/PG methods.

In closing, the observations reported in this work indicate that a practical and generalizable upwinding scheme may exist that is not a fragile experimental technique of limited applicability. The arguments proposed by earlier critics of upwinding have not been entirely put to rest, as there is a definite need for further theoretical development to explain the results presented here. Many interesting questions remain to be addressed in this line of research. The answers to these questions will provide useful information regarding the performance of upwinded finite elements and Eulerian models in general. A simple means of generating optimally upwinded 2-D and 3-D FE models of sharp fronts in ADR transport is the ultimate goal of this investigation.

REFERENCES

Abdel-Hadi, E. A. A., Hsu, T. R., and Bhatia, K. S., "Upwind Finite Element Analysis of Advection-Diffusion Equation," In Numerical Methods in Thermal Problems: *Proceedings of the Fourth International Conference*, Swansea, Wales, Pineridge Press, Vol. 1, pp. 756-770, (1985).

Abelson, P. A. "Desalination of Brackish and Marine Waters," Science, Vol. 251, No. 4999, pp. 1289. (1991).

Adjerid, S., and Flaherty, J. E. "A Moving Finite Element Method With Error Estimation and Refinement for One-Dimensional Time Dependent Partial Differential Equations," SIAM Journal of Numerical Analysis, Vol. 23, No. 4, pp. 778-795. (1986).

Adornato, P. M., and Brown, R. A. "Petrov-Galerkin Methods for Natural Convection in Directional Solidification of Binary Alloys," International Journal for Numerical Methods in Fluids, Vol. 7, pp. 761-791. (1987).

Allen, M. B., and Curran, M. C. "Adaptive Local Grid Refinement Algorithms for Finite-Element Collocation," Numerical Methods for Partial Differential Equations, Vol. 5, pp. 121-132. (1989).

Ames, W. F., Numerical Methods for Partial Differential Equations 2nd ed., Barnes & Noble, New York, 1977.

Arney, D. C., and Flaherty, J. E. "An Adaptive Local Mesh Refinement Method for Time-Dependent Partial Differential Equations," Applied Numerical Mathematics, Vol. 5, pp. 257-274. (1989).

Babuska, I., and Szabo, B. "On the Rates of Convergence of the Finite Element Method," International Journal for Numerical Methods in Engineering, Vol. 18, pp. 323-341. (1982).

Barrett, J. W., and Morton, K. W. "Approximate Symmetrization and Petrov-Galerkin Methods for Diffusion-Convection Problems," Computer Methods in Applied Mechanics and Engineering, Vol. 45, pp. 97-122. (1984).

Baskharone, E. A. "Finite-Element Analysis of Turbulent Flow in Annular Exhaust Diffusers of Gas Turbine Engines," Transactions of the ASME, Vol. 113, pp. 104-110. (1991).

Basu, P. K., and Peano, A. "Adaptivity in *p*-version Finite Element Analysis," Journal of Structural Engineering, Vol. 109, No. 10, pp. 2310-2324. (1983).

Bear, J., Hydraulics of Groundwater, McGraw-Hill, New York, 1979.

Benim, A. C. "Finite Element Analysis of Confined Turbulent Swirling Flows," International Journal for Numerical Methods in Fluids, Vol. 11, pp. 697-717. (1990).

Berger, M. J., and Oliger, J. "Adaptive Mesh Refinement for Hyperbolic Partial Differential Equations," Journal of Computational Physics, Vol. 53, pp. 484-512. (1984).

Bermudez, A., Durany, J., Posse, M., and Vázquez, C. "An Upwind Method for Solving Transport-Diffusion-Reaction Systems," International Journal for Numerical Methods in Engineering, Vol. 28, pp. 2021-2039. (1989).

Bieterman, M., and Babuska, I. "The Finite Element Method for Parabolic Equations. II. A Posteriori Error and Adaptive Approach," Numerische Mathematik, Vol. 40, pp. 373-406. (1982).

Bouloutas, E. T., and Celia, M. A., "An Analysis of Some Classes of Petrov-Galerkin and Optimal Test Function Methods," In Numerical Methods for Transport and Hydrologic Processes, *Proceedings of the Seventh International Conference on Computational Methods in Water Resources*, M. A. Celia, L. A. Ferrand, C. A. Brebbia, W. G. Gray, and G. F. Pinder Eds., Cambridge, MA, Elsevier, Vol. 2, pp. 15-20, (1988).

Bramble, J. H., Ewing, R. E., Pasciak, J. E., and Schatz, A. H. "A Preconditioning Technique for the Efficient Solution of Problems with Local Grid Refinement," International Journal for Numerical Methods in Engineering, Vol. 67, pp. 1988. (1988).

Brueckner, F. P., and Heinrich, J. C. "Petrov-Galerkin Finite Element Model for Compressible Flows," International Journal for Numerical Methods in Engineering, Vol. 32, pp. 255-274. (1991).

Burdette, S. R., Coates, P. J., Armstrong, R. C., and Brown, R. A. "Calculations of Viscoelastic Flow Through an Axisymmetric Corrugated Tube Using the Explicitly Elliptic Momentum Equation Formulation (EEME)," Journal of Non-Newtonian Fluid Mechanics, Vol. 33, pp. 1-23. (1989).

Burkart, M. R., Onstad, C. A., and Bubenzer, G. D. "Research on Agrichemicals in Water Resources," Eos, Vol. 71, No. 29, pp. 980-981 ,988-989. (1990).

Cantekin, M. E., and Westerink, J. J. "Non-Diffusive N+2 Degree Petrov-Galerkin Methods For Two-Dimensional Transient Transport Computations," International Journal for Numerical Methods in Engineering, Vol. 30, pp. 397-418. (1990).

Carey, G. F., and Seager, M. "Projection and Iteration in Adaptive Finite Element Refinement," International Journal for Numerical Methods in Engineering, Vol. 21, pp. 1681-1695. (1985).

Christie, I., Griffiths, D. F., and Mitchell, A. R. "Finite Element Methods for Second Order Differential Equations with Significant First Derivatives," International Journal for Numerical Methods in Engineering, Vol. 10, pp. 1389-1396. (1976).

Christie, I., and Mitchell, A. R. "Upwinding of High Order Galerkin Methods in Conduction-Convection Problems," International Journal for Numerical Methods in Engineering, Vol. 12, pp. 1764-1771. (1978).

Cohen, R. "Cosmos Engineering Application Retooled," MacWeek, Vol. 6, No. 10, pp. 9. (1992).

Conservation Foundation, "Groundwater: Saving The Unseen Resource," Conservation Foundation, Washington, D.C., (1985).

Cornew, F. H., and Miller, C. T., "An Adaptive Petrov-Galerkin Finite-Element Method for Approximating the Advective-Dispersive-Reactive Equation," In Computational Methods in Subsurface Hydrology, *Proceedings of the Eighth International Conference on Computational Methods in Water Resources*, G. Gambolati, A. Rinaldo, C. A. Brebbia, W. G. Gray, and G. F. Pinder Eds., Venice, Italy, Computational Mechanics Publications/Springer-Verlag, Vol. 1, pp. 437-442, (1990).

Darcy, H., Les Fontaines Publiques de la Ville de Dijon, Victor Dalmont, Paris, 1856.

de Oliveira, P., and Oliveira, F. A. "On a Theoretical Justification of Adaptive Gridding for Finite Difference Approximations," International Series of Numerical Mathematics, Vol. 86, pp. 391-401. (1988).

de S.R. Gago, J. P., Kelly, D. W., and Zienkiewicz, O. C. "*A Posteriori* Error Analysis and Adaptive Processes in the Finite Element Method: Part II-Adaptive Mesh Refinement," International Journal for Numerical Methods in Engineering, Vol. 19, pp. 1621-1656. (1983).

de Sampaio, P. A. B. "A Petrov-Galerkin/Modified Operator Formulation for Convection-Diffusion Problems," International Journal for Numerical Methods in Engineering, Vol. 30, pp. 331-347. (1990).

de Sampaio, P. A. B. "A Petrov-Galerkin Formulation for the Incompressible Navier-Stokes Equations Using Equal Order Interpolation for Velocity and Pressure," International Journal for Numerical Methods in Engineering, Vol. 31, pp. 1135-1149. (1991).

Demkowicz, L., Devloo, P., and Oden, J. T. "On an *h*-Type Mesh-Refinement Strategy Based on Minimization of Interpolation Errors," Computer Methods in Applied Mechanics and Engineering, Vol. 53, pp. 67-89. (1985).

Demkowicz, L., and Oden, J. T. "An Adaptive Characteristic Petrov-Galerkin Finite Element Method for Convection-Dominated Linear and Nonlinear Parabolic Problems in Two Space Variables," Computer Methods in Applied Mechanics and Engineering, Vol. 55, pp. 63-87. (1986a).

Demkowicz, L., and Oden, J. T. "On a Mesh Optimization Method Based on a Minimization of Interpolation Error," International Journal of Engineering Science, Vol. 24, No. 1, pp. 55-68. (1986b).

Demkowicz, L., Oden, J. T., Rachowicz, W., and Hardy, O. "Toward a Universal *h-p* Adaptive Finite Element Strategy. Part 1. Constrained Approximation and Data Structure," Computer Methods in Applied Mechanics and Engineering, Vol. 77, pp. 79-112. (1989).

Devloo, P., Oden, J. T., and Strouboulis, T. "Implementation of an Adaptive Refinement Technique for the SUPG Algorithm," Computer Methods in Applied Mechanics and Engineering, Vol. 61, pp. 339-358. (1987).

Dick, E. "Accurate Petrov-Galerkin Methods for Transient Convective Diffusion Problems," International Journal for Numerical Methods in Engineering, Vol. 19, pp. 1425-1433. (1983).

Dickinson, B., "Officials Say Leaks a Growing Danger," Chapel Hill/Durham Herald-Sun, pp. 1-2, (12/23/90).

Donea, J., Giuliani, S., Laval, H., and Quartapelle, L. "Time Accurate Solution of Advection-Diffusion Problems by Finite Elements," Computer Methods in Applied Mechanics and Engineering, Vol. 45, pp. 123-145. (1984).

Dorr, M. R. "The Approximation Theory for the *p*-Version of the Finite Element Method," SIAM Journal of Numerical Analysis, Vol. 21, No. 6, pp. 1180-1207. (1984).

Dutra Do Carmo, E. G., and Galeão, A. C. "Feedback Petrov-Galerkin Methods for Convection-Dominated Problems," Computer Methods in Applied Mechanics and Engineering, Vol. 88, pp. 1-16. (1991).

Eliason, M., "Water well suggests ancient man smarter than we thought," The Durham Sun, pp. 8-A, (10/1/90).

Environmental Protection Agency, "Septic Systems and Ground Water Protection: An Executive's Guide," E.P.A. Office of Groundwater Protection, Washington D.C., (1986).

Espedal, M. S., and Ewing, R. E. "Characteristic Petrov-Galerkin Subdomain Methods for Two-Phase Immiscible Flow," Computer Methods in Applied Mechanics and Engineering, Vol. 64, pp. 113-135. (1987).

Galeão, A. C., and Dutra do Carmo, E. G. "A Consistent Approximate Upwind Petrov-Galerkin Method for Convection-Dominated Problems," Computer Methods in Applied Mechanics and Engineering, Vol. 68, pp. 83-85. (1988).

Ganjoo, D. K., and Tezduyar, T. E. "Petrov-Galerkin Formulations for Electrochemical Processes," Computer Methods in Applied Mechanics and Engineering, Vol. 65, pp. 61-83. (1987).

Garbow, B. S., Hillstrom, K. E., and More, J. J., MINPACK Project, Argonne National Laboratory, 1980.

Givoli, D. "Non-Local and Semi-Local Optimal Weighting Functions for Symmetric Problems Involving a Small Parameter," International Journal for Numerical Methods in Engineering, Vol. 26, pp. 1281-1298. (1988).

Gray, W. G., and Pinder, G. F. "An Analysis of the Numerical Solution of the Transport Equation," Water Resources Research, Vol. 12, No. 3, pp. 547-555. (1976).

Gresho, P., and Lee, R. L., "Don't Suppress the Wiggles-They're Telling You Something," In Finite Element Methods for Convection Dominated Flows, *Proceedings of the Winter Annual Meeting of the American Society of Mechanical Engineers*, T. J. R. Hughes Ed., New York, ASME, Vol. AMD-34, pp. 37-62, (1979).

Griffiths, D. F., and Mitchell, A. R., "On Generating Upwind Finite Element Methods," In Finite Element Methods for Convection Dominated Flows, *Proceedings of the Winter Annual Meeting of the American Society of Mechanical Engineers*, T. J. R. Hughes Ed., New York, ASME, Vol. AMD-34, pp. 91-104, (1979).

Gui, W., and Babuska, I. "The *h*, *p*, and *h-p* Versions of the Finite Element Method in 1 Dimension: Part III. The Adaptive *h-p* Version," Numerische Mathematik, Vol. 49, pp. 659-683. (1986a).

Gui, W., and Babuska, I. "The *h*, *p*, and *h-p* Versions of the Finite Element Method in 1 Dimension: Part I. The Error Analysis of the *p*-Version," Numerische Mathematik, Vol. 49, pp. 577-612. (1986b).

Guymon, G. L., Scott, V. H., and Herrmann, L. R. "A General Numerical Solution of the Two-Dimensional Diffusion-Convection Equation by the Finite Element Method.," Water Resources Research, Vol. 6, No. 6, pp. 1161-1617. (1970).

Heinrich, J., and Zienkiewicz, O. C., "The Finite Element Method and 'Upwinding' Techniques in the Numerical Solution of Convection Dominated Flow Problems," In Finite Element Methods for Convection Dominated Flows, *Proceedings of the Winter Annual Meeting of the American Society of Mechanical Engineers*, T. J. R. Hughes Ed., New York, ASME, Vol. AMD-34, pp. 105-136, (1979).

Heinrich, J. C., Huyakorn, P. S., Zienkiewicz, O. C., and Mitchell, A. R. "An 'Upwind' Finite Element Scheme for Two- Dimensional Convective Transport Equation," International Journal for Numerical Methods in Engineering, Vol. 11, pp. 131-143. (1977).

Heinrich, J. C., and Zienkiewicz, O. C. "Quadratic Finite Element Schemes for Two-Dimensional Convective-Transport Problems," International Journal for Numerical Methods in Engineering, Vol. 11, pp. 1831-1844. (1977).

Hughes, T. J. R. "A simple Scheme for Developing 'Upwind' Finite Elements," International Journal for Numerical Methods in Engineering, Vol. 12, pp. 1359-1365. (1978).

Hughes, T. J. R. "Recent Progress in the Development and Understanding of SUPG Methods with Special Reference to the Compressible Euler and Navier-Stokes Equations," International Journal for Numerical Methods in Fluids, Vol. 7, pp. 1261-1275. (1987).

Hughes, T. J. R., and Brooks, A., "A Multi-Dimensional Upwind Scheme With No Crosswind Diffusion," In Finite Element Methods for Convection Dominated Flows, *Proceedings of the Winter Annual Meeting of the American Society of Mechanical Engineers*, T. J. R. Hughes Ed., New York, ASME, Vol. AMD-34, pp. 19-36, (1979).

Hughes, T. J. R., Mallet, M., and Mizukami, A. "A New Finite Element Formulation for Computational Fluid Dynamics: II. Beyond SUPG," Computer Methods in Applied Mechanics and Engineering, Vol. 54, pp. 341-355. (1986).

Huyakorn, P. S., and Pinder, G. F., Computational Methods in Subsurface Flow, Academic Press, San Diego, CA, 1983.

Imre, L., and Környev, T. "Computer Simulation of Salami Drying," International Journal for Numerical Methods in Engineering, Vol. 30, pp. 767-777. (1990).

Istok, J., Groundwater Modeling by the Finite Element Method, American Geophysical Union, Washington, D.C., 1989.

Kelly, D. W., de S.R. Gago, J. P., and Zienkiewicz, O. C. "*A Posteriori* Error Analysis and Adaptive Processes in the Finite Element Method: Part I-Error Analysis," International Journal for Numerical Methods in Engineering, Vol. 19, pp. 1593-1619. (1983).

Kelly, D. W., Nakazawa, S., and Zienkiewicz, O. C. "A Note on Upwinding and Anisotropic Balancing in Finite Element Approximations to Convective Diffusion Problems," International Journal for Numerical Methods in Engineering, Vol. 15, pp. 1705-1711. (1980).

Kikuchi, N. "Adaptive Grid-Design Methods for Finite Element Analysis," Computer Methods in Applied Mechanics and Engineering, Vol. 55, pp. 129-160. (1986).

Langtangen, H. P. "Implicit Finite Element Methods for Two-Phase Flow in Oil Reservoirs," International Journal for Numerical Methods in Fluids, Vol. 10, pp. 651-681. (1990).

Lantz, R. B. "Quantitative Evaluation of Numerical Diffusion (Truncation Error)," Soc. Pet. Eng. J., Vol. 251, pp. 315-320. (1971).

Leonard, B. P. "A Stable and Accurate Convective Modelling Procedure Based on Quadratic Upstream Interpolation," Computer Methods in Applied Mechanics and Engineering, Vol. 19, pp. 59-98. (1979a).

Leonard, B. P., "A Survey of Finite Differences of Opinion on Numerical Muddling of the Incomprehensible Defective Confusion Equation," In Finite Element Methods for Convection Dominated Flows, *Proceedings of the Winter Annual Meeting of the American Society of Mechanical Engineers*, T. J. R. Hughes Ed., New York, ASME, Vol. AMD-34, pp. 1-18, (1979b).

Levi, B. G. "Hanford Seeks Short- and Long-Term Solutions to its Legacy of Waste," Physics Today, Vol. 45, No. 3, pp. 17-21. (1992).

Liou, J., Deans, H. A., and Tezduyar, T. E. "Finite Element Simulation of Deep-Well Wet-Oxidation Reactor," Journal of Engineering Mechanics, Vol. 116, No. 8, pp. 1780-1797. (1990).

Liou, J., and Tezduyar, T. E. "Iterative Adaptive Implicit-Explicit Methods for Flow Problems," International Journal for Numerical Methods in Fluids, Vol. 11, pp. 867-880. (1990).

Loula, A. F. D., Hughes, T. J. R., and Franca, L. P. "Petrov-Galerkin Formulations of the Timoshenko Beam Problem," Computer Methods in Applied Mechanics and Engineering, Vol. 63, pp. 115-132. (1987).

Marechal, Y., and Meunier, G. "Computation of 2D and 3D Eddy Currents in Moving Conductors of Electromagnetic Retarders," IEEE Transactions on Magnetics, Vol. 26, No. 5, pp. 2382-2384. (1990).

Mikhlin, S. G., Variational Methods in Mathematical Physics, (T. Boddington, Trans.)., Pergamon, New York, 1964.

Mittal, S., Deans, H. A., and Tezduyar, T. E. "Numerical Simulation of Deep-Well Wet Oxidation Reactor Using Steam," Journal of Engineering Mechanics, Vol. 117, No. 4, pp. 798-819. (1991).

Mizukami, A. "An Implementation of the Streamline-Upwind-Petrov-Galerkin Method for Linear Triangular Elements," International Journal for Numerical Methods in Engineering, Vol. 49, pp. 357-364. (1985).

Mizukami, A., and Hughes, T. J. R. "A Petrov-Galerkin Finite Element Method for Convection-Dominated Flows: An Accurate Upwinding Technique for Satisfying the Maximum Principle," International Journal for Numerical Methods in Engineering, Vol. 50, pp. 181-193. (1985).

Neuman, S. P., "Adjoint Petrov-Galerkin Method with Optimum Weight and Interpolation Functions Defined on Multi-Dimensional Nested Grids," In Computational Methods in Surface Hydrology, *Proceedings of the Eighth International Conference on Computational Methods in Water Resources*, G. Gambolati, A. Rinaldo, C. A. Brebbia, W. G. Gray, and G. F. Pinder Eds., Venice, Italy, Computational Mechanics Publications and Springer-Verlag, , pp. 347-356, (1990).

Oden, J. T., Demkowicz, L., Rachowicz, W., and Westermann, T. A. "Toward a Universal *h-p* Adaptive Finite Element Strategy. Part 2.A Posteriori Error Estimation," Computer Methods in Applied Mechanics and Engineering, Vol. 77, pp. 113-180. (1989).

Pinder, G. F., and Gray, W. G., Finite Element Simulation in Surface and Subsurface Hydrology 1st ed., Academic Press, New York, 1977.

Pini, G., and Gambolati, G., "3-D Finite Element Transport Models by Upwind Preconditioned Conjugate Gradients," In Numerical Methods for Transport and Hydrologic Processes, *Proceedings of the Seventh International Conference on Computational Methods in Water Resources*, M. A. Celia, L. A. Ferrand, C. A. Brebbia, W. G. Gray, and G. F. Pinder Eds., Cambridge, MA, Elsevier, Vol. 2, pp. 35-43, (1988).

Press, W. H., Flannery, B. P., Teukolsky, S. A., and Vetterling, W. T., Numerical Recipes (FORTRAN version) 1st ed., Cambridge University Press, Cambridge, England, 1989.

Price, H. S., Cavendish, J. C., and Varga, R. S. "Numerical Methods of Higher-Order Accuracy for Diffusion-Convection Equations," Soc. Petrol. Eng. J., Vol. 8, No. 3, pp. 293-303. (1968).

Prickett, T. A., Naymik, T. G., and Lonnquist, C. G., "A "Random-Walk" Solute Transport Model for Selected Groundwater Quality Evaluations," Bulletin No. 65, Illinois State Water Survey, Champaign, IL, (1981).

Rachowicz, W., Oden, J. T., and Demkowicz, L. "Toward a Universal *h-p* Adaptive Finite Element Strategy. Part 3. Design of *h-p* Meshes," Computer Methods in Applied Mechanics and Engineering, Vol. 77, pp. 181-212. (1989).

Rajagopalan, D., Armstrong, R. C., and Brown, R. A. "Calculation of Steady Viscoelastic Flow Using a Multimode Maxwell Model: Application of the Explicitly Elliptic Momentum Equation (EEME) Formulation," Journal of Non-Newtonian Fluid Mechanics, Vol. 36, pp. 135-157. (1990a).

Rajagopalan, D., Armstrong, R. C., and Brown, R. A. "Finite Element Methods for Calculation of Steady, Viscoelastic Flow Using Constitutive Equations With a Newtonian Viscosity," Journal of Non-Newtonian Fluid Mechanics, Vol. 36, pp. 159-192. (1990b).

Ramos, J. I. "Finite Element Methods for One-Dimensional Combustion Problems," International Journal for Numerical Methods in Fluids, Vol. 11, pp. 893-906. (1990).

Rank, E., and Werner, H. "An Adaptive Finite Element Approach for the Free Surface Seepage Problem," International Journal for Numerical Methods in Engineering, Vol. 23, pp. 1217-1228. (1986).

Ritter, W. F. "Pesticide Contamination of Ground Water in the United States - A Review," Journal of Environmental Science and Health, Vol. B25, No. 1, pp. 1-29. (1990).

Rivara, M.-C. "Selective Refinement/Derefinement Algorithms for Sequences of Nested Triangulations," International Journal for Numerical Methods in Engineering, Vol. 28, pp. 2889-2906. (1989).

Robertson, W. D., Cherry, J. A., and Sudicky, E. A. "Ground-Water Contamination from Two Small Septic Systems on Sand Aquifers," Ground Water, Vol. 29, No. 1, pp. 82-92. (1990).

Russell, T. F., and Trujillo, R. V., "Eulerian-Lagrangian Localized Adjoint Methods with Variable Coefficients in Multiple Dimensions," In Computational Methods in Surface Hydrology, *Proceedings of the Eighth International Conference on Computational Methods in Water Resources*, G. Gambolati, A. Rinaldo, C. A. Brebbia, W. G. Gray, and G. F. Pinder Eds., Venice, Italy, Computational Mechanics Publications and Springer-Verlag, , pp. 357-363, (1990).

Sharma, M., and Carey, G. F. "Semiconductor Device Simulation Using Adaptive Refinement and Flux Upwinding," IEEE Transactions on Computer-Aided Design, Vol. 8, No. 6, pp. 590-598. (1989).

Steffler, P. M. "Upwind Basis Finite Elements for Convection-Dominated Problems," International Journal for Numerical Methods in Fluids, Vol. 9, pp. 385-403. (1989).

Stewart, I. B., and Unsworth, K. "A Petrov-Galerkin Method for the Numerical Solution of the Bradshaw-Ferriss-Atwell Turbulence Model," International Journal for Numerical Methods in Fluids, Vol. 8, pp. 493-517. (1988).

Sun, N.-Z., and Yeh, W. W.-G. "A Proposed Upstream Weight Numerical Method for Simulating Pollutant Transport in Groundwater," Water Resources Research, Vol. 19, No. 6, pp. 1489-1500. (1983).

Tezduyar, T. E., and Ganjoo, D. K. "Petrov-Galerkin Formulations with Weighting Functions Dependent upon Spatial and Temporal Discretization: Applications to Transient Convection-Diffusion Problems," International Journal for Numerical Methods in Engineering, Vol. 59, pp. 49-71. (1986).

Tezduyar, T. E., Glowinski, R., and Liou, J. "Petrov-Galerkin Methods on Multiply Connected Domains for the Vorticity-Stream Function Formulation of the Incompressible Navier-Stokes Equations," International Journal for Numerical Methods in Fluids, Vol. 8, pp. 1269-1290. (1988).

Tezduyar, T. E., and Park, Y. J. "Discontinuity-Capturing Finite Element Formulations for Nonlinear Convection-Diffusion-Reaction Equations," Computer Methods in Applied Mechanics and Engineering, Vol. 59, pp. 307-325. (1986).

Tezduyar, T. E., Park, Y. J., and Deans, H. A. "Finite Element Procedures for Time-Dependent Convection-Diffusion-Reaction Systems," International Journal for Numerical Methods in Fluids, Vol. 7, pp. 1013-1033. (1987).

Thompson, J. F. "A Survey of Dynamically-Adaptive Grids in the Numerical Solution of Partial Differential Equations," Applied Numerical Mathematics, Vol. 1, No. 1, pp. 3-27. (1985).

Tsang, T. H., and Huang, L. K. "On a Petrov-Galerkin Finite Element Method for Evaporation of Polydisperse Aerosols," Aerosol Science and Technology, Vol. 12, pp. 578-597. (1990).

van Genuchten, M. T., "On the Accuracy and Efficiency of Several Numerical Schemes for Solving the Convective-Dispersive Equation," In *Proceedings of the First International Conference on Finite Elements in Water Resources*, W. G. Gray, G. F. Pinder, and C. A. Brebbia Eds., Princeton University, Princeton, N.J., Pentech Press, , pp. 1.71-1.90, (1976).

Wang, C., Sun, N.-Z., and Yeh, W. W.-G. "An Upstream Weight Multiple-Cell Balance Finite Element Method for Solving Three-Dimensional Convection-Dispersion Equations," Water Resources Research, Vol. 22, No. 11, pp. 1575-1589. (1986).

Westerink, J. J., and Cantekin, M. E., "Non-Diffusive N+2 degree Upwinding Methods for the Finite Element Solution of the Time Dependent Transport Equation," In Numerical Methods for Transport and Hydrologic Processes, *Proceedings of the Seventh International Conference on Computational Methods in Water Resources*, M. A. Celia, L. A. Ferrand, C. A. Brebbia, W. G. Gray, and G. F. Pinder Eds., Cambridge, MA, Elsevier, Vol. 2, pp. 57-62, (1988).

Westerink, J. J., and Shea, D. "Consistent Higher Degree Petrov-Galerkin Methods for the Solution of the Transient Convection-Diffusion Equation," International Journal for Numerical Methods in Engineering, Vol. 28, pp. 1077-1101. (1989).

Wiberg, N.-E. "Adaptive and Hierarchical Weighted Residual and Least-Squares Time Integration of Convection-Diffusion Problems," Communications in Applied Numerical Methods, Vol. 4, pp. 499-507. (1988).

Yeh, G. T., "A Zoomable and Adaptable Hidden Fine-Mesh Approach to Solving Advection-Dispersion Equations," In Numerical Methods for Transport and Hydrologic Processes, *Proceedings of the Seventh International Conference on Computational Methods in Water Resources*, M. A. Celia, L. A. Ferrand, C. A. Brebbia, W. G. Gray, and G. F. Pinder Eds., Cambridge, MA, Elsevier, Vol. 2, pp. 69-74, (1988).

Yeh, G. T. "A Lagrangian-Eulerian Method With Zoomable Hidden Fine-Mesh Approach to Solving Advection-Dispersion Equations," Water Resources Research, Vol. 26, No. 6, pp. 1133-1144. (1990).

Yu, C.-C., and Heinrich, J. C. "Petrov-Galerkin Method for Multidimensional, Time-Dependent, Convective-Diffusion Equations," International Journal for Numerical Methods in Engineering, Vol. 24, pp. 2201-2215. (1987).

Yu, C. C., and Heinrich, J. C. "Petrov-Galerkin Methods for the Time-Dependent Convective Transport Equation," International Journal for Numerical Methods in Engineering, Vol. 23, pp. 883-901. (1986).

Zienkiewicz, O. C., The Finite Element Method 3rd ed., McGraw-Hill, London, 1977.

Zienkiewicz, O. C., and Zhu, J. Z. "A Simple Error Estimator and Adaptive Procedure for Practical Engineering Analysis," International Journal for Numerical Methods in Engineering, Vol. 24, pp. 337-357. (1987).

Zienkiewicz, O. C., Zhu, J. Z., and Gong, N. G. "Effective and Practical *h-p*-Version Adaptive Analysis Procedures for the Finite Element Method," International Journal for Numerical Methods in Engineering, Vol. 28, pp. 879-891. (1989).